Using Plot Photographs to Estimate Tundra Vegetation Cover in Northern Alaska

Hana L. Christoffersen

A Thesis Submitted to the Graduate Faculty of

GRAND VALLEY STATE UNIVERSITY

In

Partial Fulfillment of the Requirements

For the Degree of

Master of Science

Biology

August 2022

Thesis Approval Form

GRAND VALLEY STATE UNIVERSITY

The signatories of the committee members below indicate that they have read and approved the thesis of Hana L. Christoffersen in partial fulfillment of the requirements for the degree of Master of Science in Biology.

06/29/2022

Dr. Robert D. Hollister, Thesis committee chair — Date

06/29/2022

Dr. Alexandra Locher, Committee member — Date

06/29/2022

Dr. Sergio ~~A. Vargas/Ecsati~~, Committee member — Date

Accepted and approved on behalf of the College of Liberal Arts and Sciences

Dean of the College

8-29-2022

Date

Accepted and approved on behalf of the Graduate Faculty

Associate Vice-Provost for the Graduate School

8/31/2022

Date

Acknowledgements

I am thankful for the help that I have received from trusted mentors, colleagues, and friends throughout my academic journey. Thank you to my graduate committee – Robert (Bob) Hollister, Alexandra (Ali) Locher, and Sergio Vargas – for continual support and oversight. My research has benefitted from your thoughtful questions and suggestions.

I am one of many students in the Arctic Ecology Program at Grand Valley State University (GVSU) that has benefitted from funding through the National Science Foundation. Thank you to Bob Hollister, Craig Tweedie, Steven Oberbauer, Jeremy May, and William Gould for shepherding this research project through multiple rounds of funding.

Perhaps some of my best, although brief, conversations were with Karl (Fred) Huemmrich and Sarah Elmendorf. Thank you for reminding me that science is collaborative and imperfect. These conversations left me feeling lighter about my research and more confident in my role.

I am also thankful to the biology graduate committee for their guidance throughout a difficult program. Ali Locher is a stellar advocate. Meg Woller-skar introduced me to Brené Brown and statistics; both have made my personal and professional life better. Thank you for reminding me to practice self-compassion.

I owe a great deal of technical support to Kin Ma (GVSU – Geography Department) and Scott Benjamin (GVSU – IT Department). Thank you for working with me to format laptops and resolve internal program bugs or the dreaded Blue Screen of Death.

Thank you to countless students for their help during my tenure as a graduate student. Kailey Keenan-Whittemore – thank you for choosing to travel with me on a whim. I am less wary of Arctic ground squirrels because of your fondness for them. Jake Harris – thank you for

patiently teaching me how to code in R. I always enjoyed your existential questions in the field, which make the walk to the research site feel shorter. Katlyn Betway-May – no question was too insignificant for you. Thank you for answering each of them and supporting me through the program. Sarah Ansbro and Mackenzie Lift – thank you for reminding me why I am choosing to become a scientist. I found the courage to continue and finish this program because of you. Tabby Fuson and Mariana Mora – thank you for showing me how we can support each other in STEM, even from thousands of miles away.

Thank you to the indigenous communities in northern Alaska, who have allowed me to study the plants on their land at Utqiaġvik and Atqasuk, Alaska. Every field season has been unforgettable. I have been privileged to join in Nalukataq (blanket toss), taste muktuk (bowhead whale), and glimpse one polar bear from a very far distance. I would also like to thank Jerry Brower for his quiet, steadfast help on the North Slope, especially for his diligent repairs of malfunctioning ATVs and the Atqasuk house.

I am thankful for Paul Krieger, Dale, Robin, and Evan Christoffersen for lending me external support, wisdom, and a sounding board when I most needed it. To Cory, my lifeline, thank you for keeping the faith when I did not, and encouraging me on what has been less of a solitary, arduous journey because of you. Copper and Tikaani, our hound dog and wolf pup, thank you for reminding me how to take breaks, whether we walked to the park or napped on the couch.

Abstract

Plot photography can provide a quick, robust method to measure vegetation, especially in polar environments where logistics can be expensive and challenging. The success and widespread adoption of plot photography in the Arctic hinges on the accuracy of image analysis and data product interpretation. The relative cover of eight vegetation classes was estimated using a point frame and digital camera across thirty, 1-m^2 plots at Utqiaġvik, Alaska from 2012 to 2021. Geographic object-based image analysis (GEOBIA) was applied to generate objects and classify the three band (red, green, blue) images. Machine learning classifiers (random forest, gradient boosted model, classification and regression tree, support vector machine, k-nearest neighbor) were applied, and random forest performed the highest (60.5% overall accuracy). Objects were classified reliably in six out of the eight vegetation classes using the random forest classification, including bryophytes, forbs, graminoids, litter, shadow and standing dead. Deciduous shrubs and lichens were not reliably classified.

We also assessed whether estimates of relative vegetation cover from plot photography were comparable to estimates using the point frame. Based on Spearman-Rank correlations within each year, graminoid cover was consistently, positively correlated. Most of the remaining vegetation classes showed moderate positive associations except for litter and standing dead, which showed a negative association. We then used multinomial regression models to gauge if the cover estimates from plot photography could accurately predict the abundance estimates from the point frame across space or time. Currently, our approach to image analysis is best suited to detect large shifts in composition over spatial gradients rather than the more subtle temporal shifts in vegetation over time. Together these results suggest that plot photography coupled with

semi-automated image analysis maximizes time, funding, and available technology to monitor vegetation cover in the Arctic.

Table of Contents

List of Tables

List of Figures

Abbreviations

Research Networks:

ARCSS: Arctic System Science

ITEX: International Tundra Experiment

AON: Arctic Observing Network

Vegetation Classes:

BRYO: Bryophytes

DSHR: Deciduous Shrubs

FORB: Forbs

GRAM: Graminoids

LICH: Lichens

LITT: Litter

SHAD: Shadow

STAD: Standing Dead

Machine Learning Classifiers:

RF: Random forest

GBM: Gradient boosted model

CART: Classification and regression tree

SVM: Support vector machine

KNN: K-Nearest neighbor

Image Analysis:

GEOBIA: Geographic object-based image analysis

OBIA: Object-based image analysis

RGB: Red green blue bands

NIR: Near-infrared band

HSV: Hue saturation value transformation

DGPS: Differential global positioning system

RMSE: Root mean square error

MRS: Multi-resolution segmentation

NDI: Normalized difference index

GLCM: Grey-level co-occurrence matrix

ASM: Angular second moment

Accuracy Assessment for Classification:

OA: Overall accuracy

PA: Producer accuracy

UA: User accuracy

Accuracy Assessment for Regression:

MAE: Mean absolute error

Chapter 1

Introduction

The Arctic is warming at twice the global rate due to climate change (Allen et al., 2018). It is likely that the average temperatures in the Arctic will increase by 6 to 10°C within the next 100 years (Allen et al., 2018). Polar regions influence feedback loops that regulate global temperatures and climate, carbon release, and vegetation dynamics (Chapin et al., 2005; Pearson et al., 2013; Schuur et al., 2015). Vegetation is growing taller in response to experimental warming in the Arctic, especially shrubs and graminoids (Elmendorf et al., 2012a; Myers-Smith et al., 2011). Bryophytes and lichens are decreasing in abundance, while litter and shrubs are increasing in abundance (Elmendorf et al., 2012a; Elmendorf et al., 2012b). Changes in vegetation composition are likely to affect hydrology, the duration and thickness of snow cover, the amount of solar radiation reflected from the earth's surface, and the forage available for wildlife and indigenous human populations (Joly et al., 2009; Kelsey et al., 2021; Sturm et al., 2005; Wrona et al., 2016). It is critical to monitor vegetation cover, structure, and community dynamics over time in order to understand and predict widespread change across the Arctic (Allen et al., 2018; Post et al., 2019).

In 1990, the International Tundra Experiment (ITEX) was established by an assembly of Arctic researchers (Webber & Walker, 1991). A warming experiment was developed using open-top chambers (OTCs) to preview the effects of warmer temperature on Arctic vegetation. Open-top chambers passively raise the temperature within a vegetation plot from 1 to 3°C (Henry & Molau, 1997; Hollister et al., 2006). Protocols were developed and shared across the international research network to measure vegetation growth, abundance, productivity, and response to warming (Molau & Mølgaard, 1996). Research efforts have expanded to include

phenology, plant traits, and carbon release in recent years (Bjorkman et al., 2018; Oberbauer et al., 2013; Oberbauer et al., 2007; Prevéy et al., 2017). ITEX is considered an important research network since standardized protocols allow for coordinated syntheses and broad conclusions about the impacts of climate change on the Arctic (Fraser et al., 2012).

The International Tundra Experiment Arctic Observing Network (ITEX-AON), which is funded by the National Science Foundation (NSF), is an assembly of researchers based in the United States at Grand Valley State University (GVSU), University of Texas at El Paso (UTEP), Florida International University (FIU), and University of Alaska Anchorage (UAA). ITEX-AON maintains long-term vegetation measurements across four research sites in northern Alaska: Utqiaġvik, Atqasuk, Toolik Lake, and Imnavait Creek. The four research sites were established in 1994 (Utqiaġvik), 1995 (Atqasuk), 1994 (Toolik Lake) and 2016 (Imnaviat Creek) (Hollister, 2003; May et al., 2020; Wahren et al., 2005).

The research in this master's thesis relies on two long-term data sets collected from thirty vegetation plots in the Arctic System Science Grid (ARCSS) at Utqiaġvik, Alaska (Brown et al., 2000). Vegetation abundance and cover were sampled using the point frame method from 2010 to 2021. The same set of plots were photographed annually at the plot-level from 2012 to 2021. The plot photographs contain three bands (red, green, blue) in the visible electromagnetic spectrum. These photographs have not been incorporated into any published research to date.

This thesis analyzes the plot photographs using geographic object-based image analysis (GEOBIA). GEOBIA is a sub-discipline that originated from object-based image analysis (OBIA) (Hay & Castilla, 2008, 2006). GEOBIA is specific to the field of remote sensing, as this refers to an object-based approach applied to remotely sensed images. GEOBIA is an image analysis technique with two, fundamental steps: segmentation and classification. Image objects,

or objects, are generated from groups of homogeneous pixels determined by segmentation algorithms. Then, the objects are labeled according to class. This process is iterative and adaptive, so additional spatial, spectral, and textural features in an image, ancillary data layers, and expert user knowledge can also be incorporated to improve the results (Platt & Rapoza, 2008).

The shift from pixel-based analysis to OBIA occurred in the early 2000's (Blaschke, 2005; Blaschke et al., 2000). Images were becoming more readily available at a higher resolution, which rendered a pixel-based approach inappropriate and inaccurate (Lang, 2008). The first instances of an object-based approach to remotely sensed imagery were in aerial or satellite imagery of agricultural and urban landscapes (Hay & Castilla, 2006). Since then, an object-based approach has been applied to aerial and satellite images in polar regions, but this approach has been applied rarely to near-surface digital images of the Arctic or Antarctic (Chen et al., 2010; King et al., 2020; Liu & Treitz, 2016).

Purpose

The purpose of this research is to: (1) classify tundra vegetation cover from repeat plot photographs at Utqiaġvik, Alaska using geographic object-based image analysis (GEOBIA); (2) compare the estimates of vegetation cover from the plot photographs to the estimates from *in situ* point frame-based sampling; (3) gauge the accuracy and overall utility of plot photography and digital image analysis; and (4) predict vegetation abundance across space and time using the vegetation cover estimates from plot photography.

Scope

Vegetation cover was collected from thirty vegetation plots within the Arctic System Science grid (ARCSS) at Utqiaġvik, Alaska. There are ninety-eight vegetation plots in the ARCSS grid. This methodology could be extended to the entire grid, in addition to other tundra communities with similar vegetation structure, characteristics, and composition in the Arctic. Observations at the fine-scale may improve and validate observations of terrestrial change at coarser scales.

Assumptions

There are four core assumptions in this research study: (1) The inherent variability of the total data set (n = 2,159,693 objects) from the repeat plot photographs is captured and reflected appropriately in the labeled data set (n = 15,000 objects). In other words, the models are trained and validated appropriately on the subset of objects in the labeled data set. (2) The local vegetation composition is summarized appropriately in the thirty vegetation plots within the ARCSS grid. (3) The true baseline, or value which represents the exact amount of vegetation cover in a plot, is unknown, regardless of the vegetation sampling method. Point frame-based sampling and plot photography generate estimates of vegetation cover and abundance since error can be minimized but not eliminated from these methods. (4) The comparison is not direct between the cover estimates generated from point frame-based sampling and plot photography. The cover estimates from the point frame are calculated from every available canopy layer, not just the top canopy layer. The cover estimates from plot photography are calculated from all visible objects in the superficial, two-dimensional view of the plot.

Hypotheses

This research addresses the four questions: 1. Which model is optimal for classification of near surface, high resolution digital images of Arctic vegetation? 2. Which vegetation classes can be accurately estimated? Which classes cannot be? 3. How do estimates from plot photography and automated image analysis compare with estimates from the point frame method? 4. Can we predict vegetation abundance across space and time using the vegetation cover estimates from plot photography?

We assert that all classes can be accurately estimated, given the quality and high spatial resolution of the images. Although there is a lack of spectral information available for analysis in red, green, and blue images, other geometric and texture-based metrics may compensate for it. Point frame measurements have been proven as reliable indicators of vegetation cover. We expect that the vegetation cover estimates from plot photography will complement cover estimates from the point frame. It is unlikely that the estimates will match exactly due to methodological differences between the two methods of sampling.

Significance

Although general greening and browning trends can be determined at a global scale, there is significant variability in the magnitude and direction of the trends. In other words, vegetation change is not uniform across time and space (Bhatt et al., 2013, 2017; Myers-Smith et al., 2020). Trends in vegetation can be observed through *in situ* field studies at the plot level or remotely sensed through aerial or satellite platforms, however, these results may not correspond across scales or between sensors (Myers-Smith et al., 2020). There is a need for improved integration of *in situ* field observations with remotely sensed observations across varying scales (Davidson et al., 2016; Langford et al., 2016; Shiklomanov et al., 2019). This study helps bridge the gap

between field and remotely sensed observations and communicate information across platforms, validating or challenging existing observations and conclusions.

The framework within this thesis could be extended to digital images acquired at comparable, near-surface scales. Images taken from low-altitude aerial platforms have high spatial resolution, which may be comparable to the resolution of near-surface digital images (Anderson et al., 2016; Fraser et al., 2016; Malenovský et al., 2017; Richardson et al., 2018). Some minor changes may be necessary to the workflow, including a different set of parameters for segmentation, but the framework can be applied to other digital images. We expect that the workflow will continue to improve with technical, scientific, and practical revisions over time.

Our contribution to the existing body of research is important because few researchers have examined plot photographs using object-based image analysis (Laliberte et al., 2007; Luscier et al., 2006; Michel et al., 2010), and even fewer have assessed alpine or tundra vegetation cover from the photographs using this approach (Chen et al., 2010; King et al., 2020; Liu & Treitz, 2016). Vegetation cover was estimated in twenty-six vegetation plots in Nunavut, Canada in 2007 using an object-based approach on plot photography (Chen et al., 2010). The cover estimates of a few, dominant vegetation species were compared using a digital grid overlay, visual inspection, and semi-automated image analysis. This approach was the earliest, published example of object-based image analysis applied to plot photographs of tundra vegetation. Although the results were accurate, the methodology relied on several manual modifications, therefore it was too time-consuming and labor-intensive to adapt over a larger data set. There was no formal accuracy assessment to determine the accuracy of the object-based classification. Additionally, the approach was not extended to analyze broad vegetation classes, nor assess the change in vegetation cover over time.

More recently, vegetation cover, change, and bryophyte vigor were estimated in Antarctica using an object-based approach on plot photography from 2003 to 2014 (King et al., 2020). In this study, the vegetation classes were broad, consisting only of bryophytes, lichens, rock, and shadow. King et al. were successful with their approach, but their vegetation classes were few and visually distinctive, marked by clear boundaries between vegetation types (2020). Northern tundra communities, especially mesic vegetation communities, tend to display high species richness and complexity, necessitating a greater number of vegetation classes (van der Welle et al., 2003). This study also failed to validate their results with complementary data from an *in situ* field survey.

The research in this thesis extends previous work by applying the semi-automated image analysis approach to the vegetation in northern Alaska, quantifying the cover of eight, complex vegetation classes from plot photographs. We also use the estimates of vegetation cover from the plot photographs to predict vegetation abundance over space and time, scaling our approach to tundra communities with similar composition.

Definitions

Broad growth form: An alternative grouping to the classification of plants by scientific species, family, or genus. Vegetation species are grouped into broad forms, or categories, which are functionally-related: bryophytes (mosses), deciduous shrubs, evergreen shrubs, forbs (non-woody flowering plants), graminoids (grasses, sedges, rushes), lichen, litter, and standing dead. It is easier to detect broad trends in vegetation communities using aggregate groups of vegetation.

Geographic object-based image analysis (GEOBIA): This framework is based on object-based image analysis, where a two-step, iterative process may result in a classified image. Image

objects are created (segmentation) and classified (classification). In order to distinguish object-based image analysis from related disciplines in biomedical and computer science, geographic object-based image analysis (GEOBIA) has been accepted as the framework that often accompanies object-based image analysis of remotely-sensed imagery.

Inflorescence: The flowering part(s) of a plant.

In situ: An on-site or local observation.

Machine learning classifiers: Machine learning classifiers may also be referred to as machine learning algorithms or models. Models aim to learn and unveil patterns in a data set based on training, validating, and testing samples. Models can be developed for classification or regression-based tasks. Classification predicts a discrete value, usually in the form of a class label or category. Regression predicts a continuous value.

Resolution: Describes the spatial resolution, or visible detail, of an image. High, medium, and low resolutions vary in their definitions depending on the platform of measurement. For satellite imagery, 0 to 2 meters is generally accepted as high resolution, 2 to 20 meters is medium resolution, and more than 20 meters is low resolution. This same guideline does not apply to images acquired at the plot-level or low-altitude aerial level. In this study, images were considered high resolution if the objects of interest were at least three to five times larger than the pixels from which they were made.

Vegetation abundance: Abundance is calculated from the number of counts of a vegetation species within a plot. Relative abundance is calculated by the counts of one vegetation species divided by the counts of all vegetation species.

Vegetation cover: Cover is calculated from the area occupied by a vegetation species within a plot. Relative cover is calculated by the area of one vegetation species divided by the area of all vegetation species.

Chapter 2

Estimating tundra vegetation cover using plot photographs and semi-automated image analysis

Hana L. Christoffersen[1], Sergio A. Vargas Zesati[2], Sarah C. Elmendorf[3], Alexandra Locher[1], Craig E. Tweedie[2], Chandi Witharana[4], Robert D. Hollister[1]

[1]Department of Biological Sciences, Grand Valley State University, 1 Campus Dr., Allendale, MI 4940, USA

[2]Department of Biological Sciences, The University of Texas at El Paso, 500 W University Ave., El Paso, TX 79968, USA

[3]Institute of Arctic and Alpine Research, University of Colorado, Boulder, CO 80309, USA

[4]Department of Natural Resources and the Environment, University of Connecticut, Storrs, CT 06269, USA

Corresponding Author: Hana L. Christoffersen (e-mail: christoh@mail.gvsu.edu)

Abstract

Plot photography can provide a quick, robust method to measure vegetation, especially in polar environments where logistics can be expensive and challenging. The success and widespread adoption of plot photography in the Arctic hinges on the accuracy of image analysis and data product interpretation. The relative cover of eight vegetation classes was estimated using a point frame and digital camera across thirty, 1-m^2 plots at Utqiaġvik, Alaska from 2012 to 2021. Geographic object-based image analysis (GEOBIA) was applied to generate objects and classify the three band (red, green, blue) images. Machine learning classifiers (random forest, gradient boosted model, classification and regression tree, support vector machine, k-nearest neighbor) were applied, and random forest performed the highest (60.5% overall accuracy). Objects were classified reliably in six out of the eight vegetation classes using the random forest classification, including bryophytes, forbs, graminoids, litter, shadow and standing dead. Deciduous shrubs and lichens were not reliably classified.

We also assessed whether estimates of relative vegetation cover from plot photography were comparable to estimates using the point frame. Based on Spearman-Rank correlations within each year, graminoid cover was consistently, positively correlated. Most of the remaining vegetation classes showed moderate positive associations except for litter and standing dead, which showed a negative association. We then used multinomial regression models to gauge if the cover estimates from plot photography could accurately predict the abundance estimates from the point frame across space or time. Currently, our approach to image analysis is best suited to detect large shifts in composition over spatial gradients rather than the more subtle temporal shifts in vegetation over time. Together these results suggest that plot photography coupled with

semi-automated image analysis maximizes time, funding, and available technology to monitor vegetation cover in the Arctic.

Keywords

Abundance; Arctic; Cover; Geographic Object-Based Image Analysis (GEOBIA); Handheld digital camera; Plant; Plot photography; Point frame; Vegetation change.

Introduction

The Arctic is changing in response to warmer temperatures caused by global warming (Allen et al., 2018). Warmer temperatures in the Arctic lead to longer growing seasons, greater thaw depth, and altered snow cover and accumulation, which influences the composition of tundra vegetation communities (Kelsey et al., 2021; Leffler et al., 2016; Shiklomanov et al., 2010). As the composition shifts in tundra vegetation communities, climate-related feedback cycles may be amplified, prompting widespread change in and beyond the Arctic (Chapin et al., 2005; Pearson et al., 2013). In order to assess and forecast change across a warming Arctic, it is critical to monitor plant cover, structure, and community dynamics over time (Allen et al., 2018; Post et al., 2019).

Satellite-derived indices have documented widespread spectral greening across the Arctic for more than 40 years (Guay et al., 2014; Zhu et al., 2016), while spectral browning has also been detected in the past decade by some studies (Bhatt et al., 2013; de Jong et al., 2011; Phoenix & Bjerke, 2016). Spectral greening trends suggest an increase in vegetation productivity as a result of warming, whereas spectral browning trends suggest a decrease in vegetation productivity (Myers-Smith et al., 2020). Satellite-based observations and trends must be validated by ground-based observations, but these data do not always correspond spatially or temporally (Myers-Smith et al., 2020). It is not well understood how patterns detected by

satellites are related to patterns observed on the ground. Plot-level photographs, low-altitude drones, and manned aerial aircraft offer the potential to bridge the information gap between ground-based and satellite-based observations in the Arctic (Anderson et al., 2016; Fraser et al., 2016; King et al., 2020; Liu & Treitz, 2016; Malenovský et al., 2017).

Ground-based observations validate remotely-sensed observations through precise, accurate, and detailed measurements of tundra vegetation. The point frame method is a standard field technique for measuring *in situ* vegetation cover and abundance in the Arctic (Molau & Mølgaard, 1996). Although this method is accurate, repeatable, and robust, it is costly in terms of time and energy (May & Hollister, 2012). It can be challenging to generate a sufficiently large, representative sample size using this method, since vegetation plots are likely to be sampled at a lower temporal frequency (May & Hollister, 2012). Additionally, traditional approaches to vegetation monitoring in the Arctic are confined to a short growing season (less than 3 months), extensive logistical costs, and limited access to remote research sites. The constraints of conventional field surveys have encouraged the use of remote sensing methods in the Arctic (Dronova, 2015; Shiklomanov et al., 2019).

Plot-level photography may be more efficient, quicker, and easier to record than traditional field surveys. Plot photography may increase the sampling extent and frequency at a study site, and a photographic record can be analyzed retroactively (Booth et al., 2005; King et al., 2020). The error associated with handheld digital cameras remains consistent, whereas different observer bias may be introduced seasonally in field surveys (Chen et al., 2010; Luscier et al., 2006). Plot photographs are also advantageous because each image captures a complete bird's eye (nadir) view of the vegetation, whereas the analysis of the point frame data is limited to the point density of the sampling frame (Chen et al., 2010; Laliberte et al., 2007). Despite the

obvious advantages, the success of plot photography is reliant on the accuracy of image interpretation and analysis (Dronova, 2015).

Imagery analysis has transitioned from pixel-based to object-based image analysis over recent years (Hay & Castilla, 2008, 2006). In order to distinguish object-based image analysis from related approaches in the biomedical and computer sciences, geographic object-based image analysis (GEOBIA) has been accepted as the framework that accompanies object-based image analysis of remotely-sensed imagery (Hay & Castilla, 2008, 2006). Image objects, or objects, are generated from groups of homogeneous pixels through segmentation, then assigned to a class through classification. Spatial, spectral, and other features within an image, additional data layers, and expert user knowledge can be incorporated into the classification procedure, which further offsets object-based from pixel-based approaches (Platt & Rapoza, 2008). In this study, we refer to the GEOBIA framework as an object-based approach, or GEOBIA. Image objects and objects are used interchangeably.

As high resolution imagery becomes more accessible due to technological advancements, GEOBIA is being widely used (Blaschke et al., 2014; Chen et al., 2018; Hay & Castilla, 2008). Advantages of the object-based approach are summarized elsewhere (see Blaschke et al., 2014; Chen et al., 2018; Hussain et al., 2013). In general, object-based approaches have been shown to be accurate in analyzing high resolution imagery, especially in urban and agricultural landscapes (Myint et al., 2011; Ye et al., 2018).

GEOBIA has been used to evaluate vegetation cover primarily at the aerial and satellite levels (Ma et al., 2017). Fewer studies have applied GEOBIA to near-surface digital images (Laliberte et al., 2007; Luscier et al., 2006; Michel et al., 2010), especially in the Arctic (Chen et

al., 2010; King et al., 2020; Liu & Treitz, 2016). To our knowledge, no published studies have examined vegetation cover change from plot-level photographs in the Arctic, yet.

Chen et al. (2010) examined vegetation cover using an object-based approach on plot photographs from 2007 in the Arctic. The cover estimates of a few, dominant vegetation species were compared using a digital grid overlay, visual inspection, and semi-automated image analysis. This approach was the earliest example of object-based image analysis on plot photographs of tundra vegetation. This approach was the earliest, published example of object-based image analysis applied to plot photographs of tundra vegetation. Although the results were accurate, the methodology relied on several manual modifications, therefore it was too time-consuming and labor-intensive to adapt over a larger data set. There was no formal accuracy assessment to determine the accuracy of the object-based classification. Additionally, the approach was not extended to analyze broad vegetation classes, nor assess the change in vegetation cover over time.

More recently, King et al. (2020) examined vegetation cover, change, and vigor using an object-based approach on plot photographs from 2003 to 2014 in Antarctica. The vegetation classes were limited to a few broad categories (bryophytes, lichens, rock, and shadow) with visually distinctive boundaries. Northern tundra communities, especially mesic vegetation communities, are complex and diverse, so the rule-based framework from King et al. (2020) is not sufficient nor replicable in the Arctic, since the vegetation classes are not comparable between the two studies (van der Welle et al., 2003). King et al. also failed to validate their results with complementary data from an *in situ* field survey (2020).

The research in this thesis extends previous work by applying the semi-automated image analysis approach to the vegetation in northern Alaska, quantifying the cover of eight, complex

vegetation classes from plot photographs. We also use the estimates of vegetation cover from the plot photographs to predict vegetation abundance over space and time, scaling our approach to tundra communities with similar composition.

The following questions were addressed in this study:

1. Which machine learning classifier (model) is optimal for classification of near surface, high resolution digital images of Arctic vegetation?
2. Which vegetation classes can be accurately estimated? Which classes cannot be?
3. How do estimates from plot photography and automated image analysis compare with estimates from the point frame method?
4. Can we predict vegetation abundance across space and time using the vegetation cover estimates from plot photography?

We investigate if images from inexpensive, handheld digital cameras can be used to accurately estimate vegetation cover from 2012 to 2021 at Utqiaġvik, Alaska. We use an object-based approach to analyze Arctic tundra vegetation cover from high resolution digital images. Machine learning classifiers are investigated and compared in order to generate an accurate vegetation classification across the repeat plot photographs. Spearman-rank correlations reveal the degree of association between the cover estimates from the point frame and plot photography sampling methods. Multinomial regression models demonstrate whether the cover estimates from plot photography can predict abundance estimates from the point frame sampling method. Ultimately, we determine if plot photography is useful in estimating vegetation cover and change. We also compare the cost and benefit of both sampling methods in terms of overall investment (time, logistics, effort) and accuracy.

Materials and Methods

Study Site

In the early 1990's, a sampling grid was established at Utqiaġvik (formerly Barrow), Alaska (71˚19'N, 156˚36'W) by the Arctic System Science Program (ARCSS) to monitor long-term, landscape-level terrestrial change (Brown et al., 2000). Ninety-eight, 1-m^2 vegetation plots were installed at 100-m intervals across a 1-km^2 grid (Figure 2.1). Plots were not artificially warmed or manipulated. Plots are representative of the local variability in topography, moisture, soil, and vegetation cover at Utqiaġvik. In 2010, 30 plots were selected for annual vegetation sampling. The analysis in this study is focused on the 30 vegetation plots.

This region (W1) is defined as a wetland dominated by sedges, grasses, and mosses by the Circumpolar Arctic Vegetation Map (Raynolds et al., 2019). Vegetation plots were established over a drained lake basin and historic beach ridge. The habitat varies from moist ridges on ice-wedge polygons to saturated wet meadows. Average July temperatures for the region were historically recorded as 4^{o}C, although the region has experienced a warming trend over the past several decades (Allen et al., 2018; Box et al., 2019; Brown et al., 1980). Continuous daylight is exhibited in the Arctic for most of the growing season, which extends from early June to late August. Peak growing season, where the plants are generally at their greenest and most productive, occurs from July through mid-August (Tieszan, 1978).

Plot Photography

Plot photographs were taken at breast-height (approximately 1-m above the ground), from a bird's eye (nadir) point-of-view, centered above the plot. Although overcast conditions were preferred in order to reduce the amount of shadow in the photograph, lighting conditions were not always consistent. An object-based approach may combat inconsistent lighting by

relying on information that is independent from color, which reduces the error associated with inconsistent lighting conditions (King et al., 2020).

Plot photographs were taken using either the Panasonic DMC-TS3 or Nikon Coolpix AW120 handheld cameras. Images were considered high resolution since the objects of interest were at least three to five times larger than the number of pixels in the objects (Blaschke et al., 2014; Lang, 2008; Strahler et al., 1986). Automatic camera settings (no flash, fixed focus) were used to respond to natural ambient light in the environment. Images were recorded as uncompressed JPEG files with three visible spectral bands (red, green, blue) and an 8-bit, unsigned radiometric resolution, which ranged in digital values from 0 to 255.

Plot photographs were mostly collected on a biweekly basis during the growing season (Table 2.1). One set of photos near peak growing season were analyzed each year, although some substitutions occurred for plot photos that were not vertically positioned, missing, or out-of-focus (Figure 2.2). Photographs were substituted if an adjacent or nearby sampling date contained an acceptable image. In total, 210 plot photographs were analyzed across seven sampling years (2012, 2013, 2014, 2015, 2018, 2019, 2021). In 2016, no photographs were recorded. In 2017, photographs were not suitable because they were taken prior to peak greenness and productivity. In 2020, photographs were of low resolution and incomplete.

Image Preprocessing

The general methodology is found in Figure 2.3. Images were geometrically corrected in ArcGIS Pro v. 2.8 (ESRI Inc.; Redlands, CA, United States). Each image was registered to four ground control points, or differential global positioning system (DGPS) coordinates, which marked the plot corners (spatial reference ESPG: 26904). The base of each stake was surveyed using high precision coordinates collected with a Trimble R8 GNSS Receiver and a 2 m survey

pole in 2013. Despite some tilt over time due to freeze-thaw cycles, the base remained permanently fixed at the base in one location. Coordinates were processed using the Post Processing Kinematic approach in Trimble Business Center v. 2.70 with an overall accuracy of ± 1 to 5 cm (Trimble; München, Germany).

Images acquired in 2013 were corrected first. These were considered to be the benchmark images, since the DGPS coordinates were also acquired in 2013. Once the benchmark images were corrected, the permanent physical markers were identified in each image. The markers, or tags, served as additional ground control points for the images across all other years (Figure 2.4). Occasionally, the plot image from 2012 was a better representation of the entire series of plot photographs (i.e., more tags are visible due to low water levels, or better camera angle). In these cases, the plot image from 2012 became the benchmark for the images across all other years. Root mean square error (RMSE) averaged 1.5 to 4.8 cm across sampling years (Table 2.2). In a few cases, the RMSE extended to 8.8 to 11.5 cm on the images with the most severe distortion as a result of poor camera angle.

Orthorectification is preferred for accurate registration because it establishes a true nadir perspective, and it reduces the likelihood of an over- or under-valuation of plant cover (Clarke & Fryer, 1998). Although orthorectification is critical for a reliable analysis of pixel to pixel change, it is not critical for reliable analysis of change in relative vegetation cover within each plot in an image (King et al., 2020; Rogers et al., 1983). We assess the total number of objects, not the change between pixels, so the georeferencing procedure is acceptable for our analysis (King et al., 2020).

Nearest neighbor resampling rectified the pixel sizes of all images to a coarser resolution of 0.05 cm, which standardized the resolution and allowed for direct comparison between images

(King et al., 2020; Laliberte et al., 2007). A background mask was generated to hide the exterior of the plot. When not enough tags were visible within the plot to clearly define the area of interest, the mask generated from the benchmark image was used. Both the georeferenced images and the corresponding masks were exported for use in eCognition.

Segmentation and Preliminary Classification

An object-based approach was applied to the plot photographs in eCognition Developer v. 9.5 (Trimble; München, Germany). Chessboard segmentation was applied to mask the background of each vegetation plot. Generally, the user must define an object size that exceeds the number of pixels in the image to mask the background. We achieved the chessboard segmentation with an object size of 15,000 to create two image objects: the area of interest and exterior of the plot. The exterior of the plot was removed from analysis.

Image object candidates were generated across the entire image using the multi-resolution segmentation algorithm (MRS), which is one of the most widespread, successful segmentation algorithms for OBIA (Baatz & Schaape, 2000; Benz et al., 2004). Image objects undergo an iterative algorithm, in which pixels are grouped into objects until the threshold (defined by scale) is reached. The threshold (scale) is user-defined, and it is weighted by shape and compactness. This algorithm exacts a greater toll on the computer processor and memory, rendering it a slow technique.

Image objects were weighted by user-defined parameters in multi-resolution segmentation, including scale, color, shape, smoothness, and compactness. Scale is unit-less, not intuitive, and depends on the heterogeneity in the image, but in general, a lower value for scale results in smaller image objects. A higher value for scale results in larger image objects. Shape values range from 0 to 1.0. A higher value for shape generates image objects that are weighted

more heavily by shape, whereas a lower value for shape generates image objects that are weighted more by color, or spectral information. Compactness ranges from 0 to 1.0. Lower compactness values generate image objects that are squiggly and irregular. Higher compactness values generate image objects that are blocky, rectangular, and compact.

Although supervised and unsupervised approaches have been proposed for the automatic, objective selection of optimal segmentation parameters, there is no consensus among the remote sensing community (Hossain & Chen, 2019). We applied a supervised, stepwise approach to select the optimal segmentation parameters for our images in eCognition Developer v. 9.5 (Trimble; München, Germany). Although some scientists argue that this method lacks repeatability and robustness, trial-and-error to maximize parameters can provide strong results (Blaschke et al., 2014; Liu et al., 2018; Radoux & Bogaert, 2017). All variables were held constant while independently adjusting each of the user-defined parameters to observe the effect of each parameter on the primitive image objects. Combinations of scale, compactness, and shape were identified as potential contenders. The combinations were visually compared across different images: dry, moist, wet plots; across sampling years; across different lighting conditions, which ranged from highly reflective water to shadowed canopies). We tallied the number of mixed image objects, and we closely examined the edge delineation, meaningfulness (over- or under-segmented), and representation of each class. The final parameters, used consistently across all the images, were Scale: 30, Color/Shape: 0.5/0.5, Smoothness/Compactness: 0.7/0.3. Color and shape were equally adept at creating logical image objects. A greater weight was assigned to smoothness since tundra vegetation is rarely blocky or square. This resulted in a total of 2,159,693 image objects generated across all of the images. The total number of image objects generated in each image is summarized in Table 2.3.

An over-segmented image object is defined as one feature divided into multiple image objects. This result was preferable to under-segmented image objects, because smaller image objects can be merged into larger image objects in subsequent steps if desired. Under-segmentation results in image objects that contain multiple features in a single image-object, or in other words, are too large and mixed with multiple features. It becomes impossible to distinguish different classes from an under-segmentation (Kim et al., 2011).

After segmentation we established a non-hierarchical, multi-class classification scheme, which contained ten classes: non-vegetation, bryophytes, deciduous shrubs, forbs, graminoids, lichens, litter, shadow, standing dead, and water. It was not possible to develop an automatic ruleset to refine and classify image objects due to the lack of existing, ancillary thematic data.

Non-vegetation and water were manually identified and masked from the images. Insects, excrement, bare ground, fungi and permanent physical tags were labeled as non-vegetation. The machine learning classifiers require at least fifty samples to be trained properly. There were not enough samples to identify the non-vegetation classes accurately. In the rare case that an image object was unidentifiable from the image, it was also classified as non-vegetation.

Vascular species (deciduous shrubs, forbs, graminoids) and non-vascular species (bryophytes, lichens) were grouped by broad growth form. Litter and standing dead are the result of dead plant material, but these two classes can be classified separately, since they differ in characteristics and structure. Standing dead is typically recognizable by reflective upright stalks, while litter is degraded to the point where it is not recognizable.

Inflorescences may appear identical or vastly different in shape, color, and size as a result of their development within their phenological lifespan. Due to the low frequency and lack of pattern among the inflorescences, all inflorescences were identified and classified manually into

the corresponding class. The algorithms would not be able to learn and classify these few instances well.

Areas obscured by shadow were not able to be accurately identified, therefore shadow was assigned its own class. In the rare event that a mixed image object is encountered in the labeling procedure, then the image object was classified based on the majority class (Congalton & Green, 2009).

Feature Calculation and Extraction

A combination of spectral, shape, and textural features, which leverage the information in an object-based approach, were selected for analysis (Table 2.4). Relational (i.e., proximity to neighbors), hierarchical, and class-related features were not used in the design and implementation of this study.

Several band combinations were tested using the red, green, and blue bands. Spectral indices often minimize the effects of uneven illumination (Jensen, 2013). Some spectral indices can provide an estimation of vegetation cover, phenological shifts, or productivity, while others can distinguish soil or non-living elements from living vegetation species (Anderson et al., 2016; Beamish et al., 2016; Gitelson et al., 2002; Ide & Oguma, 2010; Richardson et al., 2007, 2009; Tucker, 1979). In our preliminary exploration, we found that ratio-based spectral indices (RSI = Band A / Band B) and reciprocal difference spectral indices (RDSI = (1 / Band A) – (1 / Band B) did not offer any new information. These redundancies were eliminated prior to classification.

Texture features were calculated from a grey-level co-occurrence matrix (GLCM) (Haralick, 1979; Haralick et al., 1973). A GLCM tabulates how often different combinations of pixel gray levels appear or exist in an image or scene. Contrast features include homogeneity, contrast, and dissimilarity, while orderliness features include entropy and angular second

moment. Descriptive statistics of the GLCM (correlation, mean, standard deviation) were not included in this analysis, nor were any third-order texture measures calculated from the grey-level difference vector (GLDV) due to the heavy computational load in eCognition Developer. Texture features were calculated from all bands in all directions (0°, 45°, 90°, 135°), and therefore show directional invariance.

Machine Learning Classifiers

There were five machine learning classifiers that were implemented in this study (Table 2.5). All classifiers are non-parametric; therefore, no statistical assumptions were made about the distribution of the data. A brief description of each classifier is provided below.

Random Forest (RF) is an ensemble tree-based classifier (Breiman, 2001). Trees are generated independently from each other. Trees are trained on in-the-bag samples, which are drawn randomly with replacement from the training data set (Breiman, 1996). Trees are validated on out-of-the-bag (OOB) samples, or hold out samples from the training data set, to assess model performance. The final tree is a result of the combination of the highest votes for the most accurate split thresholds and predictors. The resulting error estimate is generated from OOB samples. Any less than 500 trees in the forest may result in errors that have failed to stabilize, so 500 trees in the forest was maintained in this study (Belgiu & Drăgut, 2016; Lawrence et al., 2006). RF was tuned between the Gini and extratrees split rule. The number of predictors tested (mtry) ranged from 2 to 22 in even increments. Minimum node size remained at a value of 1.

Gradient Boosted Modeling (GBM) is an ensemble tree-based classifier (Friedman, 2001, 2002). Trees are created in series (sequentially) in a gradient boosted classifier rather than in parallel (concurrently) as they are in a random forest classifier. Boosting classifiers are

adaptable: as the trees are trained on the subsets from the training data set, the training subsets are purposefully edited to minimize the classification errors from earlier trees (Freund & Schapire, 1997; Schapire, 1990). The number of trees, tree complexity, learning rate, and minimum terminal node size can be adjusted in GBM. The number of trees ranged from 50 to 300 at increments of 50. Tree complexity ranged from 1, 2, 3, 5, and 9. Shrinkage remained at a value of 0.1, and minimum terminal node size remained at 10.

Classification and Regression Tree (CART) is one of the simplest tree-based classifiers and generally quickest to compute due to the inherently simple mathematics (Pal & Mather, 2003; Quinlan, 1986). CART is not an ensemble tree-based classifier: data is split into classes based on defined thresholds. Pruning the tree, or removing splits, may lower the accuracy of the final model, but it generally helps with extrapolating the model onto an unknown (new) data set. In this study, the complexity parameter was tuned across ten random values determined automatically through the caret package in RStudio.

Support Vector Machine (SVM) is a non-parametric machine learning classifier. This classifier uses a hyperplane boundary in multi-dimensional feature space to define samples into classes (Cortes & Vapnik, 1995; Huang et al., 2002; Mountrakis et al., 2011; Pal & Mather, 2005). Training samples that are closest to the hyperplane are support vectors used to develop the model. Other samples are ignored. The hyperplane starts as a linear boundary. If the training samples cannot be separated using a linear boundary, then the feature space is transformed to a higher dimension until the classes are separable. The transformation is the kernel trick, and the radial basis function kernel, which is non-linear, is used in this study. Samples are penalized at a cost if they are located on the incorrect side of the boundary, which generally occurs in data sets

where classes cannot be distinguished clearly. Cost was tuned exponentially over values ranging from 2^{-2} to 2^{7}. Sigma was determined automatically using the sigest function.

K-nearest neighbor (KNN) is a non-parametric, lazy learning classifier (Altman, 1992). KNN is frequently referred to as a lazy learning classifier, since the degree of membership is directly assessed for each unknown sample, but no model is trained (Everitt et al., 2006). Each unknown sample is assigned to the class with the nearest feature space based on the trends within the training data set. Low values for the number of neighbors, k, create complex decision boundaries between classes, while high values create general, less complex decision boundaries between classes. The greater the data set, the more computationally intensive this classifier tends to be. The parameter k was tuned over ten odd numbers ranging from 5 to 23 as determined automatically through the caret package in RStudio.

Model Optimization, Evaluation, and Application

Caret assembles a wide variety of classification and regression models into a standard framework using universal syntax for R (Kuhn, 2008). Auxiliary tasks such as data preparation, data splitting, variable selection, and model evaluation, are also integrated in this package. We relied on caret to train, validate, and test the classification models.

A total of 15,000 image-objects were selected randomly and equally across all of the plot images, which was 0.7% of the total data set (Figure 2.5). The image-objects were labeled and divided into training, validation, and test data sets using a stratified random sampling scheme (Table 2.6). As a general rule for large data sets, a minimum of 10,000 samples must be sampled (Congalton, 1991). There were also at least 50 samples per class, but most classes generally had between 75 to 100 samples, which is optimal for larger data sets (Congalton, 1991). We determined this to be an adequately-sized data set on which to train the model. The imbalance in

the labeled data set likely reflects the general trend of the entire data set assuming the variability is appropriately captured within 15,000 records.

Features may be highly correlated in eCognition, so these redundancies must be closely examined and eliminated during model development (Laliberte & Rango, 2011; Trimble Germany GmbH, 2019). Features above a 95% correlation threshold were removed from analysis, resulting in 22 features for analysis. Since the data set in this study is not high-dimensional, as in the endless possibilities of most genomic studies, it is not critical to remove features through more rigorous testing (Chandrashekar & Sahin, 2014).

Data were down sampled to adjust for class imbalance. Five repeats of 10-fold cross validation were applied to generate a stable estimates of model performance (Kuhn, 2008). A sampling grid was applied to most models to find the best hyperparameters.

Machine learning classifiers were evaluated primarily by overall accuracy. A confusion matrix, also referred to as an error matrix or contingency table, examines the thematic accuracy of a classified image (Congalton et al., 1983; Foody, 2002). Thematic accuracy is a broad term, which describes how accurately the image is labeled. Overall accuracy (OA) describes the agreement between the reference and classified data sets. It is calculated from the diagonal values along a confusion matrix. An accuracy greater than 0.8 is a strong model, a value between 0.4 to 0.8 is moderate, and a value less than 0.4 is poor (Congalton & Green, 2009). Cohen's Kappa accounts for the possibility of agreement between the reference and classified data sets based on chance (i.e., a classifier's tendency to vote yes or no), but it can also be misleading and irrelevant, so it is not discussed at depth in this study (Cohen, 1960; Congalton et al., 1983; Pontius & Millones, 2011). Individual class accuracy is analyzed by producer and user accuracies (Story & Congalton, 1986). Producer accuracy (PA) is relied on by the mapmaker to

describe the probability that a real-life object is classified correctly in the image. User accuracy (UA) is relied on by the map user to describe the probability that a classified object in an image matches the object in real-life.

The computational run time and intricacy of the model development process were also metrics of model evaluation. Not only are these metrics determinant of the success of the classification model, but they also determine if the model can be communicated and interpreted by decision makers and the general public. The highest performing model was applied to the total data set to classify each vegetation plot. Relative vegetation cover was extracted according to each vegetation class at each plot.

Comparing Estimates of Vegetation Cover

Vegetation cover in the field was assessed using the point frame method (Harris et al., 2021; May & Hollister, 2012; Molau & Mølgaard, 1996). A 0.75-m^2 gridded frame was aligned to permanent physical markers in each vegetation plot. The frame was leveled and positioned above the tallest plant species in the plot. 100 nodes, or sampling points, were distributed equally every 7.5 cm on the gridded frame. A wooden rod was dropped at every node. Species type, height, and live or dead status were recorded for each encounter until the ground was reached. Plots were sampled once within the same 14-day time frame annually from mid-July through early August.

Relative vegetation cover estimates were processed in Microsoft Access 2019 (Microsoft Corp.; Redmond, WA, United States). Plant species were grouped into seven broad growth forms, or vegetation classes: bryophytes, deciduous shrubs, forbs, graminoids, lichens, litter, and standing dead. Encounters of research equipment, permanent physical markers, and open water were removed from the data set prior to calculations of relative cover. Relative cover refers to

the total cover of each vegetation class divided by the total cover of all vegetation classes in a plot.

All statistical analyses were executed in RStudio v. 1.4 (RStudio, PBC; Boston, Massachusetts). Each vegetation class was tested for normality (Anderson-Darling Test) and equal variance (Levene's Test). Transformations were not helpful in alleviating issues of non-normality and heteroscedasticity. Spearman-Rank correlation tests were applied to each vegetation class at each sampling year. Shadow was summarized from the classified images but not evaluated in a correlation test.

Predicting Vegetation Abundance

Vegetation cover was assessed using the point frame method, yielding count-based measurements of abundance. Count-based abundance data are often zero-inflated and do not conform to standard distributions. Negative covariances among taxonomic groups are expected since the relative abundances must sum to one. Therefore, a growing number of studies have advocated for the use of the Dirichlet-multinomial model for analysis of over-dispersed, count-based abundance data (Clark et al., 2017; de Valpine & Harmon-Threatt, 2013).

Multinomial logistic regression with the default logit link was applied to predict the point frame estimates of all vegetation classes ($y_{t,p}$) using the image-based estimates from the corresponding plots and time points ($Obia_{t,p}$) (Equation 1; Kruschke, 2014).

Equation 1

$$y_{t,p} \sim Multinomial\ (\lambda_{t,p}\ N_{t,p})$$

The propensity ($\lambda_{t,p,v}$) of each vegetation class (v) in each plot (p) at each time point (t) was predicted from a linear model using a plot-specific intercept ($\alpha_{p,v}$), regression coefficient (β_v), and predictor ($Obia_{v,t,p}$) (Equation 2). The predictor variables were narrowed to a smaller

set. For each vegetation class, we used the corresponding image-based estimate in each plot at each time point as the predictor.

Equation 2

$$\lambda_{t,p,v} = \alpha_{p,v} + \beta_v * Obia_{v,t,p}$$

Random effects of plot were also included in the model to account for the repeated measurements over time (Equation 3). Random effects of plot describe the stability of vegetation composition over time within the plot. Plot-specific random intercepts ($\alpha_{p,v}$) were established using the grand mean intercept ($\beta_{0,v}$) and the plot-specific variations for each vegetation class (σ_v).

Equation 3

$$\alpha_{p,v} \sim Normal\ (\beta_{0,v}\ \sigma_v)$$

The expected proportions in each vegetation class for a particular plot were provided by the softmax function (Equation 4). This was the exponentiated propensity to be in a given vegetation class relative to the propensity to be in all possible classes. In other words, this function normalized all expected proportions in each vegetation class to sum to a maximum of one.

Equation 4

$$\varphi_{t,p,v} = softmax(\lambda_{t,p,v}) = \frac{\exp\ (\lambda_{t,p,v})}{\sum_{v \in c} \exp\ (\lambda_{t,p,v})}$$

Therefore, the expected number of counts in each vegetation class are determined by Equation 1, which relies on Equations 2, 3, and 4. The expected number of counts in each

vegetation class are the result of the expected proportions in each class ($\varphi_{t,p,v}$) multiplied by the total number of counts in that plot ($N_{t,p}$) recorded using the point frame.

Although the models were fit directly to the point frame counts, we used the expected by observed proportions of each vegetation group ($\varphi_{t,p,v} * N_{t,p}$) to evaluate model performance, as the null expectation is that the total number of counts in any given vegetation class will be higher when more points are sampled.

We calculated the mean absolute error (MAE) and bias of each vegetation class to evaluate model performance (Willmott & Matsuura, 2005). MAE was calculated as the average absolute difference between the predicted proportion of vegetation in each class and the observed proportion in each class (mean(absolute(predicted – observed))). Bias was calculated as the mean difference between the two proportions in each class ((mean(predicted – observed))). Bias describes whether a predicted class was over- or under-estimated by the model since bias accounts for directionality.

All models were fitted using the brms package with non-informative priors, specifying 'NA' for the reference category. In some cases, lack of a reference category can lead to non-identifiable models. Here, models showed satisfactory convergence using the narrowed set of predictor variables ($\widehat{R} < 1.1$). The narrowed set of predictor variables were relied upon in this study for the sake of simplicity and computational load.

We evaluated model performance using both in-sample and out-of-sample methods. For in-sample performance the full data set was used for both training and evaluation. For out-of-sample performance we used an end-sample holdout method to partition the data set temporally or spatially (Simonis et al., 2021).

We tested if the image-based estimates improved our ability to quantify the vegetation abundance from future years by partitioning the data temporally. We refit the model using data from 2012 to 2015. Then, we predicted the relative abundance of each vegetation class in all plots from 2018 to 2021. To evaluate the relative information gained from plot photography, we modeled the random effects of plot and fixed effects covariates as predictors.

Specifically, we predicted the relative abundance of each vegetation class (v) in each plot (p) at each time point (t) in the temporal comparison using three modifications to Equation 2. First, we calculated conditional predictions which included the random effects of plot and fixed effects covariates (Equation 2). Secondly, we calculated marginal predictions, eliminating random effects of plot, and only included the image-based information from the fixed effects covariates (Equation 5).

Equation 5

$$\lambda_{t,p,v} = \beta_{0,v} + \beta_v * Obia_{v,t,p}$$

Finally, we refit a model that only included the random effects of plot, predicting relative abundance of each vegetation class in each plot (Equation 6).

Equation 6

$$\lambda_{t,p,v} = \alpha_{p,v}$$

We also tested if image-based estimates improved our ability to quantify vegetation abundance from unseen vegetation plots by partitioning the data spatially. We refit the model using the data from twenty vegetation plots, or two-thirds of the data set. Then, we predicted the relative abundance of the vegetation classes in the remaining ten vegetation plots, or one-third of the data set. In this comparison, we included random effects in the model to account for the

repeated sampling. As there was no overlap between the vegetation plots used to fit and evaluate the model, the conditional predictions were essentially the same as the marginal predictions. Therefore, marginal predictions were not evaluated.

Results

Segmentation

In general, a greater number of objects were generated from the images of moist vegetation plots (Table 2.3). Plots that were inundated with standing water tended to produce fewer objects. The segmentation parameters generally captured the crenulated structure of lichens. Forbs and graminoids were often over-segmented. Deciduous shrubs, bryophytes, and standing water often existed in large, contiguous patches in the plot images, but these patches were also over-segmented due to the low scale parameter.

Evaluation of Machine Learning Classifiers

The random forest model performed the best with an overall accuracy of 60.5% (Table 2.7). The gradient boosted model performed slightly worse with an overall accuracy of 59.8%. The overall accuracies of the random forest and gradient boosted models were fairly even in the results from the training, validation, and test sets. The computational time was greatest for the gradient boosted model. The k-nearest neighbor model was the worst performing model with an overall accuracy of 46.6%.

Intensity was ranked as the feature with the highest relative importance (Table 2.8). The top five most important features were spectral or layer values. Texture features were ranked in the middle, while most of the geometric (shape, extent) predictors were ranked at the bottom.

In general, most classes demonstrated individual class accuracy above 50% using the random forest model (Table 2.9). It is important that bryophytes, graminoids, and litter exhibited

high user accuracies, as these three growth forms are especially abundant in the training data set (Table 2.6). Graminoids and litter exhibited high user accuracies, and bryophytes exhibited a moderate user accuracy. Deciduous shrubs and lichens exhibited very low user accuracies, in addition to low producer accuracies. Deciduous shrubs had the lowest producer (40.0%) and user accuracies (15.6%). Deciduous shrubs were most frequently confused with bryophytes (22.9% of the time), graminoids (33.5% of the time), and litter (21.6% of the time) in the classification. There was less confusion between deciduous shrubs and forbs than anticipated (3.2% of the time). Lichens also had an unusually low user accuracy (20.4%); this class was most frequently confused with litter (39.8% of the time) and standing dead (23.1% of the time) in the classification.

Shadow was rarely confused with the other classes. Shadow was most frequently confused with bryophytes (17.7% of the time) and litter (11.3% of the time). Shadows vary with light intensity and vegetation structure and were present to some degree in all images. Shadow occupied between 0.36% and 41.8% of a plot image (mean = 11.5%). The least amount of shadow overall (7.3% total) occurred in the images from 2013, while images from 2018 had the most shadow (16.7% total).

Comparing Estimates of Vegetation Cover

Deciduous shrubs and lichens were distributed sparsely among one-third to half of the vegetation plots using the point frame method of vegetation sampling (Table 2.10). Bryophytes, forbs, graminoids, litter, and standing dead were generally present in most, if not all, vegetation plots using the point frame method. All classes were detected across all plots and sampling years using the plot photography method, with the exception of forbs in years 2014 and 2018.

In general, there were positive correlations across classes and years (Table 2.11). Graminoids were associated positively across all sampling years. Graminoids also showed the highest significant positive association overall. Litter showed negative or no association, except for a low positive association in 2012. Standing dead also showed a few instances of negative association in 2013 and 2021. There was one instance of negative association in bryophyte cover in 2013.

Over all plots and years, there was a significant positive correlation between relative cover estimates from the point frame and plot photography methods (Figure 2.6). Litter and standing dead were the exceptions. There was no relationship detected for standing dead. Lower amounts of litter detected from the point frame were associated with higher amounts of litter detected using plot photography. This relationship often fell far from the 1:1 reference line. Plot photography generally underestimated the relative cover of graminoids.

Predicting Vegetation Abundance

In-sample performance of the multinomial regression model eliminated the bias and reduced MAE across all classes, thereby improving estimates of relative abundance (Table 2.12). The MAE of deciduous shrubs, graminoids, and litter improved the most. After accounting for the consistency in vegetation composition over time, that is, the random effects of plot, in the model, greater quantities of deciduous shrubs, forbs, and graminoids detected using the plot photography method were associated with greater quantities of those classes using the point frame method (Figure 2.7). This was marginally true for bryophytes, although the credible interval overlapped zero. Greater quantities of lichen, litter, and standing dead detected using the plot photography method were predictive of lower amounts of those growth forms in the corresponding point frame data.

Out-of-sample performance of the regression models over time demonstrated that image-based estimates, or fixed effects covariates, helped lower the MAE and bias in most cases, except for lichen and standing dead (Table 2.13). Lichen abundance exhibited little to no change, while standing dead abundance exhibited higher MAE and bias in the image-based model. However, some of the largest improvements in our ability to estimate abundance from this model came from random effects of plot, especially in deciduous shrubs and graminoids. In general, the optimal model resulted from the conditional predictions, which included the fixed effects covariates and random effects of plot. Although there was not a huge difference in predictive performance between the three models, all models notably improved the estimates of vegetation abundance over direct substitution.

Out-of-sample performance of the regression models over space demonstrated that the MAE and bias was lowered across all vegetation classes, except for lichen abundance (Table 2.14). Lichen abundance exhibited a lower MAE and bias using direct substitution. Bryophyte and forb abundance also exhibited little to no change in MAE and bias. Although there was not a large difference in predictive performance between the two models, the conditional predictions improved the estimates of vegetation abundance over direct substitution.

Discussion

Segmentation

Over-segmentation was a likely outcome for most vegetation classes in the images, since tundra vegetation is heterogeneous at a fine-scale, and it varies in structure, quantity, and color. It was impossible to designate segmentation parameters that perfectly segmented each feature in an image into objects. Although a larger scale parameter outlined the contiguous patches of deciduous shrubs, bryophytes, and standing water with fewer instances of over-segmentation, it

also failed to capture the outline of the lichens. A larger scale parameter generally resulted in more under-segmented objects, as the boundaries between the deciduous shrubs and forbs blurred.

Although it is usually possible to remedy over-segmentation by merging smaller objects into larger objects in subsequent steps, there was no clear rule to institute regarding color, shape, or texture (Laliberte et al., 2007). The three-band images in this study are limited by their available spectral information, so color, or spectral information, cannot be relied upon in later steps to merge objects and facilitate automatic classification (Lang, 2008). There is likely never a perfect setting for segmentation, so it is better to over-segment the features in an image and merge them in subsequent steps (Witharana & Civco, 2014).

In order to make GEOBIA more reproducible and robust, recent studies have suggested that the accuracy of segmentation is assessed through a formal accuracy assessment (Ma et al., 2015; Ye et al., 2018). Formal accuracy assessments often require manual delineation of an independent set of reference polygons. The reference polygons are compared to the polygons produced through the segmentation algorithms. Not only can the accuracy assessment vary according to the user, but it is often time-consuming, especially in images with great diversity or heterogeneity. Although the accuracy of the segmentation is an important consideration, a formal accuracy assessment remains an area of active, controversial research as not all researchers argue that it is necessary (Blaschke et al., 2014; Radoux & Bogaert, 2017). This assessment can be considered for future studies.

Importance Values

Importance values should be interpreted with care, since highly correlated, continuous predictors may be given higher values erroneously (Strohbl et al., 2007). eCognition produces

features that can be highly correlated (Trimble Germany GmbH, 2019). Therefore, our analysis discusses feature importance in broad terms, and the importance values were not closely analyzed in this study (Maxwell et al., 2018).

In general, spectral features were the most influential predictors in the random forest classification. Spectral features measure the fundamental properties of the objects, while texture measures the spatial relationships of pixels within an object. These features are more likely to be independent and complement each other (Kim et al., 2011; Laliberte & Rango, 2008). Shape features had the least impact on the random forest classification, which validates the theory that shape features may become more critical at greater scales (Ma et al., 2015).

Hue, saturation, and intensity (value), or HSV, has been shown to improve the segmentation or classification of digital images (Chen et al., 2010; Laliberte et al., 2007; Laliberte & Rango, 2011). HSV results from a transformation of the red, green, blue color space, which are highly correlated bands and tend to provide redundant information (Jensen, 2005). In our preliminary analysis, HSV did not improve the segmentation of the plot photographs. However, hue and intensity were both among the top five predictors of the classification. Intensity showed significant, distinctive contrast between vegetation classes at a cursory glance, especially in comparison to other spectral, textural, or geometric features. In general, shadow and standing dead were on opposite ends of the spectrum for intensity values.

Green ratio (rG), green-red vegetation index (GRVI), and greenness excess index (GEI) were also among the top five predictors. These indices measure similar information regarding the phenology and vegetation composition from the digital images. Green-Red Vegetation Index (GRVI) has performed comparably to the Normalized Difference Vegetation Index (NDVI) at the plot level; thus, GRVI may often be used interchangeably with NDVI, usually at the expense

of lower overall accuracy (Anderson et al., 2016; Marcial-Pablo et al., 2019; Motohka et al., 2010). It is clear that the green ratio (rG), green-red vegetation index (GRVI), and greenness excess index (GEI) offer important, discriminatory information on the vegetation classes based on the high importance values. Perhaps, these RGB-based indices may be used as proxies to NIR-based indices when standard, low-cost cameras are used to capture photographic information from vegetation plots.

Shadow

In general, the images with the greatest amounts of shadow also had the greatest amounts of inundation. Inundated plots exhibited a few, dominant species, and some of which were not visible in the image depending on the level of inundation in the plot. Moist vegetation plots tend to exhibit greater species diversity than inundated vegetation plots (van der Welle et al., 2003). Since any visible water was masked and removed prior to classification, the relative cover estimates of shadow tended to be inflated in inundated plots. For example, plot H3 recorded the lowest overall measurement for shadow cover in 2014 (0.36%). Plot H3 also recorded two of the highest measurements for overall shadow cover in 2018 (41.2%) and 2019 (41.8%), which were also years with a large amount of inundation.

Shadow has been shown to confuse image analysis and lower classification accuracy (Laliberte et al., 2007). In this study, very little class confusion occurred with shadow overall, except for some overlap with bryophyte and litter cover. Bryophytes vary in color and texture, especially in response to moisture level (May et al., 2018). Inundated bryophytes tend to darken in color, creating a more complicated task for the machine learning classifier to distinguish an inundated bryophyte from shadow. Litter appeared not to have distinctive color, shape, or size, since it can vary depending on the timing of the degradation and the vegetation species. Litter

tends to be darker in color due to degradation, so the minimal class confusion with shadow was also justified. It may be possible to improve the distinction between shadow, bryophytes, and litter with additional training samples.

We expected to encounter shadow in the plot photographs as a result of the constraints of plot photography. The observer can change their viewpoint easily and illuminate the plot if shadow is present during the point frame method of sampling. The reverse is not true of plot photography, where shadow is a component of every image to varying degrees. Even in ideal, overcast sampling conditions, shadows remained visible in the middle and lower canopies in the digital images. It is difficult to achieve standardized lighting conditions in the Arctic, where fieldwork is limited to a short growing season and low sun angles (Stow et al., 2004). Blocking direct sunlight in an attempt to standardize lighting conditions may be possible with additional equipment or a second field technician, but shadow cannot be eliminated from the images, only minimized (Chen et al., 2010; King et al., 2020; Laliberte et al., 2007; Luscier et al., 2006).

Comparing and Predicting Estimates of Vegetation Cover and Abundance

If the point frame and plot photography sampling methods recorded similar species composition within the plots, then there should not be a large difference between the relative cover estimates between the data sets. A difference might indicate that the plot photography method is over- or under-estimating the relative cover of one or more classes due to the constraints of the sampling methodology or parameters in the image analysis. A difference might also indicate that a larger labeled data set is necessary to train, validate, and test the random forest classifier, since the variability of the entire data set is not captured in data set. The difference could also be a result of the error inherent in the random forest classifier, which has an

overall accuracy of 60.5%. Some class confusion is inevitable, which may result in under- or over-estimates of relative cover.

There is a large discrepancy in the relative cover estimates of graminoids and standing dead from the point frame and plot photography. Graminoids and standing dead tend to be upright, tall, and narrow in structure, though they differ in color. Plot photography appears to under-estimate graminoid and standing dead cover since the topmost view of the canopy is visible only, which limits the available area that can be analyzed in the photograph.

Deciduous shrubs and lichens had the greatest individual classification error (Table 2.8). Perhaps more instances of lichens were needed to train the model, given the wide variety of color, shape, and species at Utqiaġvik. Likewise, deciduous shrubs were often under-segmented and confused with vegetation classes that exhibited similar size and shape. There was little overlap between deciduous shrubs and forbs, suggesting that spectral similarities between the two vegetation classes were not strong enough to confuse the two more often. It is difficult to rely on the classification of deciduous shrubs and lichens, since the producer and user accuracies were so low.

Standing dead is a version of dead plant material, but this class has distinctive characteristics which separate it from litter. Standing dead is tall, narrow and reflective. Litter can be difficult to classify automatically, given that this class encompasses all dead plant material that has fallen to the bottom of the canopy. Litter may appear round, brown and curled, as the leaves of the dominant forb, *Petasites frigidus*, do after senescence, or gray and formless as plant material degrades over time. Not only is it difficult to establish a repeatable classification pattern for the machine learning classifiers, but the boundaries of this class may also be difficult to define during the segmentation procedure. Class confusion occurred between

litter and all other vegetation classes, but the classification of litter ultimately performed well with the highest overall user accuracy (81.5%). Perhaps the results of the classification could be improved had the focus been on living vegetation only.

Plot photography is a reliable method for recognizing and classifying graminoids, which are the most abundant vegetation class at Utqiaġvik according to the cover estimates from the point frame. Graminoids exhibited an acceptably high user accuracy in the classification, and point frame and image-based estimates of graminoid abundance were also strongly correlated across all sampling years; therefore, the image-based estimates of graminoid cover are reliable. If graminoids are the primary focus of the research study, then this technique can be confidently, and widely, adopted in the Arctic.

However, this technique falls short in estimating the cover and abundance of deciduous shrubs and lichens. Deciduous shrubs and lichens exhibited very low user accuracies in the classification, rendering these image-based estimates of cover as unreliable. If deciduous shrubs and lichens are the focus of the research study, then researchers should not rely on this technique. Although the practicality of plot photography for Arctic researchers is limited, it is not rejected. The object-based approach failed to recognize and classify deciduous shrubs and lichens at a satisfactory level of accuracy in this study, but plot photographs can be analyzed retroactively. Image analysis and deep learning approaches may improve over time and allow for accurate classification of these two vegetation classes, provided that the images are available for analysis.

Given the amount of class confusion in the random forest classifier, false positives and negatives exist in the estimates of relative cover for each vegetation class. All classes, except for forbs, were detected across all sampling years using plot photography (Table 2.10). We assume that deciduous shrubs and lichens were over-estimated in the plot photographs, given that these

classes were only present in half or less of the vegetation plots annually using the point frame method of sampling. This trend is also visible in the direct substitution of the regression model (Figure 2.6). It appears that the point frame method of sampling captures the vegetation composition of each plot more accurately than the plot photography method of sampling.

All regression models, including the temporal and spatial comparisons, performed optimally in comparison to direct substitution. The substantial decreases in MAE and bias are a result of incorporating two additional sources of information: the fixed effects covariates, which are developed from the image-based estimates of abundance, and random effects of plot. The image-based estimates often improved the MAE and bias minimally, whereas most of the improvements originated from the plot identity, or plot-specific information.

Plot photography is a quicker field methodology than point frame sampling. In this study we tested our approach using the data from thirty vegetation plots in the ARCSS grid. This subset of thirty vegetation plots is sampled once annually using the point frame method and up to six times seasonally using the plot photography method. In contrast, the ninety-eight vegetation plots in the ARCSS grid are sampled once every five years using the point frame method, since this requires a huge investment in terms of field crew, time, energy, and logistics. The performance of the holdout space model on the thirty vegetation plots strongly suggests that plot photography could be extended to the remaining sixty-five vegetation plots with accurate results, since this sampling method accurately observes compositional shifts in vegetation abundance.

In other words, when point frame sampling is applied to a subset of the vegetation plots in the ARCSS grid, plot photography can be applied to the remaining the vegetation plots in the ARCSS grid to provide information on the spatial composition of all the vegetation plots when constrained by time and resources. More broadly, if the model were trained on a subset of plots

and performed well, larger areas could be surveyed using plot photographs and analyzed to describe spatial gradients in vegetation composition. Greater spatial coverage could be achieved using plot photography than the point frame method.

While unbiased estimates of relative cover were generated using plot photography, the estimates were not precise on a per-plot level and lacked sufficient accuracy to capture more subtle shifts in vegetation over time within individual plots. Plot photography can be relied upon to accurately measure the plot average as long as the MAE and bias is low in the regression models. Improvements to the object-based approach may improve the accuracy of the image-based estimates, thereby improving how well the estimates predict relative abundance on a per-plot level. Thus, plot photography is useful, but an imperfect, method of sampling. It may add more information spatially, where there is large compositional turnover, than temporally, where the abundance changes are more subtle. However, estimates of relative cover from the plot photography method are constrained by historical estimates of vegetation abundance from the point frame method.

Sources of Error

Uncertainties accumulated throughout the methodology, resulting in positional, interpretation, and mis-classification errors. Positional errors resulted from the error inherent in the DGPS coordinates ($\pm$ 1 to 5 cm) and the georeferencing procedure ($\pm$ 0.2 to 11.5 cm). Segmentation parameters directly impact the results of the classification (Drăguţ et al., 2014; Kim et al., 2011; Smith, 2010). In this study, the user-dependent segmentation parameters affected the shape and size of objects, therefore affecting the quality and number of objects generated. The manual labeling procedure was executed by an expert with substantial field experience and skill in Arctic plant identification. Therefore, interpretation errors were inevitable

but consistent across the data set. Interpretation errors were impossible to quantify after the procedure, and these may weaken the quality of the data set. There were inevitable mis-classification errors since the overall accuracy of the random forest classification was 60.5%.

We recommend that positional, interpretation, and mis-classification errors for the plot photography method are dealt with in the following ways. Positional errors can be minimized, but not eliminated. If the RMSE exceeds a pre-defined threshold during the georeferencing procedure, then the image should be substituted for a nearby sampling date if available. Interpretation errors could be flagged during the labeling procedure if multiple experts labeled then compared their responses (King et al., 2020). Accurate segmentation provides a better chance of an accurate classification. The segmentation parameters can be optimized using a segmentation accuracy assessment (Ma et al., 2015; Ye et al., 2018). Perhaps, a more rigorous series of rules can be included to refine the primitive image objects in the early steps of the object-based approach. Image analysis was limited by both the available data set and tools of analysis, and we expect that it will be modified and improved over time.

The errors in the point frame sampling method were fewer than the plot photography method but still present in the form of positional, interpretation, and mis-classification errors. Positional error was minimal due to the leveling and alignment of the point frame to permanent tags in the vegetation plot. Point frame sampling can be intensive and tiring, so interpretation error was possible due to the exhaustion of the field technician (Bennett et al., 2000; Vittoz & Guisan, 2007). Tall vegetation can shift with the wind, so the frequency of contact hits may be skewed during windier conditions (Gorrod & Keith, 2009). A mis-classification can result when the field technician records incorrect information about the vegetation composition of the plot. Even so, these errors are generally minimal and usually rectified in post-processing of the data.

There is strong evidence that vegetation composition, cover, and abundance at the plot level is monitored accurately using this method of sampling (Mamet et al., 2016).

The comparison between the relative cover estimates from the point frame and plot photography method of sampling was not direct. Each biomass encounter, or contact, was recorded from the upper, middle, and lower levels of the plant canopy using the point frame sampling method. Vegetation cover was assumed for each cell on the sampling grid based on the number of contact hits within each cell. In contrast, the plot photographs in this study only recorded the topmost visible layer. Therefore, the point density from the point frame sampling method may not reflect the relative cover that was obtained through image analysis (Chen et al., 2010). Every visible object was quantified in image analysis, because this method was not constrained by a grid with 100 contact points. This introduced a degree of separation between the comparisons, because the corresponding spatial resolution and level of precision was different.

Change in relative cover must be interpreted carefully for both sampling methods (Chen et al., 2010; Michel et al., 2010). A plant can be hidden beneath the topmost visible layer, rendering it invisible to the camera. Additionally, a plant can grow at a different height, angle, or location every year. Therefore, rarer vegetation classes, like deciduous shrubs, may be detected using the point frame method during some years but not all (Table 2.10). The differences in sampling techniques between the point frame and plot photography methods may explain the weaker correlations between the relative cover estimates of some of the vegetation classes (Table 2.11).

Furthermore, the removal of standing water from the plot images might explain the weaker correlations in bryophytes, litter, or standing dead. The presence of bryophytes can be detected in inundated plots using the point frame. However, the reverse is not true: standing

water can obscure bryophyte cover in plot images. In this study, all standing water was removed from the images to maintain an objective, rule-based protocol, even if vegetation was visible underneath the surface of the water. The relative cover estimates of bryophytes, litter, or standing dead might suffer from greater mismatch in inundated plots, which may also help explain the weak or negative correlations for some sampling years.

Image Processing Automation

Automatic identification and removal of water from the plot images is preferred to manual digitization and removal. In images with overcast lighting conditions, water was identified and removed more easily than in images with direct or scattered sunlight. In images with direct or scattered sunlight, a greater number of small objects were created to outline the reflections from direct sunlight, therefore water was more time-consuming to remove. In general, manual removal of water from one image required at least forty minutes to complete.

The near-infrared (NIR) band would improve the efficiency of our semi-automatic image processing routine. We could calculate Normalized Difference Water Index (NDWI), a water-specific index, which has been used to identify and remove standing water from remotely sensed images (McFeeters, 1996; Zhou et al., 2017). The NIR band would also permit us to calculate Normalized Difference Vegetation Index (NDVI), which can assist in distinguishing types of vegetation cover and is a widely used metric to monitor vegetation dynamics across the Arctic (Epstein et al., 2013; Pettorelli, 2013). The band combinations that we can use are limited to the visible electromagnetic spectrum and contain a finite amount of information. While we can maintain the analysis of historic photographs with standard red, green, and blue bands, we can also benefit from technological improvements in our equipment, which might allow us to access more information across the electromagnetic spectrum, thereby improving our classification.

We encountered some limitations with the eCognition software, so our approach to image analysis was not fully contained within it. eCognition is a black box. It was not possible to understand the internal steps of the rule set since the code is proprietary with few resources available to explain it. The classification models also lacked proper transparency to validate the underlying statistics. There was no functionality to allow for the random selection of objects in eCognition, especially at a scale that encompasses all of the images in this study. We also found that the processing time to export the feature list for each image was long and computationally intensive. We calculated the spectral indices outside of eCognition to reduce the processing time for each image. The limitations of eCognition were remedied by RStudio, thus the workflow transitions between the two platforms frequently (Figure 2.3).

Moving forward, our aim is to increase the repeatability, robustness, and accuracy of the image analysis in this study. If possible, we seek to automate the process by lowering the number of platforms and transferring our approach to RStudio. It is critical that this process meets expectations from technical, scientific, and practical perspectives. Workflows and conceptualizations must be shared to make this approach transferable and more robust, and that is still lacking amongst the remote sensing community (Arvor et al., 2013; Witharana et al., 2021).

Recommendations for Future Studies

A ranking system should be established for the digital images. The seasonal timing of the photography can be inconsistent. Plot images were acquired on a more frequent basis during some sampling years, but not all. In order to provide evidence of why some digital images were analyzed or substituted, each image should be ranked based on quality (resolution, camera angle, plot within view, lighting conditions, blur), quantity (missing images), and proximity to the point

frame sampling date. The images in this study were examined and selected based on the number of available images near the peak season. The quality, quantity, and proximity were considered, but the images were not ranked prior to digital analysis. We also recommend that if the RMSE exceeds a pre-defined threshold in the georeferencing procedure, then the image should be replaced if another is available.

In our preliminary analysis, we applied a color balancing tool in ArcGIS Desktop to normalize spectral variations between the images, given that the lighting conditions were not the same between sampling years. This tool is error-prone and depreciated, and spatial analysts have migrated towards using ArcGIS Pro since the platform release (Menon, 2014). Our preliminary results were permanent and showed minimal improvement, even on plots exhibiting large spectral variation due to the harshness of direct sunlight. We are unaware of a tool to normalize spectral variations across plot-level images in ArcGIS Pro. Perhaps, our results would improve if normalization or correction were applied across images, allowing for a more accurate classification and comparison across time.

A larger labeled data set might improve the results of this study. Recent studies suggested that 1,000 samples per class is optimal for training the neural network classification of large data sets (Maxwell et al., 2018; Ramezan et al., 2021). This new guideline would require a data set of at least 8,000 objects to classify the eight classes of interest in this study. Given the known imbalance in the data set in this study, a larger data set is necessary. An additional 5,000 records added to the 15,000 labeled records could be added to potentially meet the suggestion of 1,000 samples per class. A larger data set might capture more spatial variability, in addition to allowing for rigorous feature selection and feature validation during model development (Maxwell et al., 2018; Ramezan et al., 2021).

Directionality in texture features is not widely adopted in object-based image analysis. In this study, texture features were calculated from all bands in all directions (0°, 45°, 90°, 135°), and therefore show directional invariance, since this is the average of four directions. Texture can add information where spectral layers may offer limited information, such as differentiating between visibly distinct vegetation classes (water, vegetation, and soil) in high resolution images (Johansen et al., 2007; Kim et al., 2011). Herbaceous vegetation in wetlands may not benefit from texture at a coarser resolution (Dronova et al., 2012, 2015; Nie & Li, 2011). Yet, most published studies rely on directional invariance in texture, since there is a high computational cost associated with texture calculation (Benz et al., 2004). A specific direction (0°, 45°, 90°, 135°) might be a more informative in identifying the texture of vegetation classes, resulting in a more accurate classification.

Additional machine learning classifiers may be investigated, perhaps leading to a classification model with a higher overall accuracy. Artificial neural networks could be explored. Neural networks require large, uncorrelated data sets and an in-depth understanding of the mechanism underpinning the classifier to obtain concrete, reliable results (Maxwell et al., 2018; Olden et al., 2008; Rawat & Wang, 2017). Neural networks can be easily over- or under-trained, resulting in spurious, noisy, and non-reproducible results (Olden et al., 2008; Rawat & Wang, 2017). Although we applied other classifiers to this data set in our preliminary analysis, the models either produced poor results or failed, since they did not meet the base assumptions of a gaussian distribution, or possessed parametric training data, binary classes, categorical predictors, or overwhelming computational demands (Kuhn, 2008). Those models were: Bayesian, boosting, discriminant, prototyping, and support vector machines (with different

kernels). Ensemble-based classification models, or a combination of machine learning classifiers, may also lead to more powerful classification model, but these were not tested in this study.

Conclusion

An object-based approach was applied to high resolution, plot photographs with three spectral bands (red, green, blue) to estimate the relative cover of eight vegetation classes. The random forest classifier performed better than the other machine learning classifiers (gradient boosted model, classification and regression tree, support vector machine, k-nearest neighbor) with an overall accuracy of 60.5%. Although the random forest classifier required more processing time, the overall accuracy was substantially higher than most of the other classifiers. The gradient boosted classifier performed similarly, but at the expense of a greater computational load and processing time, which made this classifier less desirable for future use. Random forest is the optimal machine learning classifier for the classification of near surface, high resolution digital images of Arctic vegetation.

The object-based approach accurately classified some vegetation classes, but not all. Bryophytes, forbs, graminoids, litter, shadow, and standing dead were classified accurately using the random forest classifier. Deciduous shrubs and lichens were not classified accurately using the random forest classifier. Perhaps, a larger training data set or improvements to the shape or size of objects might improve the individual class accuracies of the problematic vegetation classes, thereby improving the overall accuracy of the classification. We recommend including a comprehensive accuracy assessment for segmentation parameters in future studies (Ma et al., 2015; Ye et al., 2018).

RGB-based spectral indices and layer values were the most influential in the classification. Geometric and textural features were less influential in the random forest

classification; that is, these features complemented existing spectral information to a limited degree. Our study reinforces that valuable information can be gained through standard imagery, which only consists of red, green, and blue spectral bands. That said, improvements to our digital cameras could improve our semi-automatic image analysis routine and classification results in the future if we could access more of the electromagnetic spectrum, notably the NIR band.

Spearman-Rank correlations revealed that the relative cover estimates of graminoids were closely linked between the point frame and plot photography methods of sampling through all sampling years. Litter and standing dead or more generally, dead plant material, were more problematic. Litter and standing dead often showed negative associations between the relative cover estimates from the point frame and plot photography methods of sampling. Most likely, this can be attributed to the limitations of plot photography. Litter varies in appearance; therefore, the classifiers may have more difficulty in separating this class from the other vegetation classes due to the lack of spectral, geometric, or textural pattern. Standing dead is generally upright and narrow, therefore there is less surface area to analyze from a two-dimensional digital image. Other classes, which are wider and can be captured in an image more easily from a vertical viewpoint, are likely to be analyzed more accurately.

After our investigation into the multinomial regression models, we discovered that the estimates of relative cover from plot photographs were not precise on a per-plot level. The plot average was accurate, provided that the bias and MAE were also low in the models. The object-based approach to analyzing the plot photographs is useful, but it requires improvement before the estimates of relative cover on a per-plot basis can be trusted for a finer scale analysis. Plot photography is a useful, but imperfect, method of sampling. It may add more information

spatially, where there is large compositional turnover, than temporally, where the abundance changes are more subtle.

A photographic record can be revisited and re-analyzed in the future, and it is versatile, quick, and cost-effective. An object-based approach to image analysis provides reliable, although limited, information from fine-scale digital images of tundra vegetation. Information from near-surface digital photographs can complement existing field observations. We recommend using our near-surface plot photographs to advance our understanding of the link between ground-based and satellite-based observations without allocating resources towards traditional, intensive field surveys across the Arctic tundra. Both techniques are expected to maximize time, funding, and technology in order to monitor terrestrial change in the Arctic.

Acknowledgements

Field logistics were provided by UIC Science. Funding was provided by the Arctic Sciences Division of the National Science Foundation (awards: 0856516, 1432277, 1504224, 1836839). We thank the current and former field technicians of the Arctic Ecology Program (Grand Valley State University) and Systems Ecology Lab (University of Texas at El Paso) for assistance with data collection. We also thank Ryan Cody and Mariana Mora (University of Texas at El Paso) and Katlyn Betway-May (Grand Valley State University) for providing clean data sets.

References

Allen, M. R., Dube, O. P., Solecki, W., Aragón-Durand, F., Cramer, W., Humphreys, S., Kainuma, M., Kala, J., Mahowald, N., Mulugetta, Y., Perez, R., Wairiu, M., & Zickfeld, K. (2018). IPCC 2018: Framing and Context. In V. Masson-Delmotte, P. Zhai, H.-O. Pörtner, D. Roberts, J. Skea, P. R. Shukla, A. Pirani, W. Moufouma-Okia, C. Péan, R. Pidcock, S. Connors, J. B. R. Matthews, Y. Chen, X. Zhou, M. I. Gomis, E. Lonnoy, T. Maycock, M. Tignor, & T. Waterfield (Eds.), *Global Warming of 1.5°C. An IPCC Special Report on the impacts of global warming of 1.5°C above pre-industrial levels and related global greenhouse gas emission pathways, in the context of strengthening the global response to the threat of climate change*.

Altman, N. S. (1992). An introduction to kernel and nearest-neighbor nonparametric regression. *The American Statistician*, *46*(3), 175–185. https://doi.org/10.1080/00031305.1992.10475879

Anderson, H. B., Nilsen, L., Tommervik, H., Rune Karlsen, S., Nagai, S., & Cooper, E. J. (2016). Using ordinary digital cameras in place of near-infrared sensors to derive vegetation indices for phenology studies of high Arctic vegetation. *Remote Sens.*, *8*(847), 1–17.

Arvor, D., Durieux, L., Andrés, S., & Laporte, M. A. (2013). Advances in Geographic Object-Based Image Analysis with ontologies: A review of main contributions and limitations from a remote sensing perspective. *ISPRS Journal of Photogrammetry and Remote Sensing*, *82*, 125–137. https://doi.org/10.1016/j.isprsjprs.2013.05.003

Baatz, M., & Schaape, A. (2000). A multiresolution segmentation: an optimization approach for high quality multi-scale image segmentation. In J. Strobl (Ed.), *Proceedings of Angewandte*

Geographische Informations-verarbeitung XII (pp. 12–23).

Beamish, A. L., Nijland, W., Edwards, M., Coops, N. C., & Henry, G. H. R. (2016). Phenology and vegetation change measurements from true colour digital photography in high Arctic tundra. *Arctic Science*, *2*, 33–49. https://doi.org/10.1139/as-2014-0003

Belgiu, M., & Drăgut, L. (2016). Random forest in remote sensing: A review of applications and future directions. *ISPRS Journal of Photogrammetry and Remote Sensing*, *114*, 24–31. https://doi.org/10.1016/j.isprsjprs.2016.01.011

Bennett, L. T., Judd, T. S., & Adams, M. A. (2000). Close-range vertical photography for measuring cover changes in perennial grasslands. *J. Range Manage.*, *53*(6), 634–641.

Benz, U. C., Hofmann, P., Willhauck, G., Lingenfelder, I., & Heynen, M. (2004). Multi-resolution, object-oriented fuzzy analysis of remote sensing data for GIS-ready information. *ISPRS J. Photogramm. Remote Sens.*, *58*, 239–258.

Bhatt, U. S., Walker, D. A., Raynolds, M. K., Bieniek, P. A., Epstein, H. E., Comiso, J. C., Pinzon, J. E., Tucker, C. J., & Polyakov, I. V. (2013). Recent declines in warming and vegetation greening trends over pan-Arctic tundra. *Remote Sens.*, *5*(9), 4229–4254. https://doi.org/10.3390/rs5094229

Blaschke, T., Hay, G. J., Kelly, M., Lang, S., Hofmann, P., Addink, E., Queiroz Feitosa, R., van der Meer, F., van der Werff, H., van Coillie, F., & Tiede, D. (2014). Geographic Object-Based Image Analysis - Towards a new paradigm. *ISPRS J. Photogramm.*, *87*, 180–191.

Booth, D. T., Cox, S. E., Fifield, C., Phillips, M., & Willlamson, N. (2005). Image analysis compared with other methods for measuring ground cover. *Arid Land Research and*

Management, *19*(2), 91–100. https://doi.org/10.1080/15324980590916486

Box, J. E., Colgan, W. T., Christensen, T. R., Schmidt, N. M., Lund, M., Parmentier, F.-J. W., Brown, R., Bhatt, U. S., Euskirchen, E. S., Romanovsky, V. E., Walsh, J. E., Overland, J. E., Wang, M., Corell, R. W., Meier, W. N., Wouters, B., Mernild, S., Mård, J., Pawlak, J., & Olsen, M. S. (2019). Key indicators of Arctic climate change: 1971–2017. *Environ. Res. Lett.*, *14*, 045010. https://doi.org/10.1088/1748-9326/aafc1b

Breiman, L. (1996). Bagging predictors. *Mach. Learn.*, *24*, 123–140.

Breiman, L. (2001). Random Forest. *Machine Learning*, *45*, 5–32.

Brown, J., Hinkel, K. M., & Nelson, F. E. (2000). The Circumpolar Active Layer Monitoring (CALM) program: Research designs and initial results. *Polar Geogr.*, *24*(3), 165–258.

Brown, J., Miller, P. C., Tieszen, L. L., & Bunnell, F. L. (Eds.). (1980). *An arctic ecosystem: the coastal tundra at Barrow, Alaska*. Dowden, Hutchinson, & Ross, Inc.

Chandrashekar, G., & Sahin, F. (2014). A survey on feature selection methods. *Computers & Electrical Engineering*, *40*(1), 16–28.

Chapin, F. S., Sturm, M., Serreze, M. C., McFadden, J. P., Key, J. R., Lloyd, A. H., McGuire, A. D., Rupp, T. S., Lynch, A. H., Schimel, J. P., Beringer, J., Chapman, W. L., Epstein, H. E., Euskirchen, E. S., Hinzman, L. D., Jia, G., Ping, C. L., Tape, K. D., Thompson, C. D. C., … Welker, J. . (2005). Role of land-surface changes in Arctic summer warming. *Science*, *310*(5748), 657–660. https://doi.org/10.1126/science.1117368

Chen, G., Weng, Q., Hay, G. J., & He, Y. (2018). Geographic object-based image analysis (GEOBIA): emerging trends and future opportunities. *GIScience and Remote Sensing*,

55(2), 159–182. https://doi.org/10.1080/15481603.2018.1426092

Chen, Z., Chen, E. W., Leblanc, S. G., Henry, G. H. R., & Chen, W. (2010). Digital photograph analysis for measuring percent plant cover in the Arctic. *Arctic*, *63*(3), 315–326.

Clark, J. S., Nemergut, D., Seyednasrollah, B., Turner, P. J., & Zhang, S. (2017). Generalized joint attribute modeling for biodiversity analysis: median-zero, multivariate, multifarious data. *Ecol. Monogr.*, *87*, 34–56. https://doi.org/10.1002/ecm.1241

Clarke, T. A., & Fryer, J. G. (1998). The development of camera calibration methods and models. *Photogrammetric Record*, *16*(91), 51–66.

Cohen, J. (1960). A coefficient of agreement for nominal scales. *Educational and Psychological Measurement*, *20*(1), 37–40.

Congalton, R. G. (1991). A review of assessing the accuracy of classifications of remotely sensed data. *Remote Sensing of Environment*, *37*(1), 35–46. https://doi.org/10.1016/0034-4257(91)90048-B

Congalton, R. G., & Green, K. (2009). *Assessing the Accuracy of Remotely Sensed Data: Principles and Practices* (2nd Editio). Lewis Publishers.

Congalton, R. G., Oderwald, R. G., & Mead, R. A. (1983). Assessing Landsat classification accuracy using discrete multivariate analysis statistical techniques. *Photogrammetric Engineering and Remote Sensing*, *49*, 1671–1678.

Cortes, C., & Vapnik, V. (1995). Support-vector networks. *Machine Learning*, *20*, 273–297. https://doi.org/10.1007/BF00994018.

de Jong, R., de Bruin, S., de Wit, A., Schaepman, M. E., & Dent, D. L. (2011). Analysis of

monotonic greening and browning trends from global NDVI time-series. *Remote Sens. Environ.*, *115*, 692–702.

de Valpine, P., & Harmon-Threatt, A. N. (2013). General models for resource use or other compositional count data using the Dirichlet-multinomial distribution. *Ecology*, *94*(12), 2678–2687. https://doi.org/10.1890/12-0416.1

Drăguţ, L., Csillik, O., Eisank, C., & Tiede, D. (2014). Automated parameterisation for multi-scale image segmentation on multiple layers. *ISPRS Journal of Photogrammetry and Remote Sensing*, *88*, 119–127. https://doi.org/10.1016/j.isprsjprs.2013.11.018

Dronova, I. (2015). Object-based image analysis in wetland research: a review. *Remote Sens.*, *7*, 6380–6413.

Dronova, I., Gong, P., Clinton, N. E., Wang, L., Fu, W., Qi, S., & Liu, Y. (2012). Landscape analysis of wetland plant functional types: The effects of image segmentation scale, vegetation classes and classification methods. *Remote Sens. Environ.*, *127*, 357–369.

Dronova, I., Gong, P., Wang, L., & Zhong, L. (2015). Mapping dynamic cover types in a large seasonally floodedwetland using extended principal component analysis and object-based classification. *Remote Sens. Environ.*, *158*, 193–206.

Epstein, H. E., Myers-Smith, I. H., & Walker, D. A. (2013). Recent dynamics of Arctic and sub-Arctic vegetation. *Environ. Res. Lett.*, *8*, 1–6.

Everitt, B. S., Laundau, S., Leese, M., & Stahl, D. (2006). *Miscellaneous Cluster Methods in Cluster Analysis* (5th ed.). John Wiley & Sons, Ltd.

Foody, G. M. (2002). Status of land cover classification accuracy assessment. *Remote Sens.*

Environ., *80*, 185–201.

Fraser, R. H., Olthof, I., Lantz, T. C., & Schmitt, C. (2016). UAV photogrammetry for mapping vegetation in the low-Arctic. *Arctic Science*, *2*, 79–102.

Freund, Y., & Schapire, R. E. (1997). A decision-theoretic generalization of on-line learning and an application to boosting. *J. Comput. Syst. Sci.*, *55*(119–139).

Friedman, J. H. (2001). Greedy function approximation: A gradient boosting machine. *Ann. Statist.*, *29*(5), 1189–1232. https://doi.org/10.1214/aos/1013203451

Friedman, J. H. (2002). Stochastic gradient boosting. *Computational Statistics & Data Analysis*, *38*(4), 367–378. https://doi.org/10.1016/S0167-9473(01)00065-2

Gitelson, A. A., Kaufman, Y. J., Stark, R., & Rundquist, D. (2002). Novel algorithms for remote estimation of vegetation fraction. *Remote Sens.*, *80*, 76–87.

Gorrod, E. J., & Keith, D. A. (2009). Observer variation in field assessments of vegetation condition: implications for biodiversity conservation. *Ecol. Manag. Restor.*, *10*, 31–40. https://doi.org/10.1111/j.1442-8903.2009.00437.x

Guay, K. C., Beck, P. S. A., Berner, L. T., Goetz, S. J., Baccini, A., & Buermann, W. (2014). Vegetation productivity patterns at high northern latitudes: a multi-sensor satellite data assessment. *Glob Chang Biol*, *20*, 3147–3158.

Haralick, R. (1979). Statistical and structural approaches to texture. *Proceedings of the IEEE*, *67*(5), 786–804.

Haralick, R. M., Shanmugan, K., & Dinstein, I. (1973). Textural features for image classification. *IEEE Transactions on Systems, Man and Cybernetics*, *SMC-3*(6), 610–621.

Harris, J. A., Hollister, R. D., Botting, T. F., Tweedie, C. E., Betway, K. R., May, J. L., Barrett, R. T. S., Leibig, J. A., Christoffersen, H. L., Vargas, S. A., Orejel, M., & Fuson, T. L. (2021). Understanding the climate impacts on decadal vegetation change in northern Alaska. *Arctic Science*. https://doi.org/10.1139/as-2020-0050

Hay, G. J., & Castilla, G. (2008). Geographic object-based image analysis (GEOBIA): A new name for a new discipline. In Thomas Blaschke, S. Lang, & G. J. Hay (Eds.), *Lecture Notes in Geoinformation and Cartography* (1st ed., Vol. 0, Issue 9783540770572, pp. 75–89). Springer-Verlag. https://doi.org/10.1007/978-3-540-77058-9_4

Hay, G. J., & Castilla, G. (2006). Object-Based Image Analysis: Strengths, Weaknesses, Opportunities and Threats (SWOT). *The International Archives of the Photogrammetry, Remote Sensing and Spatial Information Sciences*, 1–3.

Hossain, M. D., & Chen, D. (2019). Segmentation for Object-Based Image Analysis (OBIA): A review of algorithms and challenges from remote sensing perspective. *ISPRS J. Photogramm.*, *150*, 115–134.

Huang, C., Davis, L. S., & Townshend, J. R. G. (2002). An assessment of support vector machines for land cover classification. *International Journal of Remote Sensing*, *23*(4), 725–749. https://doi.org/10.1080/01431160110040323

Hussain, M., Chen, D., Cheng, A., Wei, H., & Stanley, D. (2013). Change detection from remotely sensed images: From pixel-based to object-based approaches. *ISPRS Journal of Photogrammetry and Remote Sensing*, *80*, 91–106. https://doi.org/10.1016/j.isprsjprs.2013.03.006

Ide, R., & Oguma, H. (2010). Use of digital cameras for phenological observations. *Ecol.*

Inform., *5*, 339–347.

Jensen, J. R. (2005). *Introductory Digital Image Processing: A Remote Sensing Perspective*. Prentice Hall, Inc.

Jensen, J. R. (2013). *Remote Sensing of the Environment: An Earth Resource Perspective* (2nd Edn.). Harlow: Pearson Eduction Ltd.

Johansen, K., Coops, N. C., Gergel, S. E., & Stange, Y. (2007). Application of high spatial resolution satellite imagery for riparian and forest ecosystem classification. *Remote Sens. Environ.*, *110*(1), 29–44. https://doi.org/10.1016/j.rse.2007.02.014

Kelsey, K., Pedersen, S., Leffler, A. J., Sexton, J., Feng, M., & Welker, J. M. (2021). Winter snow and spring temperature have differential effects on vegetation phenology and productivity across Arctic plant communities. *Global Change Biology*, *27*(8), 1572–1586.

Kim, M., Warner, T. A., Madden, M., & Atkinson, D. S. (2011). Multi-scale GEOBIA with very high spatial resolution digital aerial imagery: Scale, texture and image objects. *Int. J. Remote Sens.*, *32*, 2825–2850.

King, D. H., Wasley, J., Ashcroft, M. B., Ryan-colton, E., Lucieer, A., Chisholm, L. A., Robinson, S. A., & King, D. H. (2020). Semi-automated analysis of digital photographs for monitoring east Antarctic vegetation. *Frontiers in Plant Science*, *11*(766), 1–16. https://doi.org/10.3389/fpls.2020.00766

Kruschke, J. K. (2014). *Doing Bayesian Data Analysis: A tutorial with R, JAGS, and Stan* (2nd Editio). Elsevier Inc.

Kuhn, M. (2008). Building predictive models in R using the caret package. *Journal of Statistical*

Software, *28*(5), 1–26. https://doi.org/https://doi.org/10.18637/jss.v028.i05

Laliberte, A. S., & Rango, A. (2011). Image processing and classification procedures for analysis of sub-decimeter imagery acquired with an unmanned aircraft over arid rangelands. *GIScience and Remote Sensing*, *48*(1), 4–23. https://doi.org/10.2747/1548-1603.48.1.4

Laliberte, A. S., Rango, A., & Herrick, J. (2007). Unmanned aerial vehicles for rangeland mapping and monitoring: A comparison of two systems. *American Society for Photogrammetry and Remote Sensing - ASPRS Annual Conference 2007: Identifying Geospatial Solutions*, *1*, 379–388.

Laliberte, A. S., Rango, A., Herrick, J. E., Fredrickson, E. L., & Burkett, L. (2007). An object-based image analysis approach for determining fractional cover of senescent and green vegetation with digital plot photography. *Journal of Arid Environments*, *69*(1), 1–14. https://doi.org/10.1016/j.jaridenv.2006.08.016

Laliberte, Andrea S., & Rango, A. (2008). Incorporation of texture, intensity, hue, and saturation for rangeland monitoring with unmanned aircraft imagery. *GEOBIA Proceedings*, *37*, 4.

Lang, S. (2008). Object-based Image Analysis for remote sensing applications: modeling reality – dealing with complexity. In T. Blaschke, S. Lang, & G. J. Hay (Eds.), *Object-based Image Analysis* (pp. 1–25). Springer.

Lawrence, R. L., Wood, S. D., & Sheley, R. L. (2006). Mapping invasive plants using hyperspectral imagery and Breiman Cutler classifications (randomForest). *Remote Sens. Environ.*, *100*, 356–362.

Leffler, A. J., Klein, E. S., Oberbauer, S. F., & Welker, J. M. (2016). Coupled long-term summer

warming and deeper snow alters species composition and stimulates gross primary productivity in tussock tundra. *Oecologia*, *181*(1), 287–297.

Liu, N., & Treitz, P. (2016). Modelling high arctic percent vegetation cover using field digital images and high resolution satellite data. *Int. J. Appl. Earth Obs.*, *52*, 445–456.

Liu, T., Abd-Elrahman, A., Morton, J., & Wilhelm, V. L. (2018). Comparing fully convolutional networks, random forest, support vector machine, and patch-based deep convolutional neural networks for object-based wetland mapping using images from small unmanned aircraft system. *GIScience and Remote Sensing*, *55*(2), 243–264. https://doi.org/10.1080/15481603.2018.1426091

Luscier, J. D., Thompson, W. L., Wilson, J. M., Gorhara, B. E., & Dragut, L. D. (2006). Using digital photographs and object-based image analysis to estimate percent ground cover in vegetation plots. *Front. Ecol. Environ.*, *4*(8), 408–413.

Ma, L., Cheng, L., Li, M., Liu, Y., & Ma, X. (2015). Training set size, scale, and features in Geographic Object-Based Image Analysis of very high resolution unmanned aerial vehicle imagery. *ISPRS Journal of Photogrammetry and Remote Sensing*, *102*, 14–27. https://doi.org/10.1016/j.isprsjprs.2014.12.026

Ma, L., Manchun, L., Ma, X., Cheng, L., Du, P., & Liu, Y. (2017). A review of supervised object-based land-cover image classification. *ISPRS J. Photogramm.*, *130*, 277–293.

Malenovský, Z., Lucieer, A., King, D. H., Turnbull, J. D., & Robinson, S. A. (2017). Unmanned aircraft system advances health mapping of fragile polar vegetation. *Methods in Ecology and Evolution*, *8*(12), 1842–1857. https://doi.org/10.1111/2041-210X.12833

Mamet, S. D., Young, N., Chun, K. P., & Johnstone, J. F. (2016). What is the most efficient and effective method for long-term monitoring of alpine tundra vegetation? *Arctic Science*, *2*(3), 127–141. https://doi.org/10.1139/as-2015-0020

Marcial-Pablo, M. de J., Gonzalez-Sanchez, A., Jimenez-Jimenez, S. I., Ontiveros-Capurata, R. E., & Ojeda-Bustamante, W. (2019). Estimation of vegetation fraction using RGB and multispectral images from UAV. *International Journal of Remote Sensing*, *40*(2), 420–438. https://doi.org/10.1080/01431161.2018.1528017

Maxwell, A. E., Warner, T. A., & Fang, F. (2018). Implementation of machine-learning classification in remote sensing: An applied review. *International Journal of Remote Sensing*, *39*(9), 2784–2817. https://doi.org/10.1080/01431161.2018.1433343

May, J.L., Parker, T., Unger, S., & Oberbauer, S. F. (2018). Short term changes in moisture content drive strong changes in Normalized Difference Vegetation Index and gross primary productivity in four Arctic moss communities. *Remote Sens. Environ.*, *212*, 114–120.

May, Jeremy L., & Hollister, R. D. (2012). Validation of a simplified point frame method to detect change in tundra vegetation. *Polar Biol.*, *35*, 1815–1823.

McFeeters, S. (1996). The use of the Normalized Difference Water Index (NDWI) in the delineation of open water features. *Int. J. Remote Sens.*, *17*, 1425–1432.

Menon, S. (2014). *ArcGIS 10.3: The next generation of GIS is here*. ESRI, Inc. https://www.esri.com/arcgis-blog/products/apps/3d-gis/arcgis-10-3-the-next-generation-of-gis-is-here/

Michel, P., Mathieu, R., & Mark, A. F. (2010). Spatial analysis of oblique photo-point images

for quantifying spatio-temporal changes in plant communities. *Applied Vegetation Science*, *13*(2), 173–182. https://doi.org/10.1111/j.1654-109X.2009.01059.x

Molau, U., & Mølgaard, P. (1996). *International Tundra Experiment (ITEX) Manual* (2nd ed.). Danish Polar Center.

Motohka, T., Nasahara, K. N., Oguma, H., & Tsuchida, S. (2010). Applicability of green-red vegetation index for remote sensing of vegetation phenology. *Remote Sens.*, *2*, 2369–2387.

Mountrakis, G., Im, J., & Ogole, C. (2011). Support vector machines in remote sensing: A review. *ISPRS Journal of Photogrammetry and Remote Sensing*, *66*(3), 247–259. https://doi.org/10.1016/j.isprsjprs.2010.11.001

Myers-Smith, I. H., Kerby, J. T., Phoenix, G. K., Bjerke, J. W., Epstein, H. E., Assmann, J. J., John, C., Andreu-Hayles, L., Angers-Blondin, S., Beck, P. S. A., Berner, L. T., Bhatt, U. S., Bjorkman, A. D., Blok, D., Bryn, A., Christiansen, C. T., Cornelissen, J. H. C., Cunliffe, A. M., Elmendorf, S. C., … Wipf, S. (2020). Complexity revealed in the greening of the Arctic. *Nat. Clim. Change*, *10*, 106–117.

Myint, S. W., Gober, P., Brazel, A., Grossman-Clarke, S., & Qihao, W. (2011). Per-pixel vs. object-based classification of urban land cover extraction using high spatial resolution imagery. *Remote Sens. Environ.*, *115*(5), 1145–1161. https://doi.org/10.1016/j.rse.2010.12.017

Nie, Y., & Li, A. (2011). Assessment of alpine wetland dynamics from 1976-2006 in the Vicinity of Mount Everest. *Wetlands*, *31*, 875–884.

Olden, J. D., Lawler, J. J., & Poff, N. L. (2008). Machine learning methods without tears: A

primer for ecologists. *Quarterly Review of Biology*, *83*(2), 171–193. https://doi.org/10.1086/587826

Pal, M., & Mather, P. M. (2003). An Assessment of the Effectiveness of Decision Tree Methods for Land Cover Classification. *Remote Sens. Environ.*, *86*, 554–565. https://doi.org/10.1016/S0034-4257 (03)00132-9

Pal, M., & Mather, P. M. (2005). Support vector machines for classification in remote sensing. *International Journal of Remote Sensing*, *26*(5), 1007–1011. https://doi.org/doi:10.1080/01431160512331314083

Pearson, R. G., Phillips, S. J., Loranty, M. M., Beck, P. S. A., Damoulas, T., Knight, S. J., & Goetz, S. J. (2013). Shifts in Arctic vegetation and associated feedbacks under climate change. *Nat. Clim. Change*, *3*, 673–677.

Pettorelli, N. (2013). *The Normalized Difference Vegetation Index*. Oxford University Press.

Phoenix, G. K., & Bjerke, J. W. (2016). Arctic browning: extreme events and trends reversing arctic greening. *Glob. Change Biol.*, *22*, 2960–2962.

Platt, R. V., & Rapoza, L. (2008). An evaluation of an object-oriented paradigm for land use/land cover classification. *Prof. Geog.*, *60*(1), 87–100.

Pontius, R. G., & Millones, M. (2011). Death to Kappa: birth of quantity disagreement and allocation disagreement for accuracy assessment. *Int. J. Remote Sens.*, *32*(15), 4407–4429. https://doi.org/10.1080/01431161.2011.552923

Post, E., Alley, R. B., Christensen, T. R., Macias-Fauria, M., Forbes, B. C., Gooseff, M. N., Iler, A., Kerby, J. T., Laidre, K. L., Mann, M. E., Olofsson, J., Stroeve, J. C., Ulmer, F., R.A.,

V., & Wang, M. (2019). The polar regions in a 2°C warmer world. *Sci. Adv.*, *5*(1–12).

Quinlan, J. R. (1986). Induction of decision trees. *Machine Learning*, *1*, 81–106.

Radoux, J., & Bogaert, P. (2017). Good practices for object-based accuracy assessment. *Remote Sensing*, *9*(7). https://doi.org/10.3390/rs9070646

Ramezan, C. A., Warner, T. A., Maxwell, A. E., & Price, B. S. (2021). Effects of training set size on supervised machine-learning land-cover classification of large-area high-resolution remotely sensed data. *Remote Sensing*, *13*(3), 1–27. https://doi.org/10.3390/rs13030368

Rawat, W., & Wang, Z. (2017). Deep convolutional neural networks for image classification: A comprehensive review. *Neural Computation*, *29*(9), 2352–2449. https://doi.org/10.1162/neco_a_00990

Raynolds, M. K., Walker, D. A., Balser, A., Bay, C., Campbell, M., Cherosov, M. M., Daniëls, F. J. A., Eidesen, P. B., Ermokhina, K., Frost, G. V., Jedrzejek, B., Jorgenson, M. T., Kennedy, B. E., Kholod, S. S., Lavrinenko, I. A., Lavrinenko, O. V., Magnússon, B., Matveyeva, N. V., Metúsalemsson, S., … Troeva, E. (2019). A raster version of the Circumpolar Arctic Vegetation Map (CAVM). *Remote Sens. Environ.*, *232*, 1–12.

Richardson, A. D., Braswell, B. H., Hollinger, D. Y., Jenkins, J. P., & Ollinger, S. V. (2009). Near-surface remote sensing of spatial and temporal variation in canopy phenology. *Ecol. App.*, *19*, 1417–1428.

Richardson, A. D., Jenkins, J. P., Braswell, B. H., Hollinger, D. Y., Ollinger, S. V., & Smith, M. L. (2007). Use of digital webcam images to track spring green-up in a deciduous broadleaf forest. *Oecologia*, *152*, 323–334.

Rogers, G. F., Turner, R. M., & Malde, H. E. (1983). Using Matched Photographs to Monitor Resource Change. In J. F. Bell & T. Atterbury (Eds.), *Renewable resource inventories for monitoring changes and trends: proceedings of an international conference* (pp. 90–92).

Schapire, R. E. (1990). The strength of weak learnability. *Mach. Learn.*, *5*, 197–227.

Shiklomanov, A. N., Bradley, B. A., Dahlin, K. M., Fox, A. M., Gough, C. M., Hoffman, F. M., Middleton, E. M., Serbin, S. P., Smallman, L., & Smith, W. K. (2019). Enhancing global change experiments through integration of remote-sensing techniques. *Front. Ecol. Environ.*, *17*(4), 215–224.

Shiklomanov, N. I., Streletskiy, D. A., Nelson, F. E., Hollister, R. D., Romanovsky, V. E., Tweedie, C. E., Bockheim, J. G., & Brown, J. (2010). Decadal variations of active-layer thickness in moisture-controlled landscapes, Barrow, Alaska. *J. Geophys. Res.*, *115*, G00I04. https://doi.org/10.1029/2009JG001248

Simonis, J. L., White, E. P., & Ernest, S. K. M. (2021). Evaluating probabilistic ecological forecasts. *Ecology*, *102*, e03431. https://doi.org/10.1002/ecy.3431

Smith, A. (2010). Image segmentation scale parameter optimization and land cover classification using the Random Forest algorithm. *Journal of Spatial Science*, *55*(1), 69–79. https://doi.org/10.1080/14498596.2010.487851

Story, M., & Congalton, R. G. (1986). Accuracy assessment: A user's perspective. *Photogramm. Eng. Rem. S.*, *52*(3), 397–399.

Stow, D. A., Hope, A., McGuire, D., Verbyla, D., Gamon, J., Huemmrich, F., Houston, S., Racine, C., Sturm, M., Tape, K., Hinzman, L., Yoshikawa, K., Tweedie, C., Noyle, B.,

Silapaswan, C., Douglas, D., Griffith, B., Jia, G. J., Epstein, H., … Myneni, R. (2004). Remote sensing of vegetation and land-cover change in Arctic tundra ecosystems. *Remote Sens.*, *89*, 281–308. https://doi.org/10.1016/j.rse.2003.10.018

Strahler, A., Woodcock, C., & Smith, J. (1986). On the nature of models in remote sensing. *Remote Sens. Environ.*, *20*, 121–139.

Tieszan, L. L. (1978). Photosynthesis in the principal Barrow, Alaska species: a summary of field and laboratory responses. In L. L. Tieszen (Ed.), *Vegetation and Production Ecology of an Alaskan Arctic Tundra*. Springer.

Trimble Germany GmbH. (2019). *Trimble Documentation eCognition Developer 9.5 Reference Book* (9.5.1). Trimble Germany GmbH.

Tucker, C. J. (1979). Red and photographic infrared linear combinations for monitoring vegetation. *Remote Sens. Environ.*, *8*, 127–150.

van der Welle, M. E. W., Vermeulen, P. J., Shaver, G. R., & Berendse, F. (2003). Factors determining plant species richness in Alaskan Arctic tundra. *Journal of Vegetation Science*, *14*(5), 711–720.

Vittoz, P., & Guisan, A. (2007). How reliable is the monitoring of permanent vegetation plots? A test with multiple observers. *J. Veg. Sci.*, *18*, 413–422.

Willmott, C. J., & Matsuura, K. (2005). Advantages of the mean absolute error (MAE) over the root mean square error (RMSE) in assessing average model performance. *Climate Research*, *30*(1), 79–82. https://doi.org/10.3354/cr030079

Witharana, C., Bhuiyan, A. E., Liljedahl, A. K., Kanevskiy, M., Jorgenson, T., Jones, B. M.,

Daanen, R., Epstein, H. E., Griffin, C. G., Kent, K., & Jones, M. K. W. (2021). *An Object-Based Approach for Mapping Tundra Ice-Wedge Polygon Troughs An Object-Based Approach for Mapping Tundra Ice-Wedge Polygon Troughs from Very High Spatial Resolution Optical Satellite Imagery*. *February*. https://doi.org/10.3390/rs13040558

Witharana, C., & Civco, D. L. (2014). Optimizing multi-resolution segmentation scale using empirical methods: Exploring the sensitivity of the supervised discrepancy measure Euclidean distance 2 (ED2). *ISPRS Journal of Photogrammetry and Remote Sensing*, *87*, 108–121. https://doi.org/10.1016/j.isprsjprs.2013.11.006

Ye, S., Pontius, R. G., & Rakshit, R. (2018). A review of accuracy assessment for object-based image analysis: From per-pixel to per-polygon approaches. *ISPRS Journal of Photogrammetry and Remote Sensing*, *141*, 137–147. https://doi.org/10.1016/j.isprsjprs.2018.04.002

Zhou, Y., Dong, J., Xiao, X., Xiao, T., Yang, Z., Zhao, G., Zou, Z., & Qin, Y. (2017). Open Surface Water Mapping Algorithms: A Comparison of Water-Related Spectral Indices and Sensors. *Water*, *9*(4). https://doi.org/10.3390/w9040256

Zhu, Z., Piao, S., Myneni, R. B., Huang, M., Zeng, Z., Canadell, J. G., Ciais, P., Sitch, S., Friedlingstein, P., Arneth, A., Cao, C., Cheng, L., Kato, E., Koven, C., Li, Y., Lian, X., Liu, Y., Liu, R., Mao, J., … Zeng, N. (2016). Greening of the Earth and its drivers. *Nat. Clim. Change*, *6*, 791–795.

Table 2.1. Vegetation sampling dates using the point frame and plot photography methods (Jul = July; Aug = August). Camera specifications, including model and pixel resolution, are summarized. Photographs were substituted on occasion as noted (No.).

Year	Point Frame Dates	Photography Date	Camera Specifications		Photo Substitutions		
			Model	Resolution	No.	Date	Reason
2012	Jul 26 - Jul 30	Aug 4	Panasonic DMC-TS3	4320 x 3240	4	Jul 9	Blurry
2013	Jul 20 - Jul 29	Jul 30	Panasonic DMC-TS3	4320 x 3240	2	Jul 16	Blurry, missing
2014	Jul 21 - Jul 29	Aug 17	Panasonic DMC-TS3	4320 x 3240	6	Jul 28	Blurry, missing
2015	Jul 26 - Jul 30	Jul 8	Panasonic DMC-TS3	4320 x 3240	-	-	-
2018	Jul 26 - Aug 9 *	Jul 29	Nikon Coolpix AW120	4608 x 3456	1	Aug 6	Distortion
2019	Jul 25 - Aug 6	Aug 2	Nikon Coolpix AW120	4608 x 3456	3	Jul 25	Blurry, missing
2021	Jul 26 - Aug 7	Aug 7	Panasonic DMC-TS3	4320 x 3240	2	Jul 22	Blurry

* Plot H4 was sampled on August 26

Table 2.2. Amount of positional error in each plot photograph as a result of the first order polynomial (affline) transformation during the georeferencing procedure. At least four ground control points (GCP) were applied to register the location of each image. Root mean square sum of all the residuals, also known as the total error or root mean square error (RMSE), is expressed in centimeters. Mean ($\bar{x}$) and standard deviation (SD) are also reported.

Plot	Ground Control Points (GCP)							Root Mean Square Error (RMSE, cm)						
	2012	2013	2014	2015	2018	2019	2021	2012	2013	2014	2015	2018	2019	2021
D2	16	4	15	14	8	7	6	1.4	1.8	1.1	3.6	4.2	2.5	3.0
D3	15	4	15	15	11	10	9	1.0	2.3	1.1	3.3	3.4	2.8	1.9
D4	15	4	18	17	16	15	15	1.4	2.6	1.3	3.7	5.4	5.8	2.4
D5	8	4	7	5	4	4	4	0.8	0.2	5.0	6.2	3.8	3.0	2.4
D6	8	4	4	4	5	5	4	1.4	2.8	6.1	5.4	5.0	3.8	1.7
D7	13	4	11	8	4	4	4	1.0	2.2	2.0	3.7	2.6	2.1	1.2
E2	15	4	14	15	10	10	11	1.3	1.5	1.7	2.5	1.6	3.1	2.5
E3	10	4	9	7	6	6	6	1.7	0.9	2.3	2.8	5.4	3.2	4.5
E4	12	4	9	6	9	5	4	1.1	2.1	2.7	4.2	3.6	3.1	5.4
E5	9	4	8	7	5	5	4	1.1	1.5	2.4	4.8	5.4	2.3	3.9
E6	9	4	8	9	4	4	4	1.4	0.2	2.6	3.5	4.7	1.1	2.9
E7	15	4	15	12	8	6	7	1.6	3.0	1.7	3.5	4.5	3.9	3.0
F2	11	4	9	11	10	8	6	3.4	5.3	1.6	2.9	6.4	5.7	4.7
F3	8	4	6	4	4	4	4	1.8	1.3	5.7	4.1	7.2	9.0	1.3
F4	4	7	8	4	4	4	4	3.9	2.8	4.1	6.5	5.1	6.7	4.0
F5	4	4	6	6	5	4	4	2.7	3.5	3.2	2.9	10.8	3.3	1.4
F6	4	4	4	4	4	4	4	1.4	1.5	1.9	3.5	1.6	2.5	0.3
F7	4	14	11	6	5	6	4	4.1	1.1	1.6	3.9	2.2	3.3	3.5
G2	8	4	7	4	4	4	4	0.9	1.8	5.1	4.5	4.2	1.6	1.1
G3	7	4	5	4	5	4	6	1.3	0.7	2.3	5.3	5.2	2.8	2.9
G4	12	4	12	12	12	11	11	2.0	1.9	2.3	3.8	4.3	3.7	3.3
G5	4	4	4	4	4	4	4	0.8	2.5	6.2	5.5	4.9	3.3	2.1
G6	7	4	6	4	5	5	4	1.2	1.0	1.2	6.2	4.3	7.3	2.9
G7	4	4	4	4	4	4	4	0.2	2.0	8.8	6.0	5.9	2.2	1.0
H2	11	4	11	9	4	4	4	1.6	1.1	4.3	2.8	2.5	4.5	1.3
H3	5	4	4	4	4	4	4	0.8	0.6	3.4	5.0	11.5	6.2	1.8
H4	11	4	8	8	7	5	4	1.1	1.1	2.1	6.3	5.6	0.9	2.0
H5	13	4	13	9	5	5	4	0.9	1.7	1.7	4.4	3.3	1.7	2.0
H6	17	4	17	17	13	9	9	0.7	1.9	1.1	3.9	2.8	1.1	0.9
H7	5	4	4	4	4	4	4	1.8	1.8	3.8	6.0	6.8	0.7	3.5
$\bar{x}$	9.5	4.4	9.1	7.9	6.4	5.8	5.5	1.5	1.8	3.0	4.4	4.8	3.4	2.5
SD	4.2	1.9	4.2	4.3	3.3	2.7	2.8	0.9	1.0	1.8	1.2	2.2	2.0	1.2

Table 2.3. Number of objects generated in each plot image as a result of the multi-resolution segmentation algorithm (MRS). Plots were noted with an asterisk (*) if they exhibited inundation.

Plot	Sampling Year						
	2012	2013	2014	2015	2018	2019	2021
D2	9564	9117	11017	10454	9473	10535	9999
D3	9609	10310	11774	11586	10730	11346	12029
D4	10074	9895	10060	10971	10127	10583	10448
D5	10279	10082 *	11223	11195	11374	11133 *	10591
D6	9405	9755 *	10831 *	11053	10556	11584	11337
D7	10085	10612 *	10748	11994 *	12460 *	13127 *	13138
E2	10391	10477	12426	11647	11828	9816	11811
E3	7258	8578 *	11274	10366	9263 *	9762 *	9508
E4	8096 *	8575 *	10057	10354	10583	10905	9358
E5	8561	8262	10071	9689	10171	9907	9134
E6	10018	9432	12023	11277	11684	11959	10876
E7	10184	10353	10524	12164	11893	12490	10595
F2	7930	8969	10548	10248	9847	10200	9824
F3	7372	6634 *	8656 *	9800	9573 *	6707 *	12114
F4	10559	9005 *	11913 *	11681 *	9578 *	4614 *	4263 *
F5	8561	8361	11640	11000	10568	8176	9060
F6	8880	9684 *	11458	11053 *	11482	10707 *	12430
F7	9261	9294	10671	10350	10460	9002	10795
G2	9126	7297 *	10398 *	9286 *	10041 *	10881 *	11593
G3	10154	8422 *	10250	9696	10000 *	8337 *	10883
G4	10341	10171	11874	12094	10729	9908	11980
G5	11570	8583 *	10722 *	10507 *	10126 *	9744 *	8453 *
G6	11964	10287 *	14402 *	13416	13101 *	10512 *	12125
G7	8795	8790 *	11824 *	11007	11128 *	10250 *	11250 *
H2	12032	10859	12470 *	11966 *	12520 *	12187 *	13526
H3	9035	8832 *	8320 *	9411 *	6000 *	4397 *	6852 *
H4	8588	9950 *	10184 *	10562	9505 *	10696 *	11801 *
H5	9573	8893	10936	10377	10505 *	9994 *	10221
H6	9622	8920	11746	10016	10676	10945	8411
H7	9239	9838	14264	10578	11215 *	10349 *	12874 *

Table 2.4. List and explanation of the features calculated for each image object. 22 features were retained to train the machine learning classification models (noted by ✓). Texture features were calculated from all bands in all directions (0°, 45°, 90°, 135°), and therefore show directional invariance.

Type		Feature	Definition
Spectral Indices	✓	Green-Red Vegetation Index (GRVI)	GRVI = (G - R) / (G + R); where G = green band, R = red band.[1] Closely correlated to NDVI.[2]
	o	Normalized Difference Index Green-Blue	(G - B) / (G + B); where G = green band, B = blue band.
	o	Normalized Difference Index Red-Blue	(R - B) / (R + B); where R = red band, B = blue band.
	✓	Green Ratio (rG)	rG = G / (R + G + B); where G = green band, R = red band, B = blue band. Evaluates phenological shifts and productivity.[3]
	✓	Red Ratio (rR)	rR = R / (R + G + B); where G = green band, R = red band, B = blue band. Objective is analogous to the Green Ratio, but the primary band of interest is red.
	✓	Blue Ratio (rB)	rB = B / (R + G + B); where G = green band, R = red band, B = blue band. Objective is analogous to the Green Ratio, but the primary band of interest is blue.
	✓	Greenness Excess Index (GEI)	GEI = 2*rG - (rR + rB); where rG = Green Ratio, rR = Red Ratio, rB = Blue Ratio.[4] May be a subtler indicator of phenological shifts than the Green Ratio.[5,6]
	o	Visible atmospheric resistance index (VARI)	VARI = (G - R) / (G + R - B); where G = green band, R = red band, B = blue band.[7] Measure of canopy reflectance. VARI complements the purpose of the Atmospherically Resistant Vegetation Index (ARVI), but this index uses only RGB bands to mitigate differences in illumination and measure canopy reflectance.
Layer Values	o	Mean Red Layer	Mean pixel value in an image object using the red band
	o	Mean Green Layer	Mean pixel value in an image object using the green band
	o	Mean Blue Layer	Mean pixel value in an image object using the blue band
	o	Standard Deviation Red Layer	Standard deviation of pixel values in an image object using the red band
	✓	Standard Deviation Green Layer	Standard deviation of pixel values in an image object using the green band
	✓	Standard Deviation Blue Layer	Standard deviation of pixel values in an image object using the blue band
	o	Mean Brightness	Mean pixel intensity in an image object using all available bands
	o	Mean Maximum Difference	Maximum pixel value subtracted by the minimum pixel value in each available band for an image object. Values are averaged.
	✓	Hue	Transformation of the red, green, blue (cube) color space into the hue, saturation, intensity (cyclindrical) color space. Hue describes the dominant color of an image object.
	o	Saturation	Saturation describes the purity of color; that is, the shades of gray present in an image object. An image object without any gray (pure color) is unsaturated, while an image object with gray is fully saturated.
	✓	Intensity	Also referred to as brightness or value, intensity describes the degree of brightness in an image object.

Table 2.4. Continued…

Type		Feature	Definition
Geometry (Extent)	✓	Area	Number of pixels in an image object.
	✓	Border length	Length (in pixels) of the outside border of an image object.
	✓	Length	Length (in pixels) of an image object.
	✓	Length-to-Width Ratio	Length (in pixels) divided by width (in pixels) of an image object.
	✓	Width	Width (in pixels) of an image object.
Geometry (Shape)	o	Asymmetry	Values increase with higher asymmetry. An ellipse is approximated around the image object, then the variance in length from the major to minor axis of the ellipse is calculated.
	✓	Compactness	Length (in pixels) multiplied by width (in pixels) of an image object, then divided by the total number of pixels in the image object. A image object with higher compactness generally has a smaller border and condensed core or area.
	✓	Density	Describes the pixel distribution in an image object. The most dense shape is considered to be a square, while the least dense shape is a filament. Density is calculated based on a covariance matrix by dividing the number of pixels in an image object by its approximate radius.
	✓	Elliptic fit	Measures the fit or alignment between an image object and an ellipse. Values range from 0 (no fit) to 1 (perfect fit).
	✓	Radius of largest enclosed ellipse	Measures the similarity between an image object and an ellipse with the same area as the image object. A ratio is calculated between the radius of the largest enclosed ellipse to the radius of original ellipse.
	✓	Radius of smallest enclosing ellipse	Measures the similarity between an image object and an ellipse with the same area as the image object. A ratio is calculated between the radius of the smallest enclosing ellipse to the radius of original ellipse.
	o	Roundness	Roundness describes the similarity of an image object to an ellipse. It is measured by subtracting the radius of the largest enclosed ellipse by the smallest enclosing ellipse.
Texture (GLCM)[8]	✓	Homogeneity	Measure of uniformity. Homogeneity is a weighted measure that decreases exponentially with greater distance from the GLCM diagonal.
	✓	Contrast	Measure of inertia. Contrast is a weighted measure that increases exponentially with greater distance from the GLCM diagonal. Contrast generally opposes homogeneity. The higher the contrast, the lower the homogeneity (or uniformity) tends to be.
	o	Dissimilarity	Similar to contrast, but it is calculated differently. Dissimilarity is a weighted measure that increases linearly with greater distance from the GLCM diagonal.
	o	Angular Second Moment (ASM)	Measure of energy. The value for ASM is largest when the pixel value differences are constant (uniform or orderly).
	✓	Entropy	Measure of spatial disorder or randomness. Entropy generally opposes ASM. The value for entropy is largest when the pixel value differences are inconstant (variable or disordered).

[1] Tucker, 1979; [2] Anderson et al., 2016; [3] Beamish et al., 2016; [4] Richardson et al., 2007; [5] Richardson et al., 2009; [6] Ide & Oguma, 2010; [7] Gitelson et al., 2002; [8] Haralick et al., 1973.

Table 2.5. List of classification models applied to the labeled data set. R package, dependent libraries, preprocessing requirements, and final tuning parameters are also summarized. Data were centered and scaled (CS). Near zero variance predictors were identified and removed (NZV).

Model	Preprocess	Tuning Parameters		
		Code	Definition	Final
Random Forest (RF)	None	mtry	Number of predictors	20
Package=ranger with libraries		splitrule	Splitting rule	extratrees
(e1071, ranger, dplyr)		min.node.size	Minimum node size	1
Stochastic Gradient Boosting (GBM)	None	n.trees	Number of trees	50
Package=gbm with libraries (gbm, plyr)		interaction.depth	Tree complexity	3
		shrinkage	Learning rate	0.1
		n.minobsinnode	Minimum node size	10
Classification and Regression Tree (CART)	None	cp	Complexity parameter	0.003019845
Package=rpart with library (rpart)				
Support Vector Machine (SVM)	CS	sigma	Sigma	0.04458388
Package=svmRadial with library (kernlab)		C	Cost	4
k-Nearest Neighbor (KNN)	CS, NZV	k	Number of neighbors	15
Package=knn				

Table 2.6. Number of objects by class in the labeled data set split into 70% training, 15% validation, and 15% test using a stratified random sampling technique.

Class	Training (70%)	Validation (15%)	Test (15%)	Total
Bryophytes	1652	354	354	2360
Deciduous Shrubs	397	85	85	567
Forbs	294	63	62	419
Graminoids	2136	458	457	3051
Lichens	318	68	68	454
Litter	3549	760	760	5069
Shadow	1208	259	258	1725
Standing Dead	949	203	203	1355
Total	10503	2250	2247	15000

Table 2.7. Performance of the five machine learning classification models compared across the training, validation, and the test data sets. Overall accuracy (OA) and Kappa are shown for each data set. Minimum and maximum accuracy values are reported for the training data set, while 95% confidence intervals are reported for the validation and test data sets. The five models were: Random forest = RF; stochastic gradient boosting = GBM; classification and regression tree = CART; support vector machine = SVM; and k-nearest neighbor = KNN.

Training

Model	OA	Min	Max	Kappa	Run Time (min)
RF	59.8	56.8	63.1	51.9	25.4
GBM	60.0	57.4	63.2	52.0	36.3
CART	55.5	52.0	59.8	46.8	0.1
SVM	57.4	54.9	60.7	49.3	10.6
KNN	46.8	43.1	51.3	37.6	1.9

Validation

Model	OA	Lower CI	Upper CI	Kappa
RF	60.6	58.6	62.7	52.9
GBM	60.5	58.4	62.5	52.7
CART	57.6	55.5	59.7	48.8
SVM	57.8	55.7	59.8	50.0
KNN	47.4	45.3	49.5	38.6

Test

Model	OA	Lower CI	Upper CI	Kappa
RF	60.5	58.4	62.5	52.5
GBM	59.8	57.7	61.8	51.7
CART	56.2	54.1	58.2	46.8
SVM	57.4	55.3	59.4	49.4
KNN	46.6	44.5	48.7	37.6

Table 2.8. Importance values for the features in the optimized random forest model. Importance values were normalized to a value between 0 to 100. Features are further explained in Table 2.4.

Predictor	Type	Raw	Normalized
Intensity	Layer	411.4	100.0
Green Ratio (rG)	Spectral	144.3	26.5
Green-Red Vegetation Index (GRVI)	Spectral	142.6	26.0
Greenness Excess Index (GEI)	Spectral	116.4	18.8
Hue	Layer	112.5	17.7
Density	Shape	100.8	14.5
Blue Ratio (rB)	Spectral	98.6	13.9
Red Ratio (rR)	Spectral	95.7	13.1
Homogeneity	Texture	72.5	6.7
Length-to-Width Ratio	Extent	71.9	6.5
Contrast	Texture	71.1	6.3
Length	Extent	62.1	3.8
Standard Deviation Green Layer	Layer	61.3	3.6
Radius of largest enclosed ellipse	Shape	58.8	2.9
Entropy	Texture	58.7	2.9
Standard Deviation Blue Layer	Layer	56.2	2.2
Compactness	Shape	55.8	2.1
Elliptic fit	Shape	55.7	2.0
Width	Extent	54.7	1.8
Radius of smallest enclosed ellipse	Shape	54.4	1.7
Border length	Extent	53.2	1.3
Area	Extent	48.3	0.0

Table 2.9. Thematic accuracy of the final random forest model on the test data set represented as a confusion matrix. Overall accuracy (OA) is calculated from the bolded diagonal values, which indicates the number of image objects that were correctly classified. Kappa accounts for the possibility of agreement between the reference and classified data sets based on chance. Individual class accuracy is analyzed by producer and user accuracies. Producer accuracy (PA) is relied on by the mapmaker to describe the probability that a real-life object is classified correctly in the image. User accuracy (UA) is relied on by the map user to describe the probability that a classified object in an image matches the object in real-life. Bryophytes = BRYO; Deciduous Shrubs = DSHR; Forbs = FORB; Graminoids = GRAM; Lichens = LICH; Litter = LITT; Shadow = SHAD; Standing Dead = STAD.

		Observed								
		BRYO	DSHR	FORB	GRAM	LICH	LITT	SHAD	STAD	**UA**
Predicted	BRYO	**178**	14	3	28	0	92	27	0	52.0
	DSHR	50	**34**	7	73	2	47	5	0	15.6
	FORB	2	9	**41**	22	1	3	0	0	52.6
	GRAM	16	16	8	**270**	0	35	0	4	77.4
	LICH	6	3	2	20	**38**	74	0	43	20.4
	LITT	47	8	1	18	9	**431**	9	6	81.5
	SHAD	55	1	0	3	0	35	**217**	0	69.8
	STAD	0	0	0	23	18	43	0	**150**	64.1
	PA	50.3	40.0	66.1	59.1	55.9	56.7	84.1	73.9	
	OA	60.5								
	Kappa	52.5								

Table 2.10. Comparison of relative cover estimates between the point frame (left) and plot photography (right) vegetation sampling methods. Values represent the presence (frequency, F), mean ($\bar{x}$), and standard deviation (SD) of the relative cover estimates of each growth form across sampling years. Note the mean ($\bar{x}$) are for the plots in which they occurred (noted by the frequency).

	Point Frame							Plot Photography						
	2012	2013	2014	2015	2018	2019	2021	2012	2013	2014	2015	2018	2019	2021
Bryophytes														
F	29	29	29	29	27	27	27	30	30	30	30	30	30	30
$\bar{x}$	17.9	20.5	19.0	14.5	25.8	11.6	11.9	15.5	19.3	17.9	10.1	11.0	10.6	13.0
SD	7.9	8.0	10.3	5.5	7.9	5.6	5.6	11.0	10.8	8.3	5.8	7.9	7.0	9.3
Deciduous Shrubs														
F	11	12	11	9	12	9	11	30	30	30	30	30	30	30
$\bar{x}$	16.9	16.8	6.3	15.4	9.5	18.0	17.5	4.0	4.8	3.9	4.2	3.8	3.2	3.4
SD	9.5	4.9	3.7	8.1	3.6	6.2	6.5	7.5	8.4	7.1	7.9	7.0	6.2	6.1
Forbs														
F	24	25	24	22	22	21	23	30	30	25	30	27	30	30
$\bar{x}$	4.7	8.1	2.1	5.1	2.8	12.1	6.6	3.7	5.7	3.0	5.3	3.5	4.7	4.2
SD	10.5	13.5	5.8	11.3	9.4	16.1	13.8	6.6	7.1	4.1	11.7	8.0	10.2	8.3
Graminoids														
F	30	30	30	30	30	30	30	30	30	30	30	30	30	30
$\bar{x}$	14.7	21.0	16.8	18.8	16.4	33.1	22.3	23.0	37.6	23.2	36.2	35.8	40.2	36.7
SD	10.7	10.7	15.7	14.4	14.1	14.7	15.5	9.4	12.3	8.8	13.4	14.5	12.6	18.2
Lichens														
F	20	18	19	18	19	16	16	30	30	30	30	30	30	30
$\bar{x}$	2.7	4.0	8.0	5.5	7.5	4.1	5.2	6.5	9.1	7.7	5.4	6.0	5.9	7.1
SD	1.7	1.9	3.3	2.9	3.0	2.5	1.9	8.2	11.1	9.4	7.5	8.7	8.4	9.8
Litter														
F	29	30	30	30	30	30	29	30	30	30	30	30	30	30
$\bar{x}$	35.8	20.4	31.9	29.7	24.2	12.4	24.1	10.7	11.6	19.8	24.1	24.2	21.8	30.6
SD	14.7	11.9	15.3	15.4	11.0	9.9	12.5	9.1	8.7	11.7	8.9	10.0	11.7	10.8
Standing Dead														
F	30	30	30	30	30	30	28	30	30	30	30	30	30	30
$\bar{x}$	7.3	9.2	15.8	10.9	13.8	8.8	12.4	36.5	11.9	24.5	14.7	15.8	13.6	4.9
SD	4.5	3.8	5.2	3.8	4.5	4.1	5.5	8.0	5.2	7.3	6.5	8.1	7.5	3.4

Table 2.11. Spearman-Rank correlation values (rho) show the positive, negative, or lack of association between the point frame and image estimates of relative cover by growth form and year. P-values (p) are also shown and bolded when significant (≤ 0.05).

	2012		2013		2014		2015		2018		2019		2021			
	Rho	P	Rho	P	Rho	P	Rho	P	Rho	P	Rho	P	Rho	P	Min Rho	Max Rho
Bryophytes	0.23	0.23	-0.13	0.51	0.25	0.18	**0.46**	0.01	0.33	0.08	0.28	0.14	**0.64**	0.00	-0.13	**0.64**
Deciduous Shrubs	0.14	0.45	0.17	0.38	0.20	0.29	0.16	0.41	**0.49**	0.01	0.21	0.26	**0.59**	0.00	0.14	**0.59**
Forbs	**0.38**	0.04	0.16	0.39	0.17	0.37	**0.40**	0.03	0.31	0.10	0.12	0.52	**0.47**	0.01	0.12	**0.47**
Graminoids	**0.69**	0.00	**0.60**	0.00	**0.43**	0.02	**0.82**	0.00	**0.79**	0.00	**0.73**	0.00	**0.84**	0.00	**0.43**	**0.84**
Lichens	**0.41**	0.02	**0.79**	0.00	**0.50**	0.00	**0.81**	0.00	**0.42**	0.02	**0.78**	0.00	0.30	0.11	0.30	**0.81**
Litter	0.24	0.21	0.00	0.99	-0.25	0.19	**-0.36**	0.05	-0.14	0.47	**-0.41**	0.03	-0.08	0.67	**-0.41**	0.24
Standing Dead	0.18	0.35	-0.29	0.12	0.27	0.14	0.32	0.09	0.14	0.47	**0.43**	0.02	-0.05	0.81	-0.29	**0.43**

Table 2.12. In-sample model performance. From left to right, in-sample performance of the relative abundance estimates of vegetation classes based on direct substitution of the image-based estimates and conditional predictions. Conditional predictions included the fixed effects covariates and random effects of plot. Model performance is illustrated by mean absolute error (MAE) and bias. MAE was calculated as the average absolute difference between the predicted proportion of vegetation in each class and the observed proportion in each class (mean(absolute(predicted – observed))). Bias was calculated as the mean difference between the two proportions in each class ((mean(predicted – observed))).

	Direct Substitution		Conditional	
	MAE	Bias	MAE	Bias
Bryophytes	0.09	0.03	0.05	0.00
Deciduous Shrubs	0.12	0.10	0.01	0.00
Forbs	0.04	0.02	0.01	0.00
Graminoids	0.14	- 0.13	0.06	0.00
Lichens	0.06	- 0.02	0.01	0.00
Litter	0.17	0.05	0.08	0.00
Standing Dead	0.10	- 0.06	0.08	0.00

Table 2.13. Out-of-sample model performance of the temporal comparison. From left to right, out-of-sample performance of the relative abundance estimates of vegetation classes from holdout years (2018-2021) based on direct substitution of the image-based estimates, fixed effects covariates only, random effects of plot only, and the interaction of the fixed effects covariates and random effects of plot. Model performance is illustrated by mean absolute error (MAE) and bias. MAE was calculated as the average absolute difference between the predicted proportion of vegetation in each class and the observed proportion in each class (mean(absolute(predicted – observed))). Bias was calculated as the mean difference between the two proportions in each class ((mean(predicted – observed))).

	Direct Substitution		Fixed Effects		Random Effects		Conditional	
	MAE	Bias	MAE	Bias	MAE	Bias	MAE	Bias
Bryophytes	0.09	0.05	0.06	0.03	0.07	0.04	0.07	0.03
Deciduous Shrubs	0.12	0.12	0.05	0.00	0.01	0.01	0.01	0.00
Forbs	0.04	0.03	0.03	0.01	0.02	0.00	0.02	0.01
Graminoids	0.15	- 0.14	0.08	- 0.04	0.10	- 0.08	0.07	- 0.04
Lichens	0.06	- 0.01	0.06	0.00	0.02	0.01	0.02	0.00
Litter	0.15	- 0.05	0.12	- 0.10	0.11	- 0.10	0.11	- 0.10
Standing Dead	0.07	0.00	0.11	0.10	0.12	0.11	0.10	0.09

Table 2.14. Out-of-sample model performance of the spatial comparison. From left to right, out-of-sample performance of the relative abundance estimates of vegetation classes from ten holdout plots based on direct substitution of the image-based estimates and conditional predictions. Conditional predictions included the fixed effects covariates and random effects of plot. Model performance is illustrated by mean absolute error (MAE) and bias. MAE was calculated as the average absolute difference between the predicted proportion of vegetation in each class and the observed proportion in each class (mean(absolute(predicted – observed))). Bias was calculated as the mean difference between the two proportions in each class ((mean(predicted – observed))).

	Direct Substitution		Conditional	
	MAE	Bias	MAE	Bias
Bryophytes	0.08	0.05	0.08	0.05
Deciduous Shrubs	0.10	0.09	0.05	0.01
Forbs	0.04	0.02	0.04	- 0.01
Graminoids	0.16	- 0.13	0.09	0.02
Lichens	0.07	- 0.04	0.09	- 0.05
Litter	0.22	0.10	0.11	- 0.02
Standing Dead	0.11	- 0.09	0.09	0.01

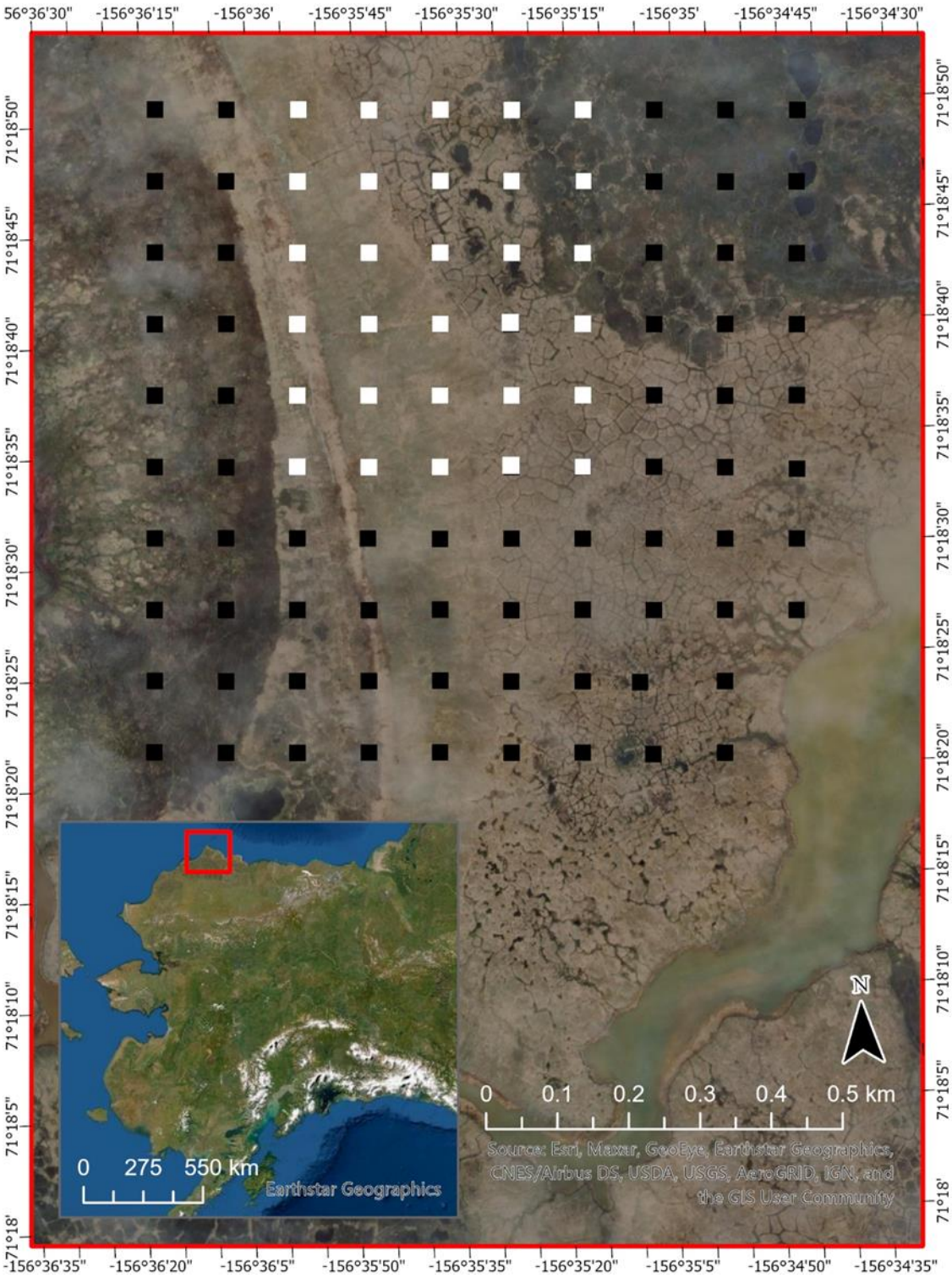

Figure 2.1. Map of the research site. The site is stationed on the Barrow Peninsula near the city of Utqiaġvik, Alaska. The 30 vegetation plots in this analysis are represented by white squares. These plots are part of a larger collection of 98 plots, which are evenly distributed at a 100-meter interval across the Arctic System Science (ARCSS) grid. The site is adjacent to the warming experiments associated with the International Tundra Experiment (ITEX).

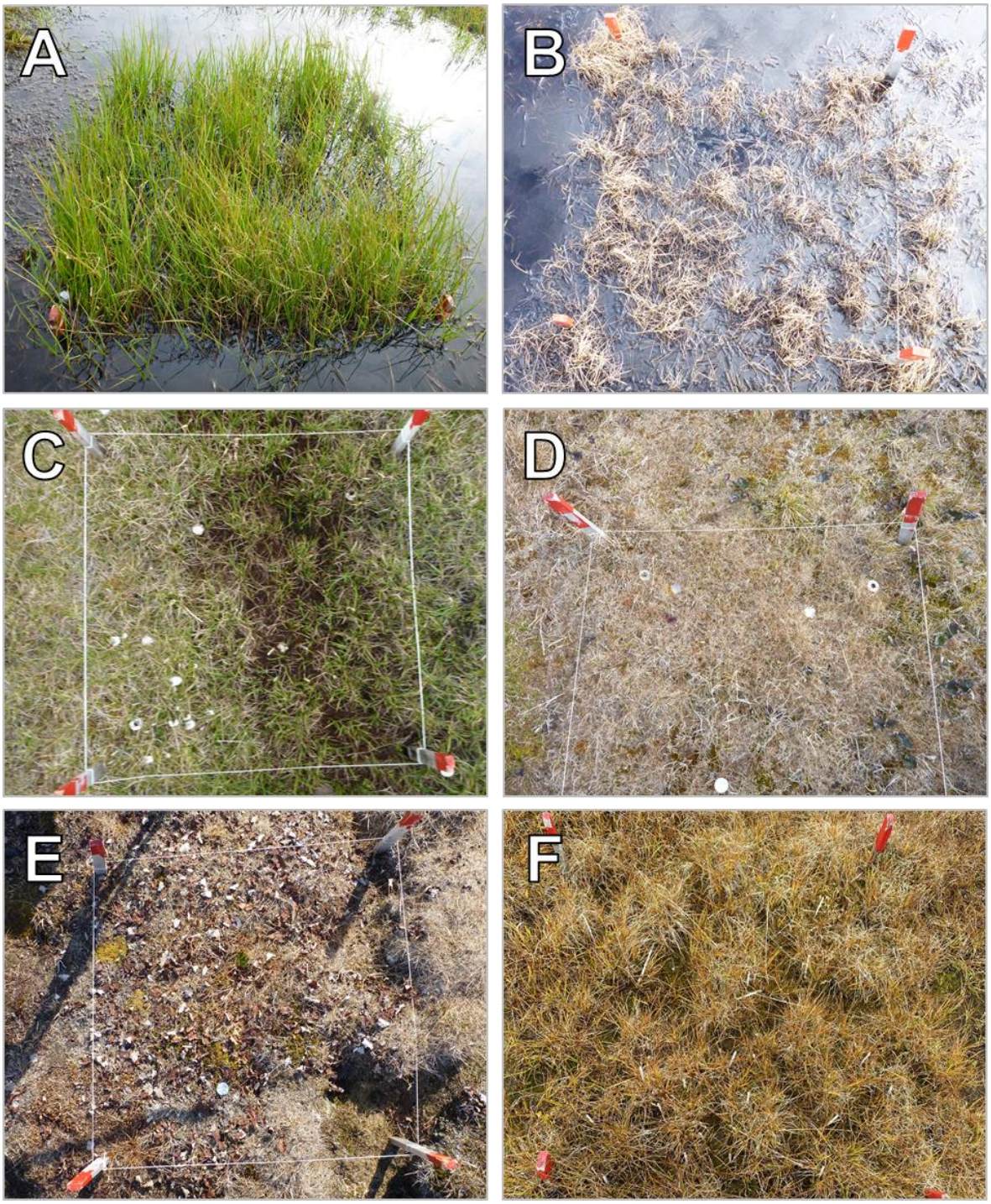

Figure 2.2. Examples of unacceptable plot images. The most common reasons to replace a plot image were (A) poor camera angle, (B) discoloration and edge distortion from direct sunlight, (C) blurriness, and (D) plot was not fully visible. If the plot was sampled too early (E) or too late in the season (F), then the images were not analyzed because the vegetation was not at peak greenness. Other issues with plot images include: missing plots, low resolution photographs, extensive areas of shadow (generally due to low solar angles and direct sunlight), and snow or standing water that obscures vegetation.

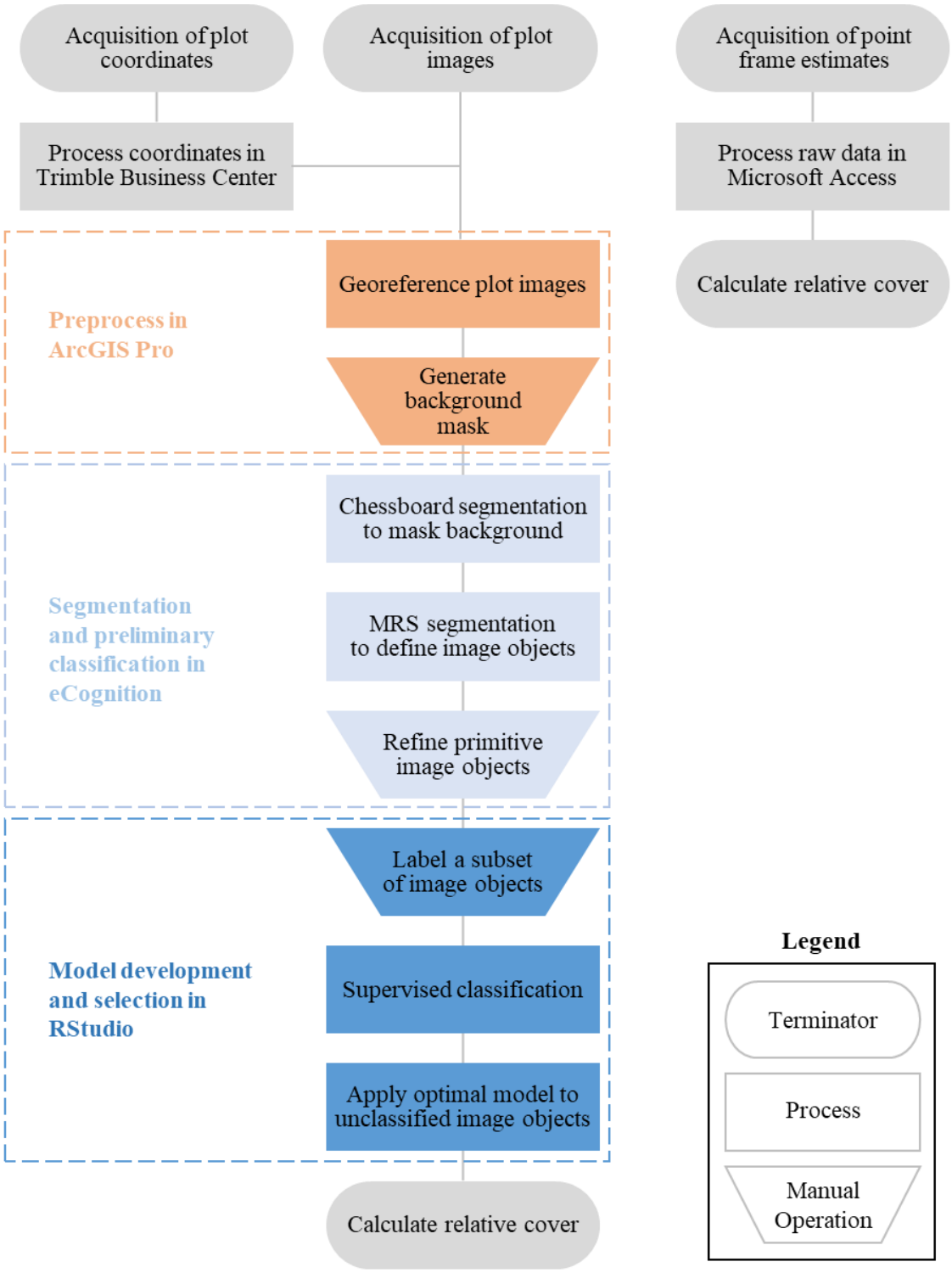

Figure 2.3. Schematic of the workflows for the plot photography (left) and point frame (right) vegetation sampling methods. The steps to process plot images were based on GEOBIA framework: data acquisition, preprocess plot images in ArcGIS Pro, segmentation and preliminary classification in eCognition, and model development and selection in RStudio. The results of image analysis are visualized in Supplemental Figures 2.S1, 2.S2, and 2.S3.

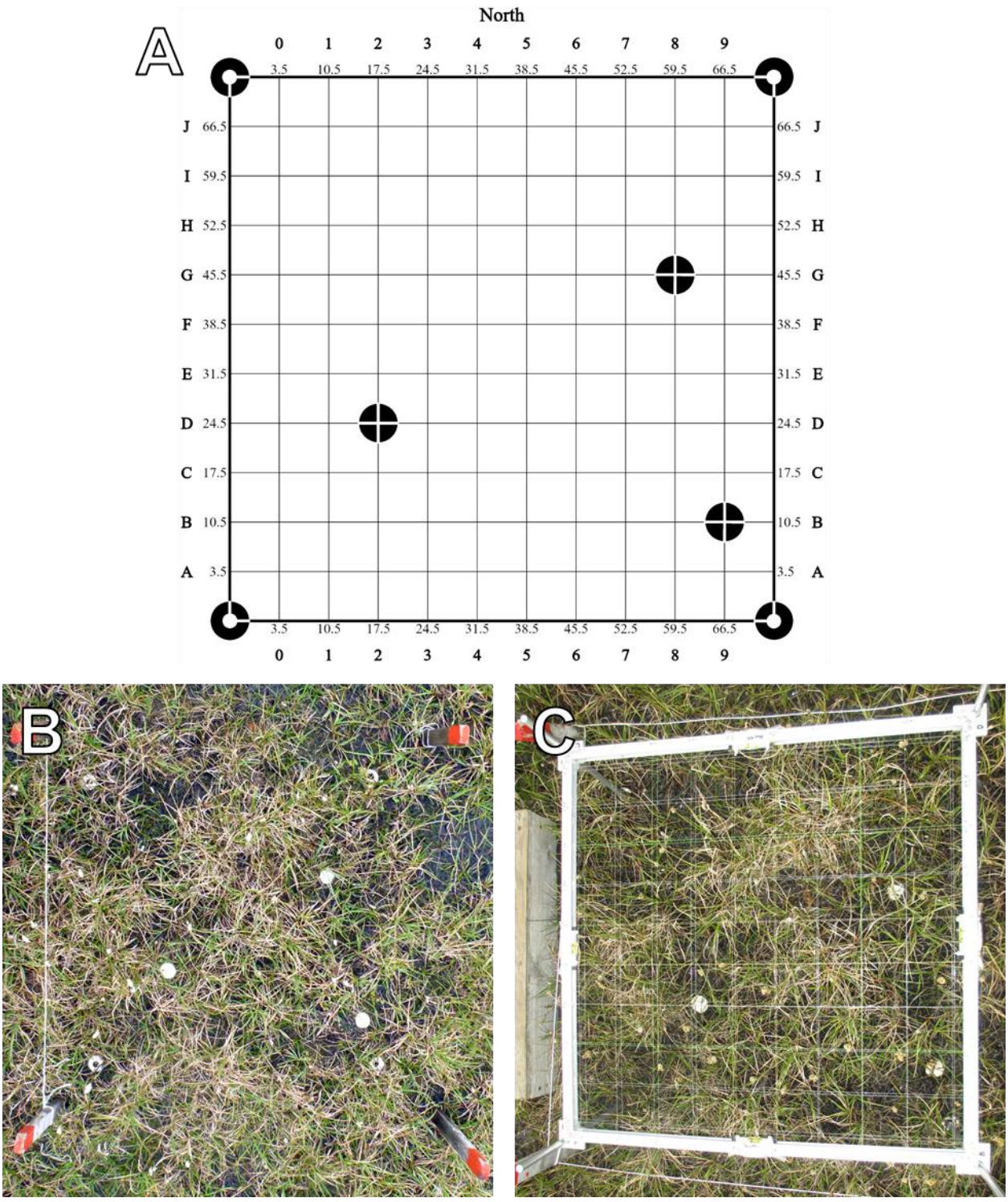

Figure 2.4. Image of a plot. (A) Field diagram shows the arrangement of the permanent tags in plot H2. (B) Plot H2 is photographed on July 30, 2013. The permanent tags in the plots, along with the corner stakes, were used to correct the orientation of the image during the georeferencing procedure. (C) The point frame was aligned using the permanent tags prior to point frame vegetation sampling on July 29, 2014.

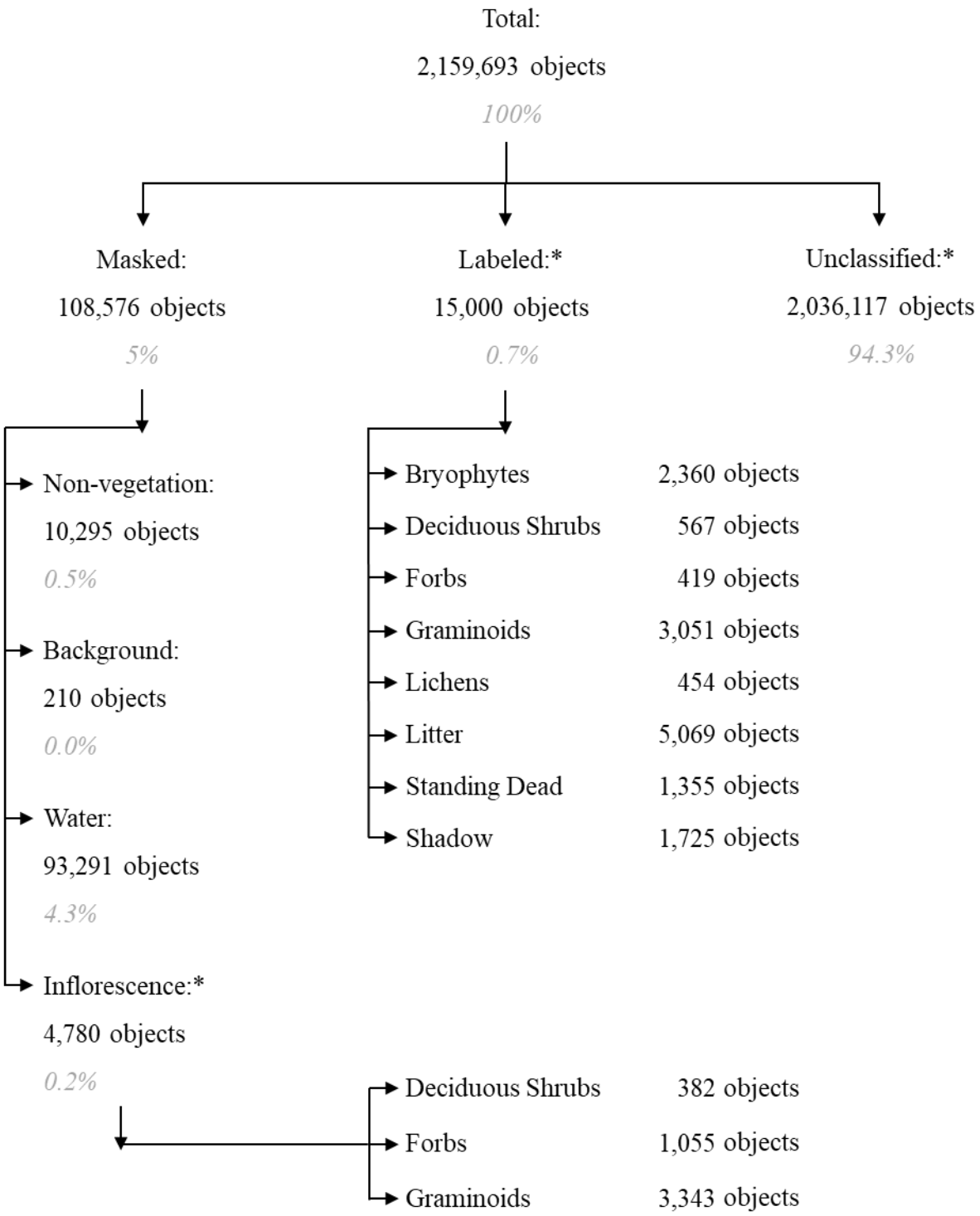

Figure 2.5. Overview of the total number of image objects. Image objects were partitioned into masked, labeled, and unclassified sets. Masked image objects were removed from analysis. Labeled image objects were used to train, validate, and test the models. Unclassified image objects were classified using the optimal machine learning classifier. Cover was calculated from the categories denoted by an asterisk (*).

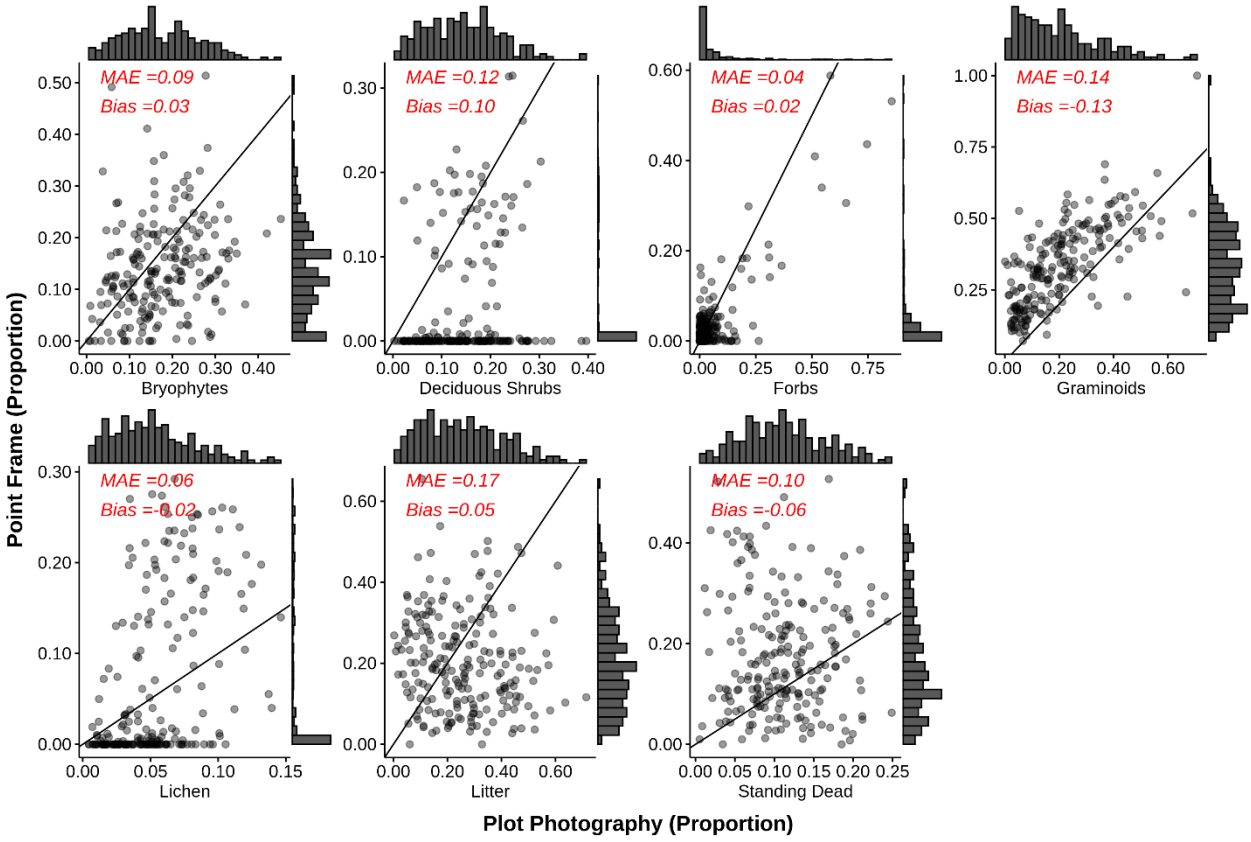

Figure 2.6. In-sample model performance of the raw data, which was based on direct substitution. Each panel shows a vegetation class. Each point shows the predicted proportion of a vegetation class in each plot at each time point. The y-axis relates to the observed point frame counts of abundance, while the x-axis relates to the image estimates. Histograms on each axis show the raw data distributions. Insets within each panel illustrate model performance using mean absolute error (MAE) and bias. The 1:1 reference line is included as a visual aid on all plots.

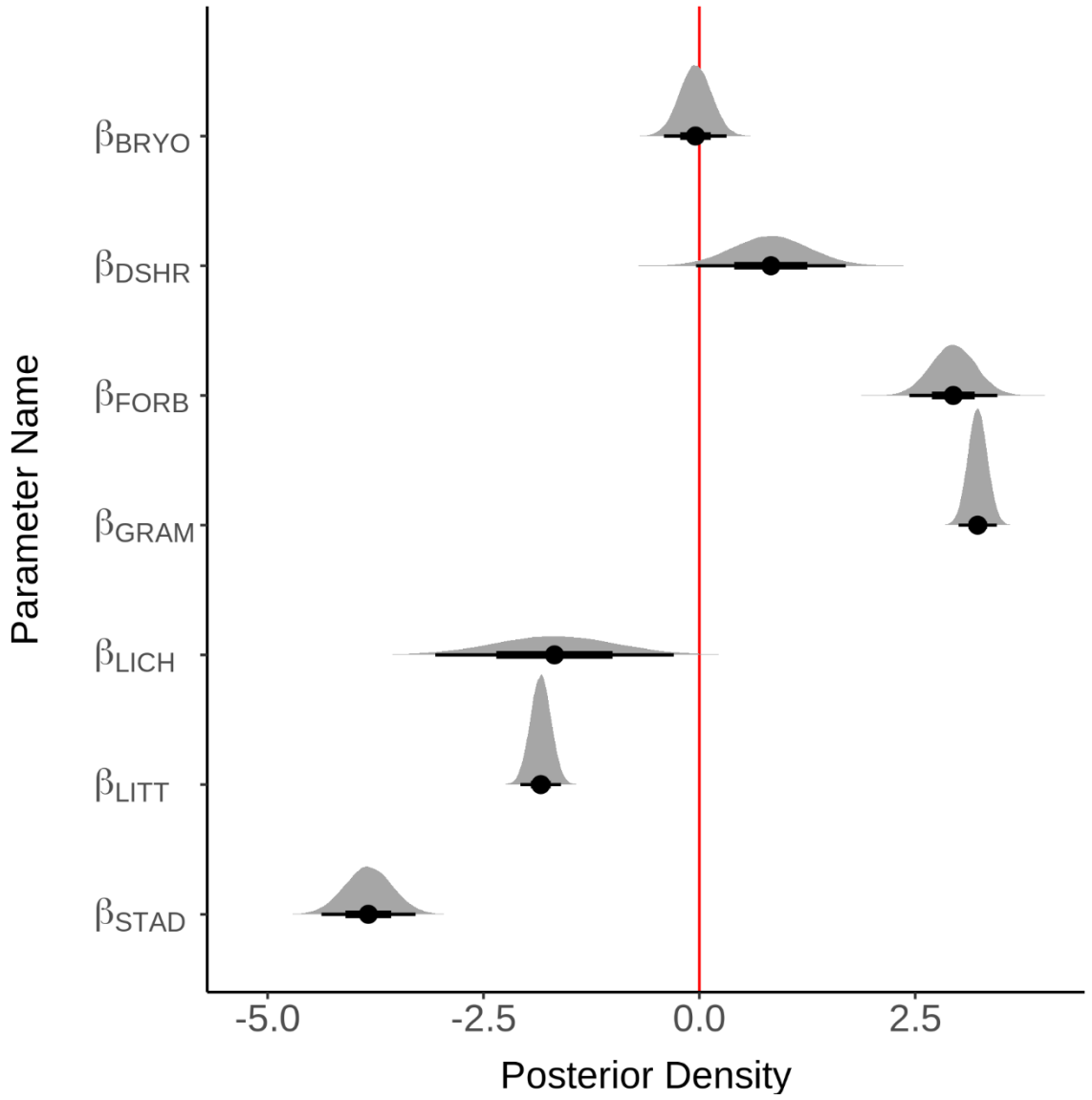

Figure 2.7. Parameter estimates shown for each vegetation class in the full model as evaluated by in-sample model performance. The credible interval is noted by a red vertical line. A distribution above the credible interval implies an analogous relationship between the two methods of sampling. A distribution below the credible interval implies an inverse relationship between the two methods of sampling. Bryophytes = BRYO; Deciduous Shrubs = DSHR; Forbs = FORB; Graminoids = GRAM; Lichens = LICH; Litter = LITT; Shadow = SHAD; Standing Dead = STAD.

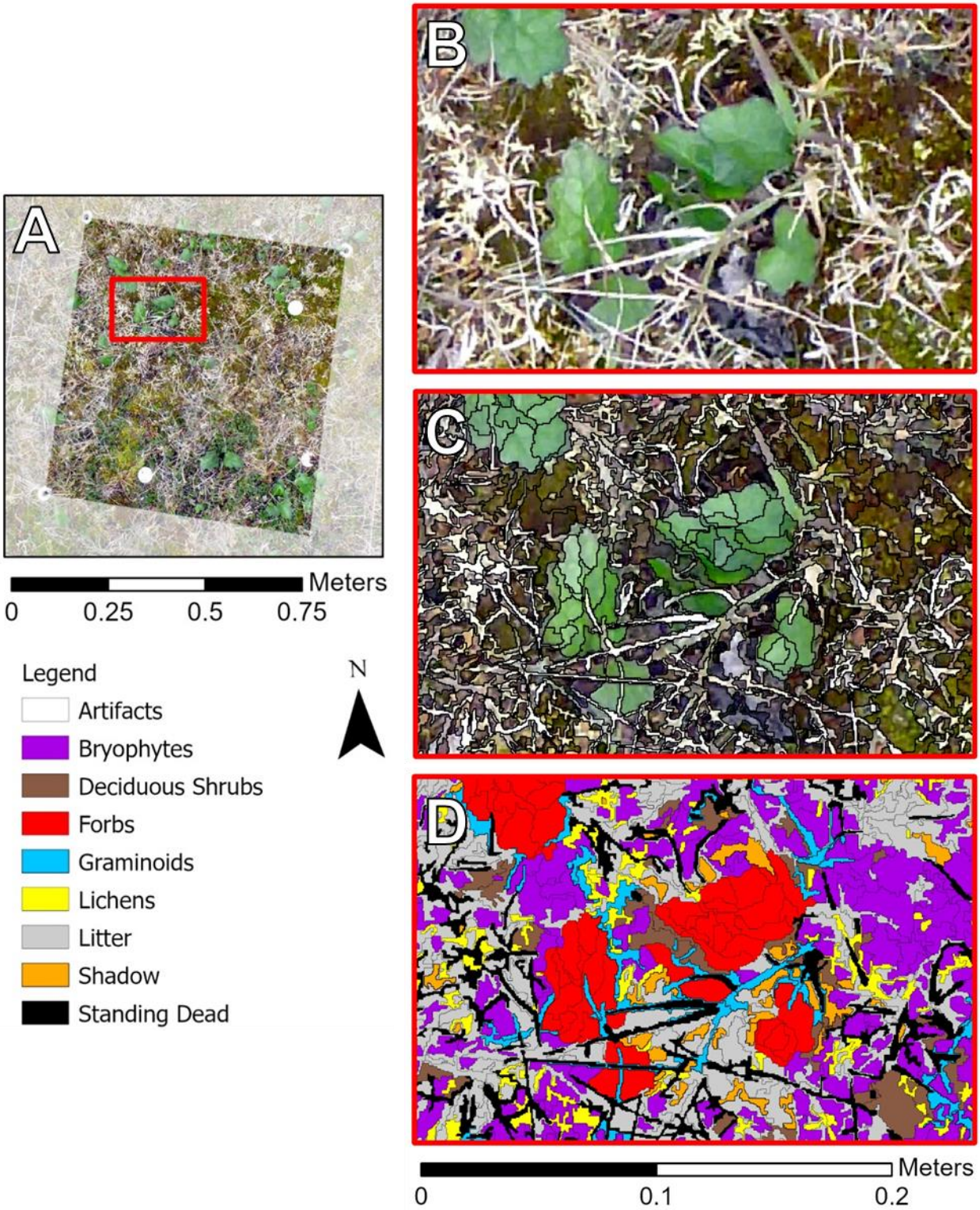

Supplemental Figure 2.S1. Example of the image segmentation and classification of a plot. (A) Extent of plot D2. Scale is increased to show the (B) vegetation in the plot, (C) primitive image objects as a result of multi-resolution segmentation, and (D) final classification of the image objects using the optimized random forest model.

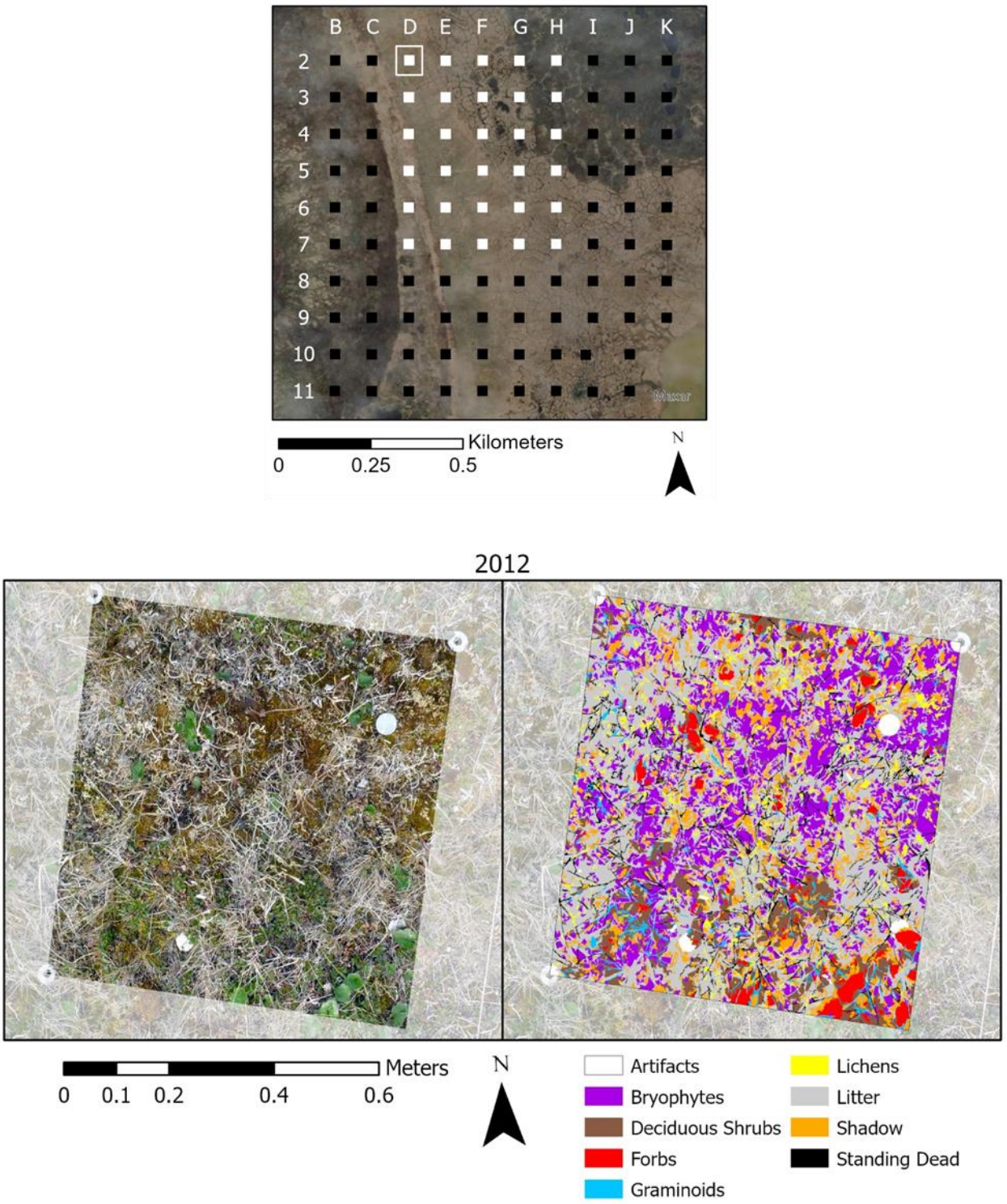

Supplemental Figure 2.S2. Classification of a non-inundated plot through time. (A) Location of plot D2 in the context of the research site. Left panels show plot photographs and right panels show the corresponding image classification across seven sampling years (2012, 2013, 2014, 2015, 2018, 2019, 2021).

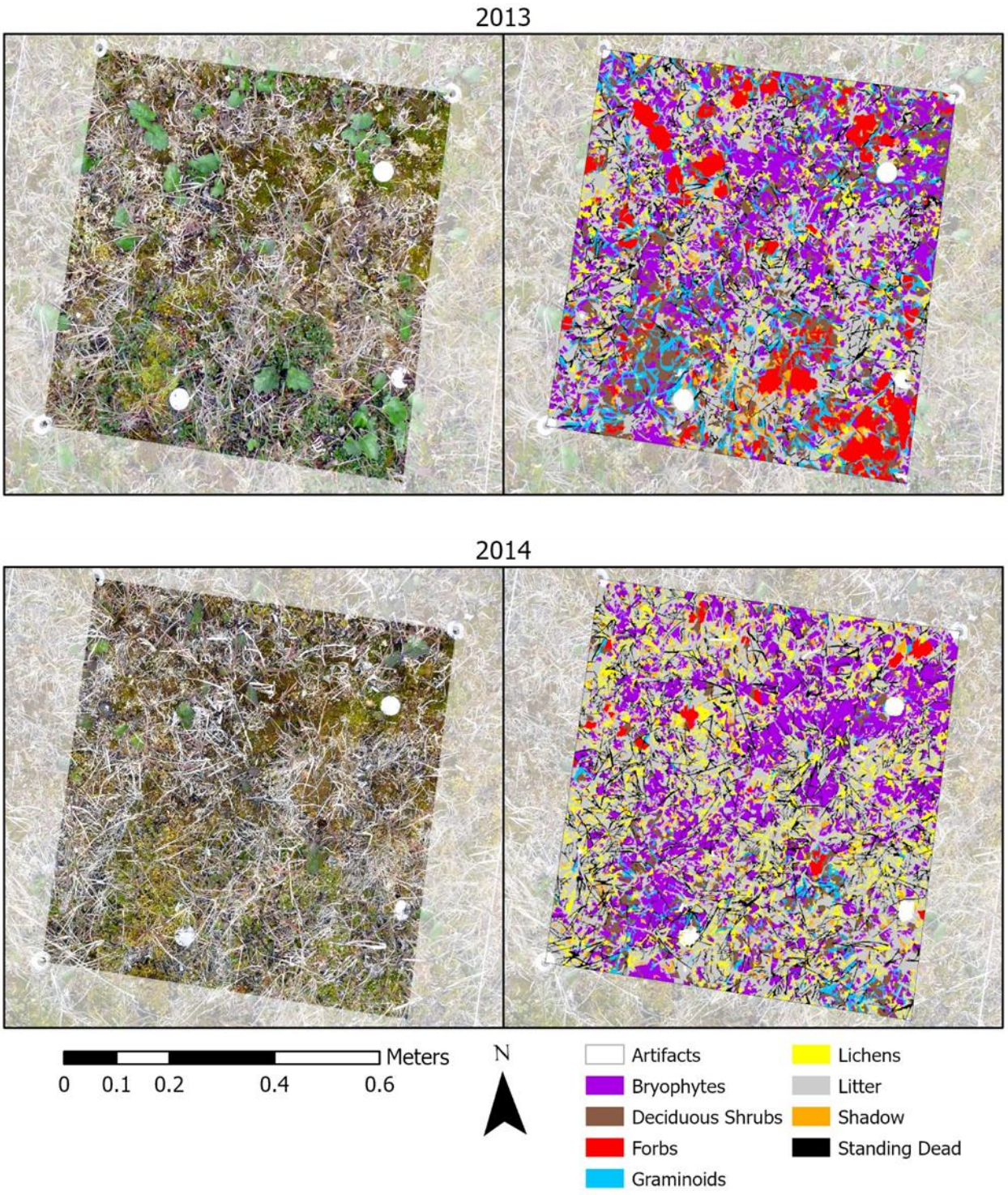

Supplemental Figure 2.S2. Continued…

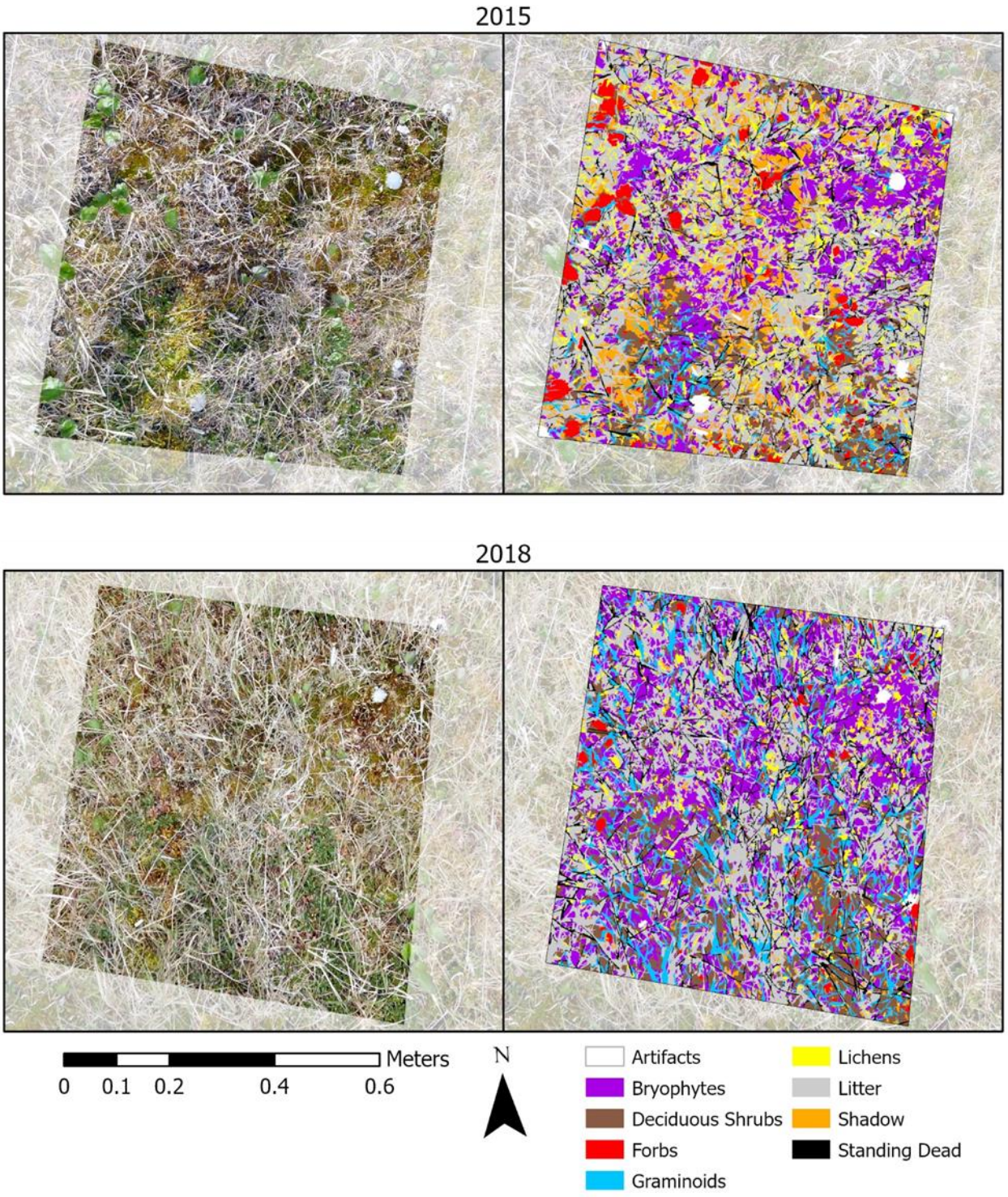

Supplemental Figure 2.S2. Continued…

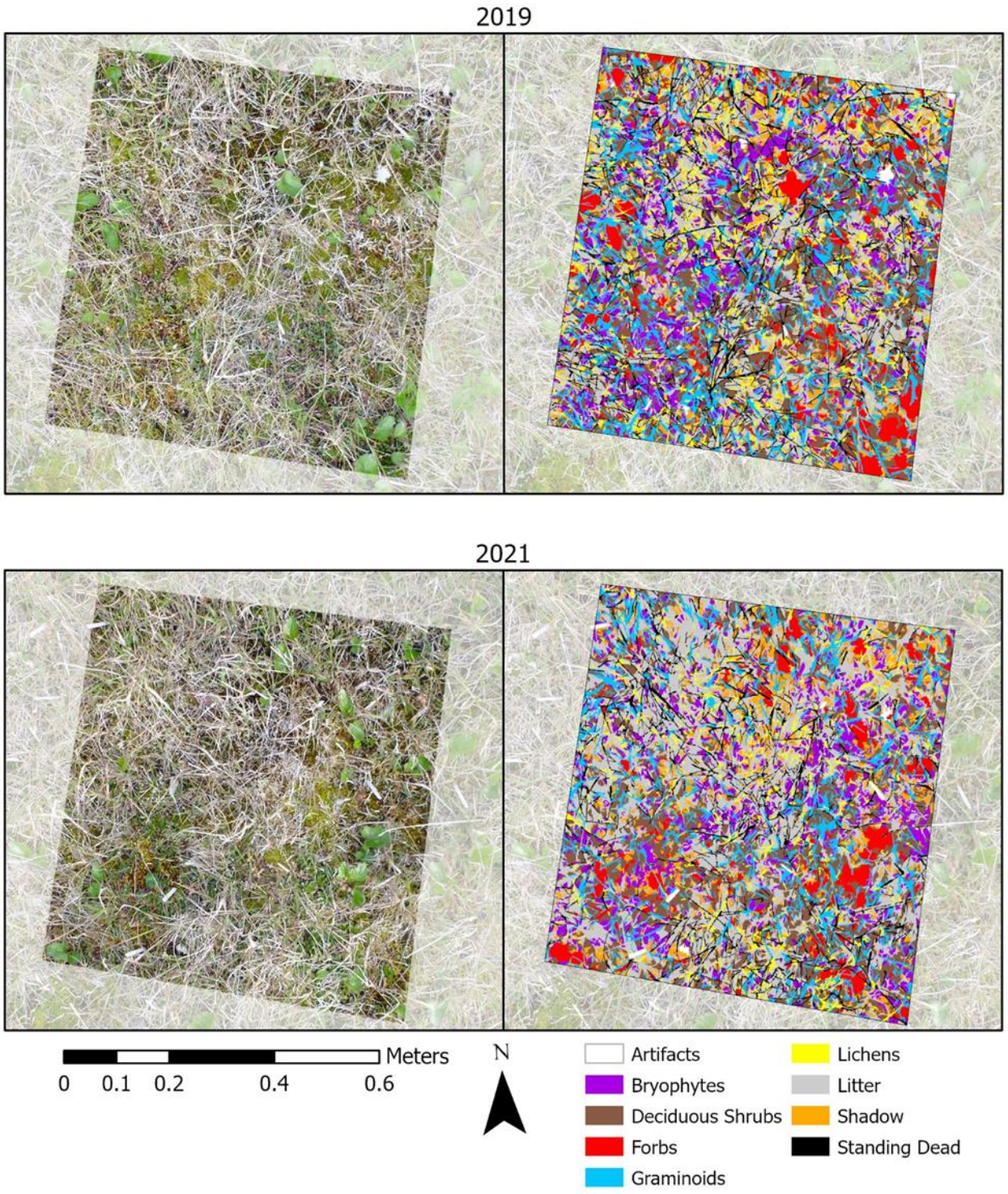

Supplemental Figure 2.S2. Continued…

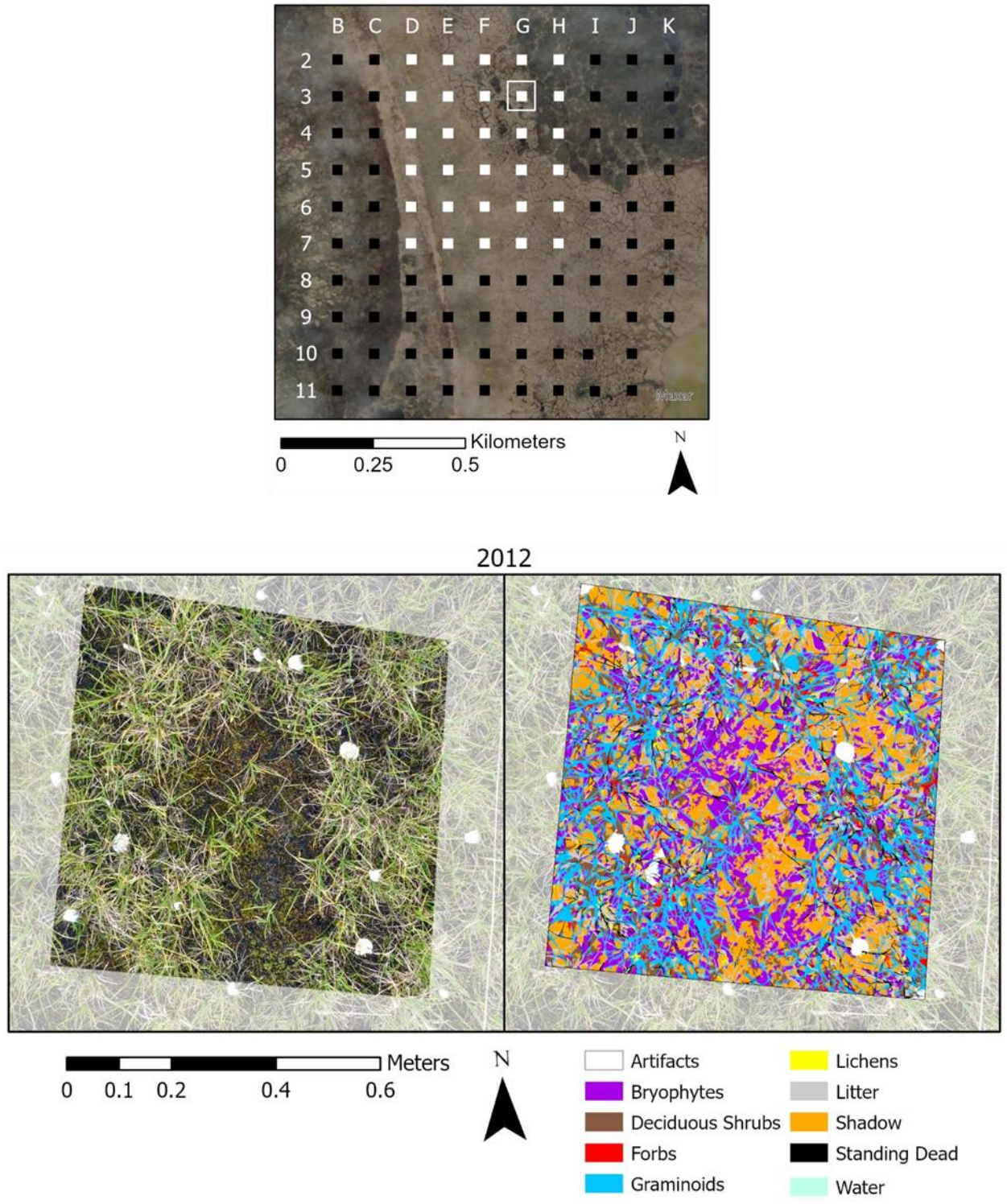

Supplemental Figure 2.S3. Classification of a frequently inundated plot through time. (A) Location of plot G3 in the context of the research site. Left panels show plot photographs and right panels show the corresponding image classification across seven sampling years (2012, 2013, 2014, 2015, 2018, 2019, 2021).

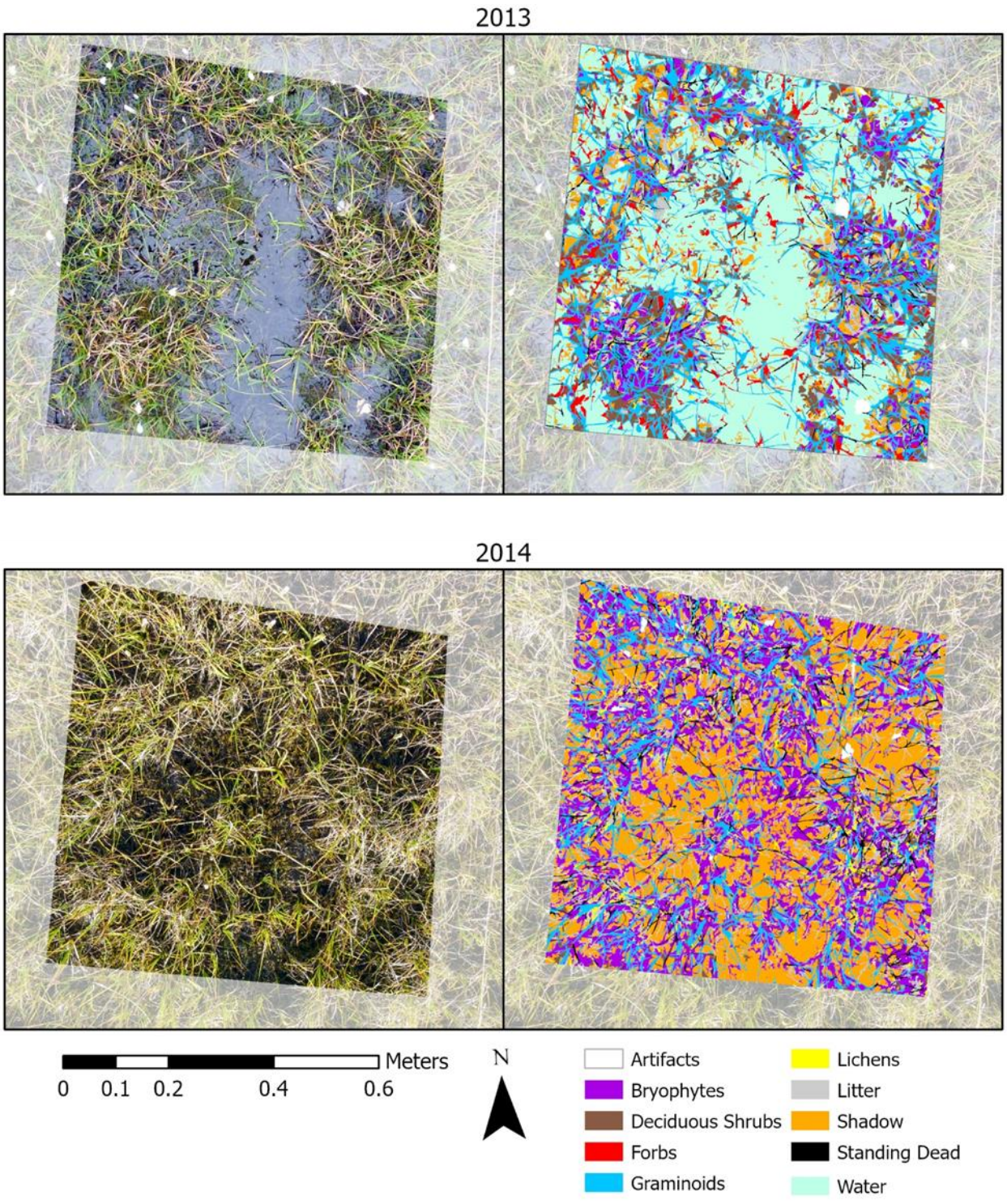

Supplemental Figure 2.S3. Continued…

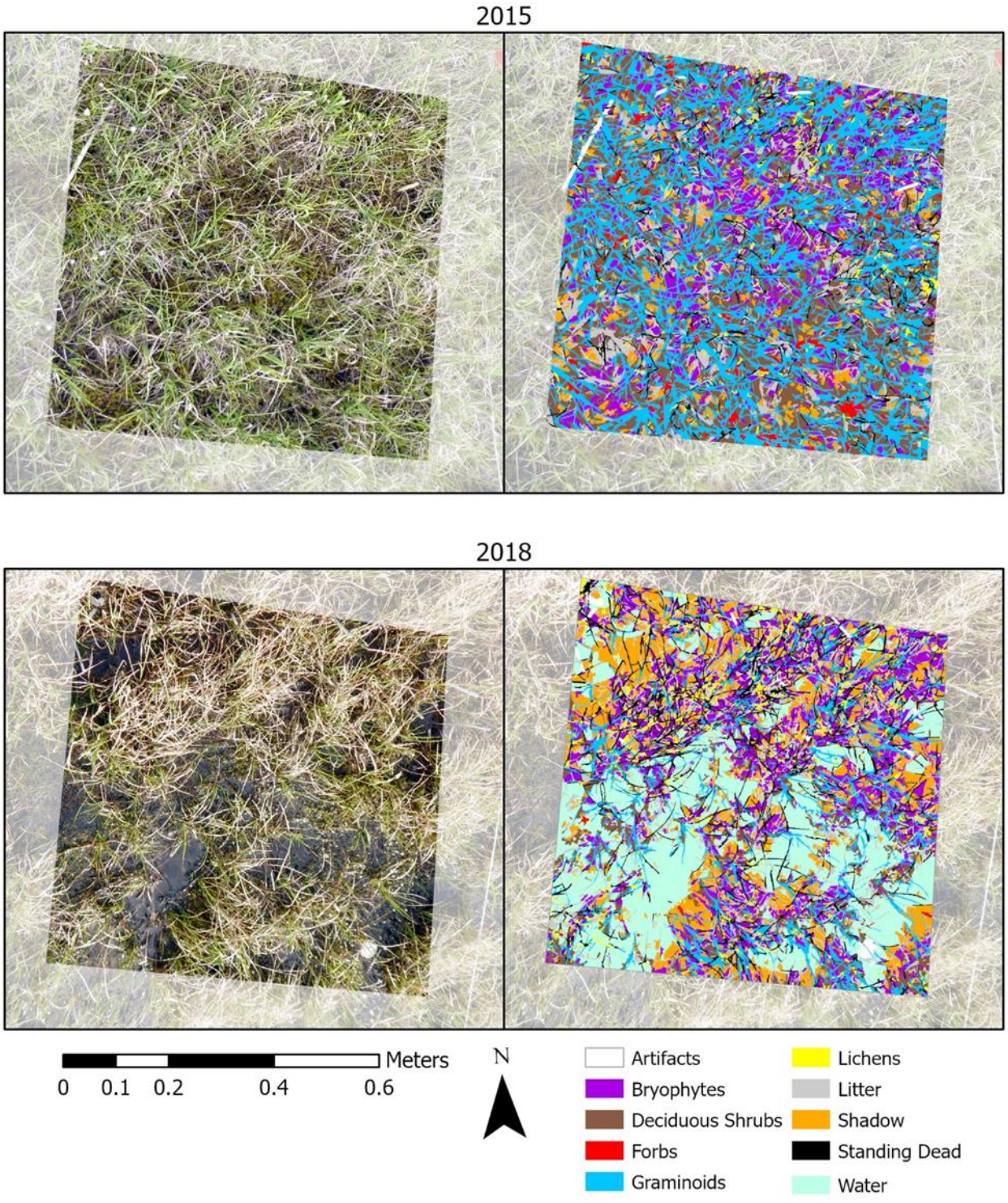

Supplemental Figure 2.S3. Continued…

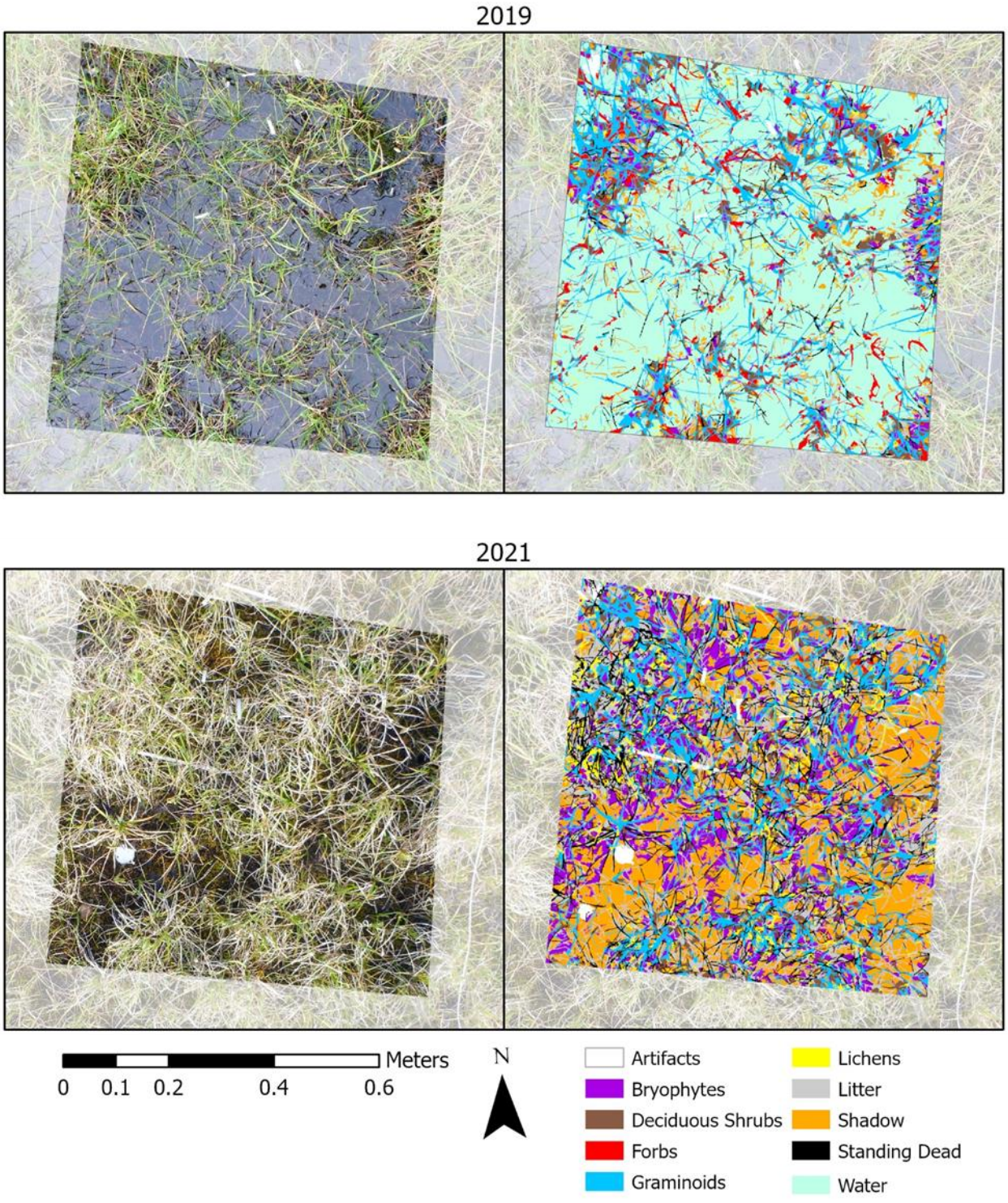

Supplemental Figure 2.S3. Continued…

Chapter 3

Extended Review of Literature

Global climate change is disturbing ecosystem structure and function (Allen et al., 2018). As the Arctic warms at an accelerated rate, Arctic ecosystems are undergoing widespread change (Chapin et al., 2005; Pearson et al., 2013). Over the last three decades, Arctic vegetation increased in height, and graminoid and shrub densities increased (Bjorkman et al., 2019; Epstein et al., 2013; Myers-Smith et al., 2019). Rising atmospheric levels of methane and carbon dioxide are attributed, in part, to permafrost thaw and collapse (Schuur et al., 2015). Sea ice, snow cover and glacial extent are also diminishing in a warming climate (Kowk, 2018; Rixen et al., 2022). As warming amplifies, we expect to see greater change in Arctic vegetation composition and structure, hydrologic processes and energy cycles with dire implications for global function and ecosystem services (Allen et al., 2018).

Vegetation plays a vital role in Arctic ecosystems (Chapin et al., 1996). Plants form the foundation of the Arctic food web and contribute to feedback mechanisms that may reinforce or diminish climatic shift (Chapin et al., 2005; Pearson et al., 2013). As the climate shifts, plants face three options: adapt, move or perish (Aitken et al., 2008). Alterations in dominant vegetation type, cover or density may affect community structure, nutrient cycling and ecosystem function in the Arctic (Epstein et al., 2013). Thus, it is critical to observe, explain and predict the complex effects of climate change on plant communities. Changing vegetation cover has global implications (Allen et al., 2018; Pearson et al., 2013; Post et al., 2019).

In situ field experiments have a long history in Arctic ecological research. Aboveground biomass sampling is precise but destructive, so this method cannot be applied to long-term monitoring studies. Visual cover estimation is non-destructive, but this method may suffer from

subjectivity based on the observer (Vittoz & Guisan, 2007). Although point frame sampling is less effected by errors than its non-destructive counterpart, this method is also time-consuming (Harris et al., 2021; May & Hollister, 2012). *In situ* field studies are particularly valuable to: provide precise terrestrial data at a fine-scale resolution, validate, or ground truth, imagery from different scales, calibrate sensors and maximize the knowledge from indigenous communities (Anderson et al., 2016; Healey et al., 2014; Myers-Smith et al., 2020). However, Arctic field studies pose logistical difficulties, which are compounded by high expense and limited spatiotemporal resolution. Although *in situ* field studies remain critical today, especially for sensor calibration and validation, the trend toward remotely-sensed spatial analyses continues (Beamish et al., 2020).

Remote sensing is a scientific field of study that uses sensors to observe, record and characterize distant objects by reflected (passive) or emitted (active) electromagnetic radiation (Tempfli et al., 2009). Standard optical sensors capture red, green, and blue wavelengths, or bands, which are visible to the human eye. Infrared and near-infrared sensors record bands that assist with classifying vegetation, but these are not visible to the human eye (Xue & Su, 2017). Broadband multispectral sensors capture electromagnetic wavelengths with several wide bands, while narrowband hyperspectral sensors capture wavelengths with hundreds of narrow bands (Goetz et al., 1985). Sensors may be affixed to remote-sensing platforms at the plot level (handheld digital photography, PhenoCams), low altitudes (drone), high altitudes (helicopter, fixed-wing plane) or spaceborne levels (satellite) (Tempfli et al., 2009).

Remote-sensing capabilities and platforms have expanded as technology improves over time (Beamish et al., 2020). Historically, traditional studies relied on satellite imagery to map land cover, identify vegetation classes and illustrate vegetation change in polar regions (Bunn &

Goetz, 2006; Stow et al., 2004). However, greater precision was needed to assess long-term trends and abrupt environmental change in the Arctic (Du et al., 2019). Arctic landscapes boast frequent cloud cover, low vegetation productivity, high biomass, shallow water bodies, uneven ice polygons and heterogenous snow melt, which makes remotely-sensed data, especially at aerial and satellite levels, more error-prone than other landscapes (Stow et al., 2004). Validation of remotely-sensed data is critical in the Arctic (Beamish et al., 2020; Du et al., 2019; Myers-Smith et al., 2020).

Recent studies have relied on PhenoCams or drones to resolve the spatiotemporal limitations of aerial or satellite platforms (Anderson & Gaston, 2013). Drones are less expensive, easy to use and offer a scale customizable by the operator. Drones became commercially available in 2005 (Marris, 2013). Due to high startup costs, there were very few users until abundance had increased and prices were lowered by 2015 (Nowak et al., 2018). Presently, drones are not widely used nor fully exploited in the Arctic (Du et al., 2019). Drones have been deployed to monitor geomorphological change in glacial valleys, which has helped capture changeable glacial patterns and eliminate the hassle of manned aerial surveys via manned aircraft (Bliakharskii et al., 2019; Ewertowski et al., 2019). Other preliminary polar studies explore sea ice extent, vegetation cover, and phenological patterns (Fraser et al., 2016; Malenovský et al., 2017; McPartland et al., 2019; Turner et al., 2019). There is great potential for drone usage in the Arctic (Nowak et al., 2018).

There is also great potential for plot photography in the Arctic. Vegetation cover and change over time has been successfully measured using high resolution, plot-level photographs in primarily temperate regions (Laliberte et al., 2007; Luscier et al., 2006; Michel et al., 2010; Wallace et al., 2019). Fewer studies have analyzed vegetation cover in plot-level photographs in

the Arctic or Antarctic using an object-based approach (Chen et al., 2010; King et al., 2020; Liu & Treitz, 2016). Plot-level photographs of Arctic vegetation could bridge the gap in observations across different scales. We expect that drones will become a more readily used tool in the Arctic, as there is an increasing need for geospatial information and integration across platforms, and plot-level photographs may be relied upon to validate this information (Du et al., 2019). We also expect advancements in satellite technology to continue to increase the resolution of readily available imagery (Shiklomanov et al., 2019). The integration of data across different platforms has become a critical focus of research in order to validate observations across different scales (Beamish et al., 2020; Du et al., 2019; Myers-Smith et al., 2020).

Improvements in the resolution and frequency of images, in addition to greater computational power available to researchers, have expanded the ways in which images can be analyzed (Blaschke & Strobl, 2001; Hay et al., 2001). Images may be evaluated using pixel-based analysis or GEographic Object-based Image Analysis (GEOBIA), or more generally, object-based image analysis (OBIA). Images are made of many pixels, therefore pixels determine the scale of an image and how a landscape can be understood and modeled (Marceau, 1999; Strahler et al., 1986). In pixel-based analysis, each pixel is examined and classified in isolation from neighboring pixels. In GEOBIA, groups of homogeneous pixels are delineated, built into objects, and analyzed (Hay & Castilla, 2008, 2006; S. Lang, 2008).

Pixel-based analysis is often successful on coarse resolution imagery, which aligned well with the data acquired from satellites launched in the 1980's to 2000's (Blaschke et al., 2014). Historically, satellite imagery was not fine enough to warrant an exact analysis (Landsat: 30 m^2; MODIS: 500 m^2). In coarse resolution imagery, one pixel may contain multiple features, so it is best to categorize these mixed pixels by their dominant spectral signature (Congalton & Green,

2009). This method has proven reliable in images depicting urban and agricultural landscapes, where features are uniform and easy to distinguish using high contrast spectral signatures (S. Lang, 2008; Platt & Rapoza, 2008). It is not as effective in high resolution imagery, where multiple pixels may contain one feature (Aplin, 2006; Chen et al., 2012). Very high resolution (VHR) satellite imagery, where the pixel resolution is greater than 5 m, renders traditional pixel-based analysis inadequate (Blaschke et al., 2014; Chen et al., 2012; Hussain et al., 2013).

GEOBIA is gaining momentum as imagery increases in spatiotemporal resolution (Blaschke, 2010; Blaschke et al., 2014; Dronova, 2015; Kucharczyk et al., 2020; Ma et al., 2017). As long as the images are high resolution, such that the objects of interest are three to five times larger than the number of pixels in the object, then this approach can be confidently applied. High resolution imagery generally contains more noise than low resolution imagery. Classifying objects, rather than pixels, may decrease the noise in high resolution images (Blaschke et al., 2014). Ancillary data, such as shape and texture, and expert knowledge from the user may improve the precision of object-based method of analysis (Blaschke et al., 2000; Platt & Rapoza, 2008). Textural, geometric, contextual features and expert knowledge from the user can be included for improved classification accuracy (Platt & Rapoza, 2008).

Arctic vegetation is a particular challenge for image analysis due to small vegetation species and structure, diverse composition, and low spectral contrast within vegetation communities (Buchhorn et al., 2013; Davidson et al., 2016; Schapeman-Strub et al., 2009). However, GEOBIA has been successful in classifying images with high spatial but low spectral resolution (Blaschke et al., 2014; Halabisky et al., 2011; Husson et al., 2016; Laliberte & Rango, 2011). GEOBIA has been implemented less frequently on plot-level photographs of Arctic

vegetation (Chen et al., 2010; King et al., 2020; Liu & Treitz, 2016). There is great potential to expand the application of GEOBIA in the Arctic.

Remote sensing greatly contributes to our understanding of historical interactions, processes, and change across landscapes (Epstein et al., 2012). As we seek to understand the effects of a warming climate on Arctic vegetation, remote sensing and image analysis remain important tools for observing vegetation trends at varying scales (Dronova, 2015; Phiri & Morgenroth, 2017; Torres-Sánchez et al., 2015). The shift from pixel-based to object-based image analysis is more likely permanent as technology continues to improve, yielding high resolution images (Blaschke et al., 2014). An object-based approach is promising, but it has not been thoroughly tested on plot-level photographs in the Arctic to analyze vegetation cover and change. Plot-level photographs may help understand the complexities of changing vegetation in response to climate change.

Extended Methodology

ITEX-AON History

The International Tundra Experiment (ITEX) was established by an assembly of Arctic researchers in 1990 (Webber & Walker, 1991). ITEX established a warming experiment using open-top chambers (OTCs) to preview the effects of warmer temperature on Arctic vegetation. An open-top chamber passively raises the temperature within a vegetation plot from 1 to 3°C (Henry & Molau, 1997; Hollister et al., 2006). The ITEX experimental design generally included an even number of control and treatment (OTC) plots across different habitat types in the Arctic. The direction of early research focused on measuring vegetation growth, abundance, productivity, and response to warming. Protocols were developed and shared (Molau & Mølgaard, 1996), which have made it an important network over time (Fraser et al., 2012). Repeat measurements of vegetation at the plot level across Arctic sites allows for synthesis studies to examine general vegetation trends across space and time (Arft et al., 1999; Elmendorf, Henry, Hollister, Björk, Bjorkman, et al., 2012; Oberbauer et al., 2007; Walker et al., 2006). Research has since expanded to examine shifts in phenology or community assemblages, intraspecific trait variation, and carbon release. Since the establishment of ITEX over thirty years ago, collaboration continues across the network, where ongoing research efforts are shared at workshops, annual (or biennial) conferences, and site visits.

The International Tundra Experiment – Arctic Observing Network (ITEX-AON) is a collaborative group of ITEX researchers based in the United States of America. ITEX-AON is currently comprised of Grand Valley State University (GVSU), University of Texas at El Paso (UTEP), Florida International University (FIU), and University of Alaska Anchorage (UAA). Four research sites are maintained and monitored on the North Slope of Alaska: Utqiaġvik,

Atqasuk, Toolik Lake, and Imnaviat Creek (Figure 3.1). This network is funded primarily by the Arctic Observing Network (AON) program by the National Science Foundation, which was established as the primary source of funding in 2006 (awards: 0856516, 1432277, 1504224, 1836839). All data are published through the Arctic Data Center. Supplemental data from this thesis are provided (Supplemental Figures 3.1-3.3).

Measurements are generally bounded by the Arctic System Science (ARCSS) grids at each research site, which span 1-km^2. The ARCSS sampling grids were established in the early to mid-1990's and funded by the Arctic System Science (ARCSS) Program of the National Science Foundation (Brown et al., 2000). Each grid contains 100 sampling points which are evenly spaced across 1-km^2. The ARCSS grid at Utqiaġvik, Alaska contains 98 vegetation plots corresponding to 98 sampling points. 30 vegetation plots are sampled annually using point frame-based sampling. A number of other vegetation-based measurements, including measures of phenology, height, and reproductive capacity, are also recorded throughout the field season. The vegetation plots are photographed using a standard handheld camera at the plot level and an unmanned aerial vehicle, or drone, at an elevation of 80 to 100 m. Soil temperature, thaw depth, and hyperspectral reflectance are also recorded at the plot level throughout the field season.

Each of the four research sites also contains a long-term warming experimental design (ITEX), a mobile-instrumented sensor platform (MISP), and a climate data tower, which monitors environmental data on a daily basis. ITEX plots are divided into two habitat types at each research site. Dry heath and moist acidic sites are stationed at Utqiaġvik, while dry heath and wet meadow sites are stationed at Atqasuk. Each ITEX site has an equal number of control and experimentally warmed vegetation plots. Open-top chambers are installed at the start of the

field season in early June. These are removed before steady snowfall begins, usually in late August.

The mobile-instrumented sensor platform (MISP) spans a 50-meter transect at Utqiaġvik, Atqasuk, Toolik Lake, and Imnaviat Creek. Spectral data are collected daily along the transect, although technical difficulties and poor weather frequently interrupt data collection at Utqiaġvik and Atqasuk. Oblique photographs are captured on an hourly basis by a PhenoCam affixed to the existing MISP infrastructure. Annual light detection and ranging (LiDAR) scans are also captured along this transect, providing information on the plant canopy and subsidence or heave from underlying permafrost. Kite aerial photography transitioned permanently to drone photography in 2018.

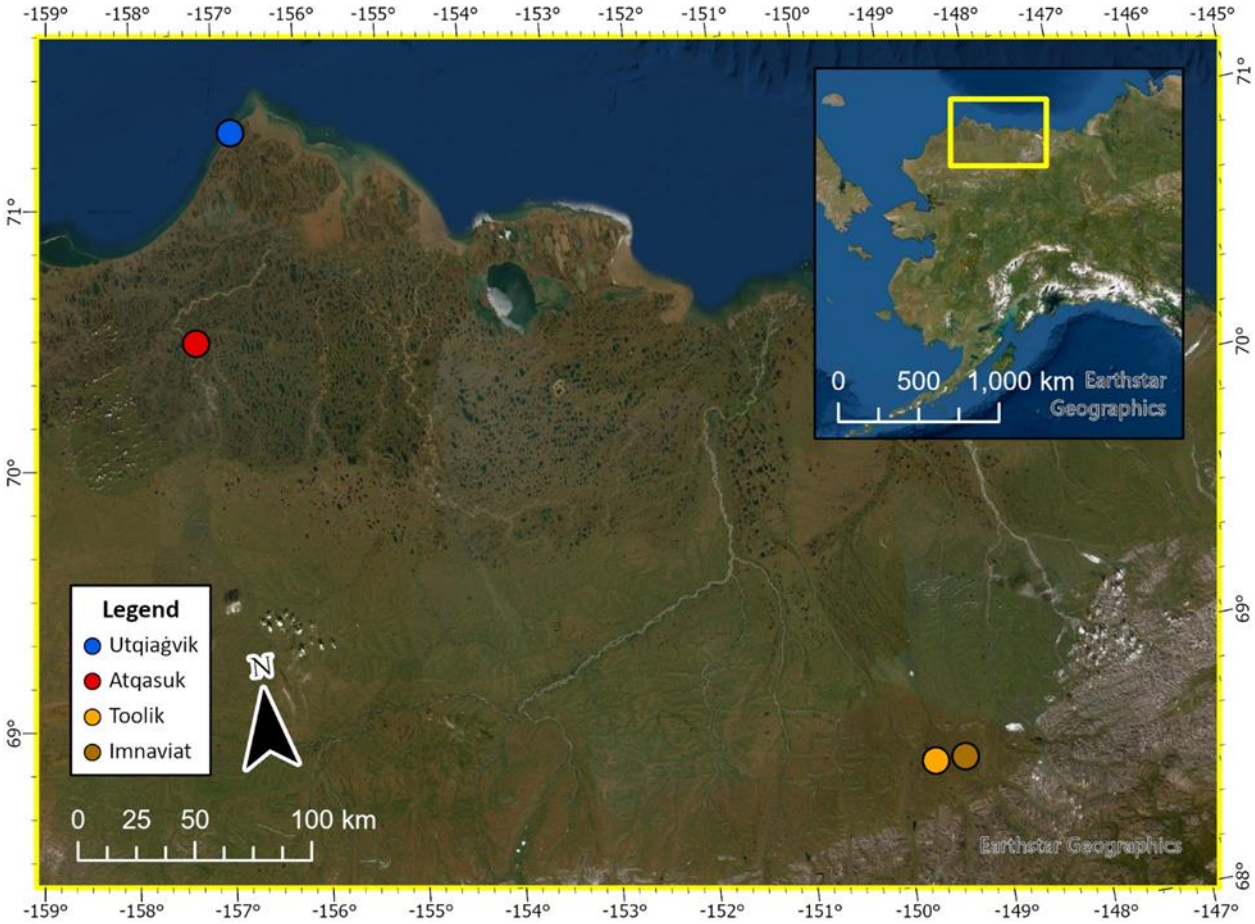

Figure 3.1. Four research sites are maintained and monitored by ITEX-AON on the North Slope of Alaska: Utqiaġvik (blue), Atqasuk (red), Toolik Lake (light yellow), and Imnaviat Creek (dark yellow).

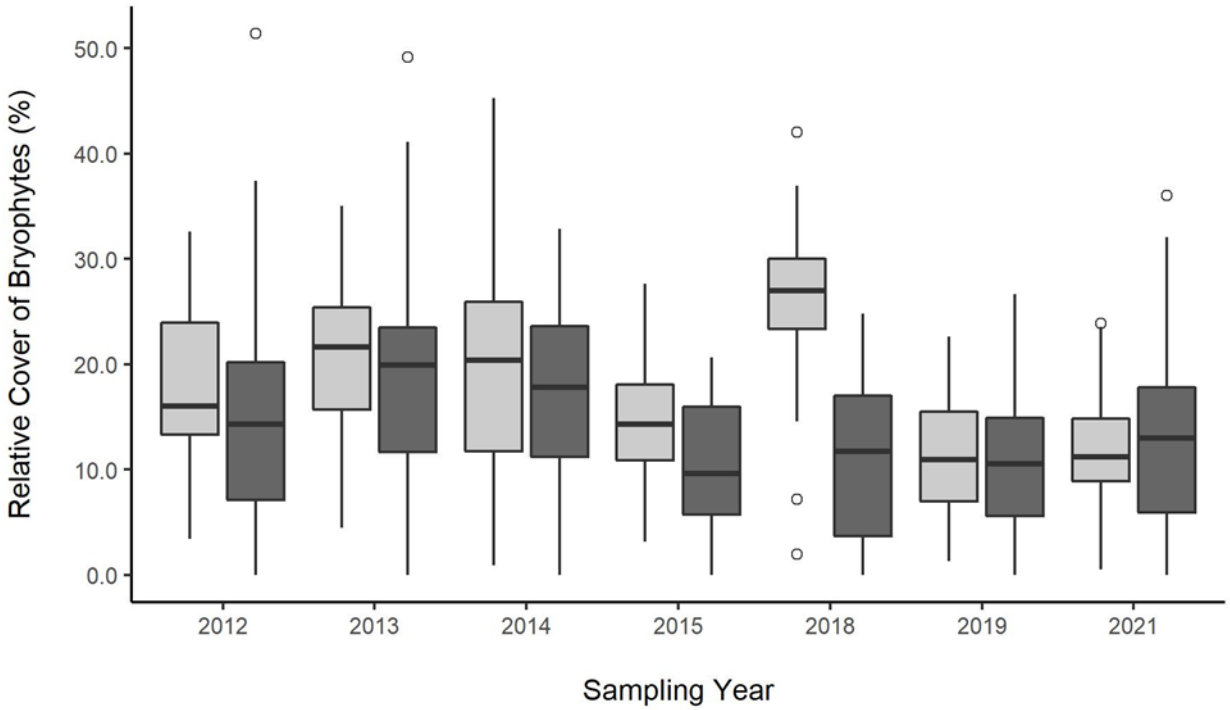

Supplemental Figure 3.S1. Box and whisker plots showing the relative cover of each growth form across seven sampling years. Image estimates are shown in light gray, while point frame estimates are shown in dark grey (n = 30 plots).

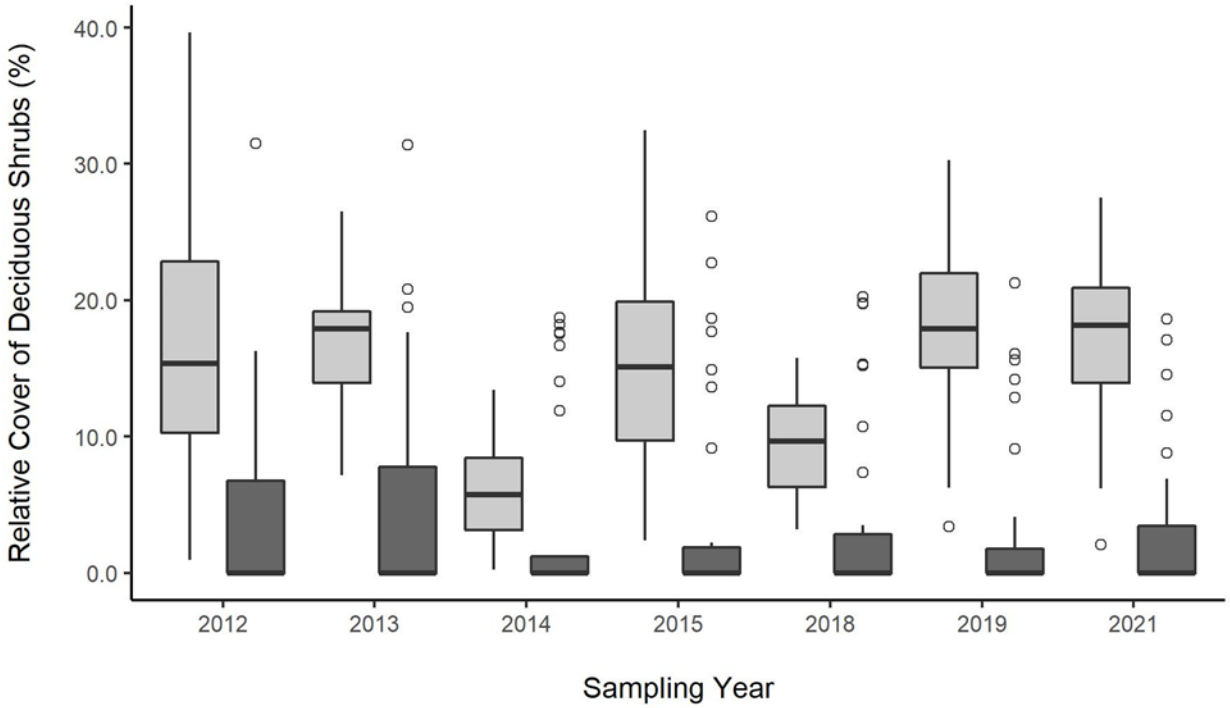

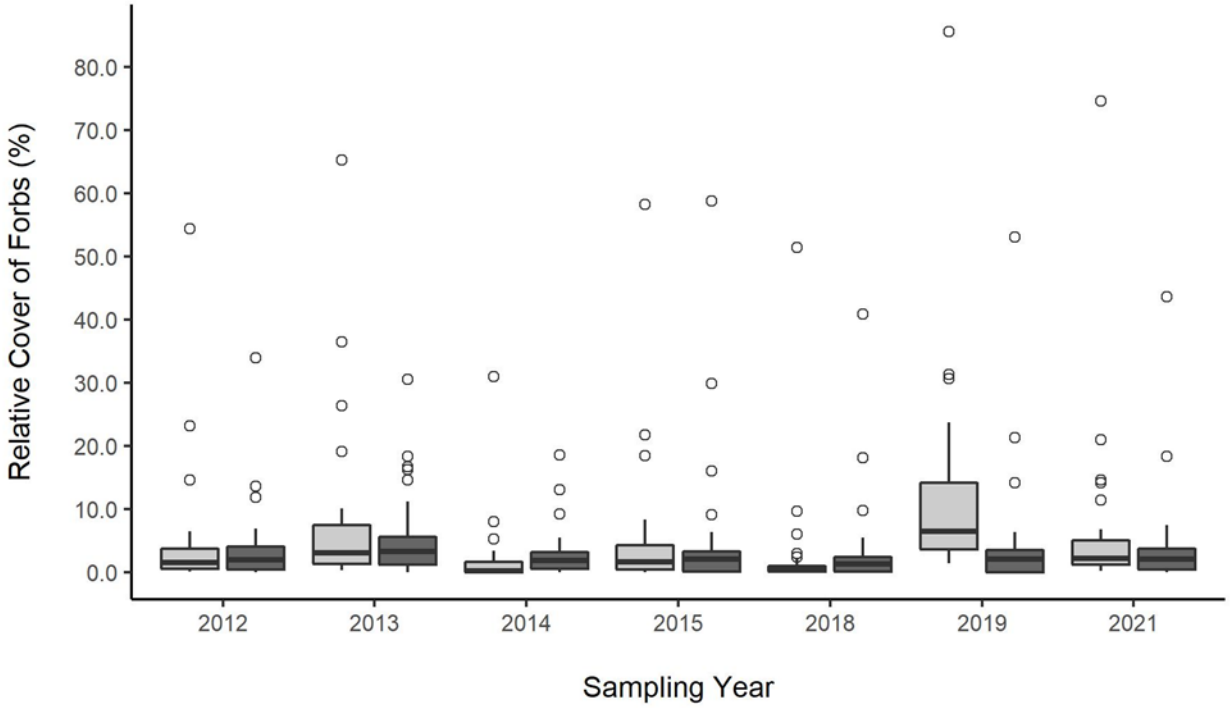

Supplemental Figure 3.S1. Continued…

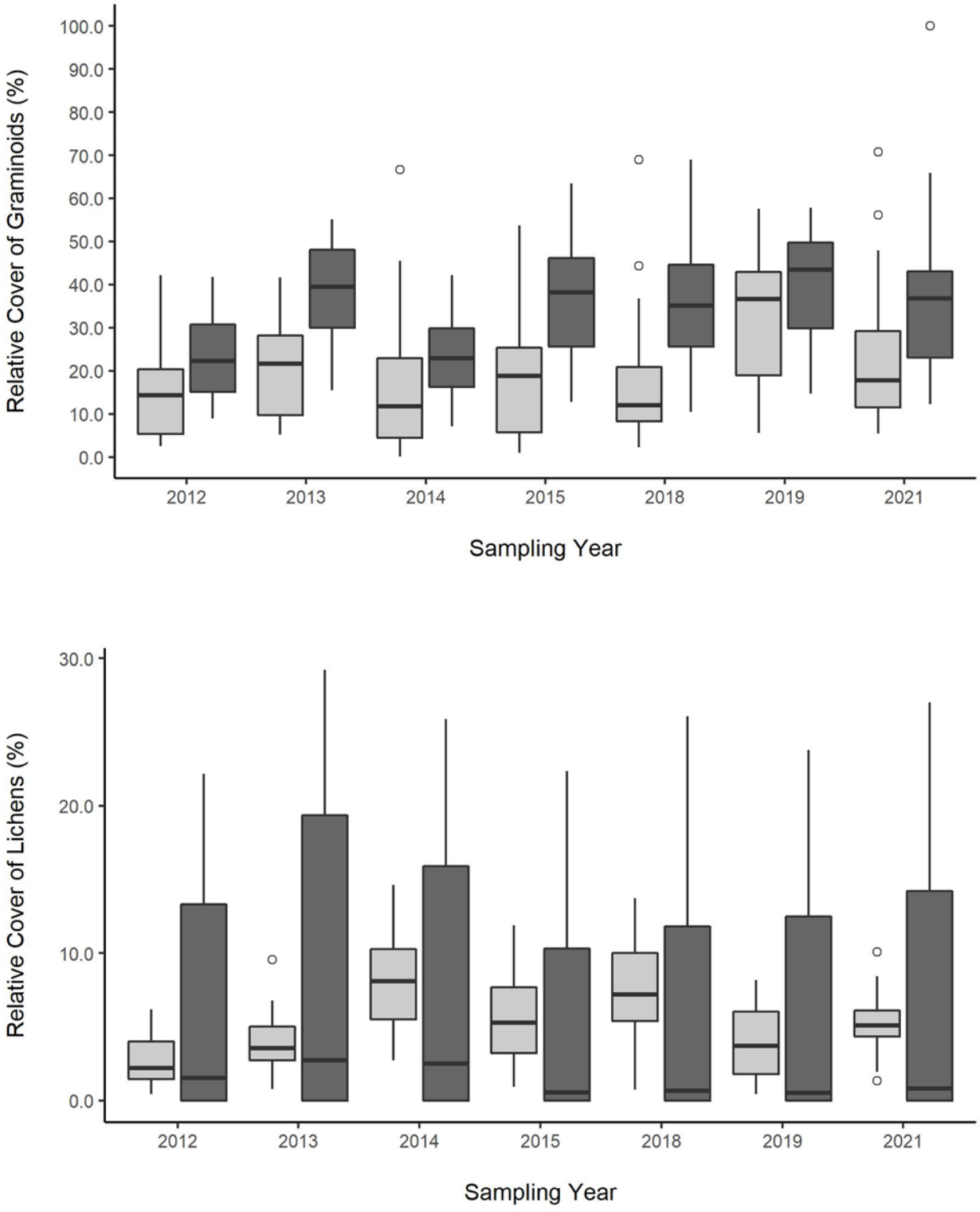

Supplemental Figure 3.S1. Continued…

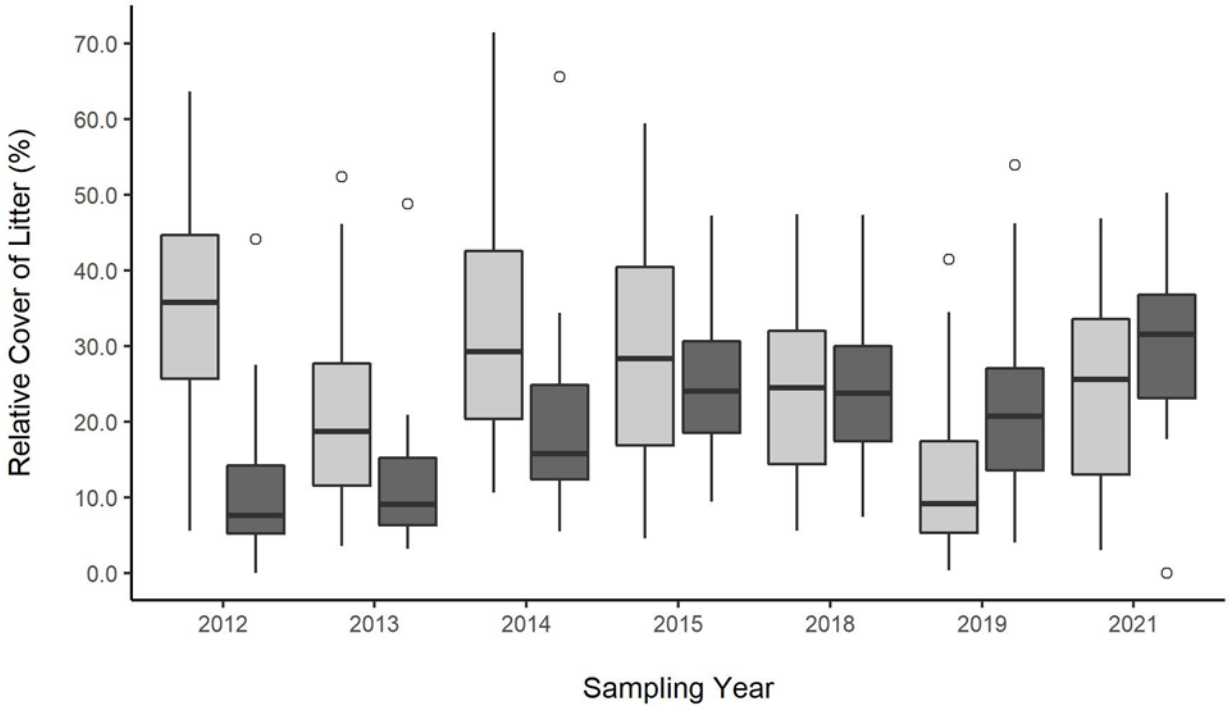

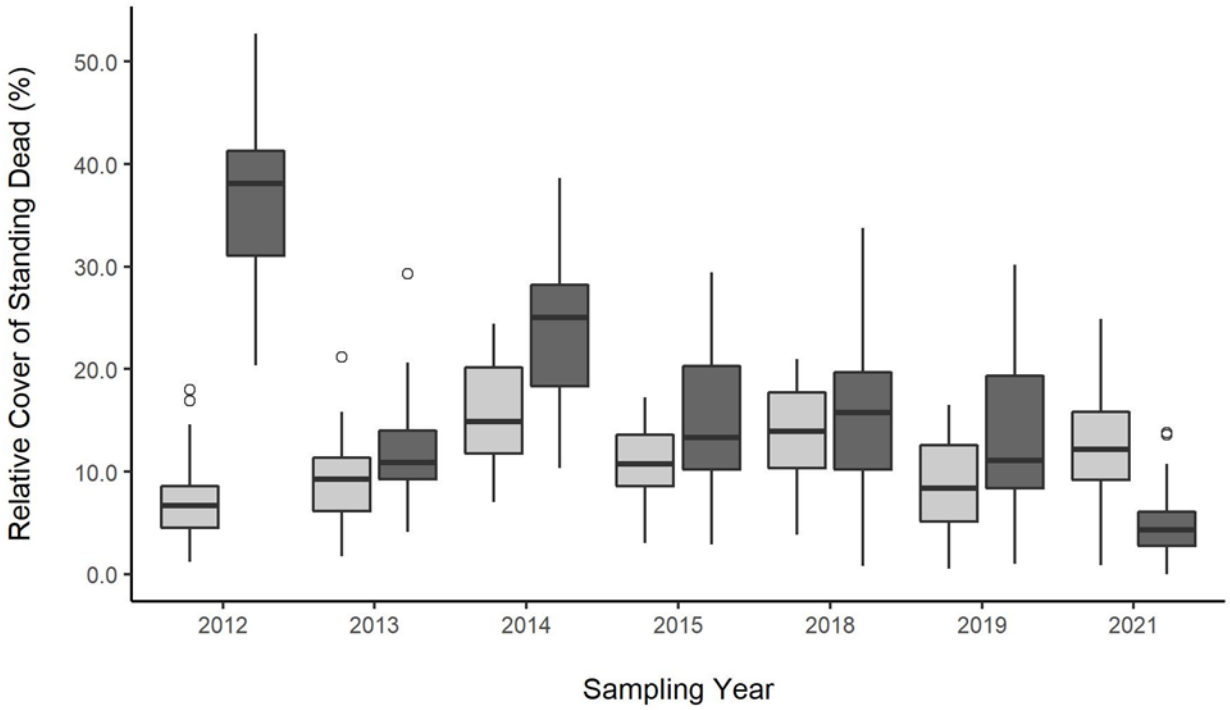

Supplemental Figure 3.S1. Continued…

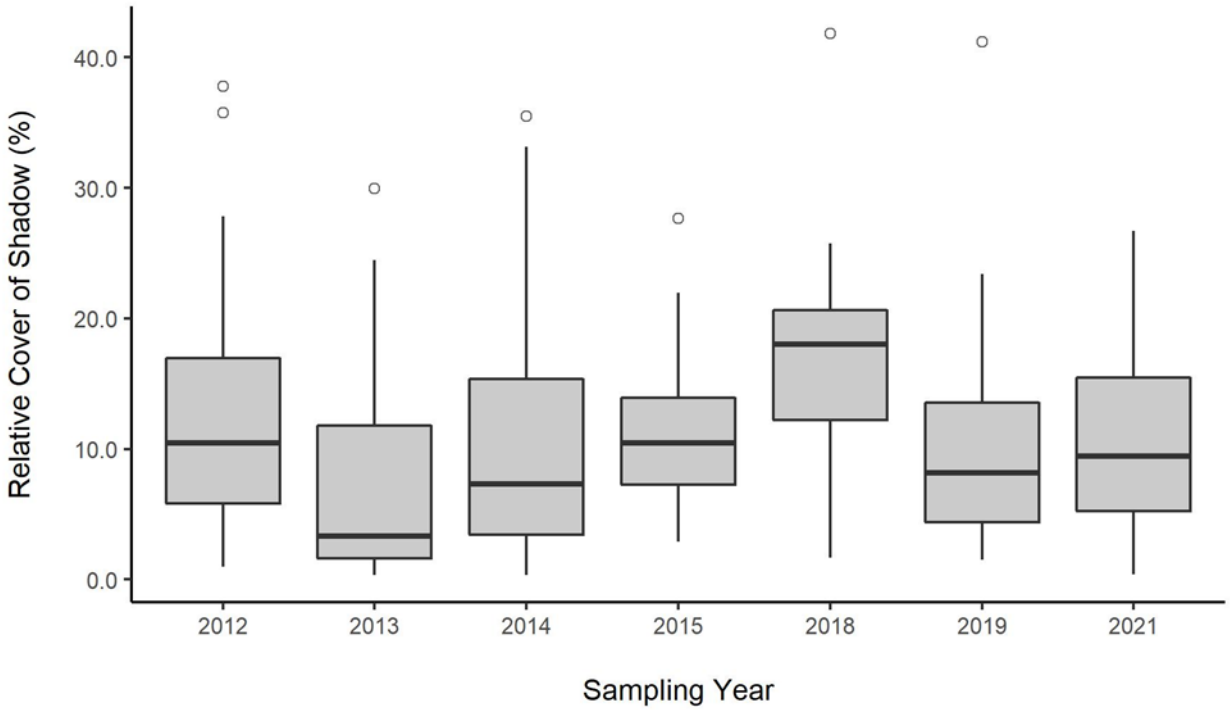

Supplemental Figure 3.S2. Box and whisker plot showing the relative cover of shadow from the image estimates across seven sampling years (n = 30 plots).

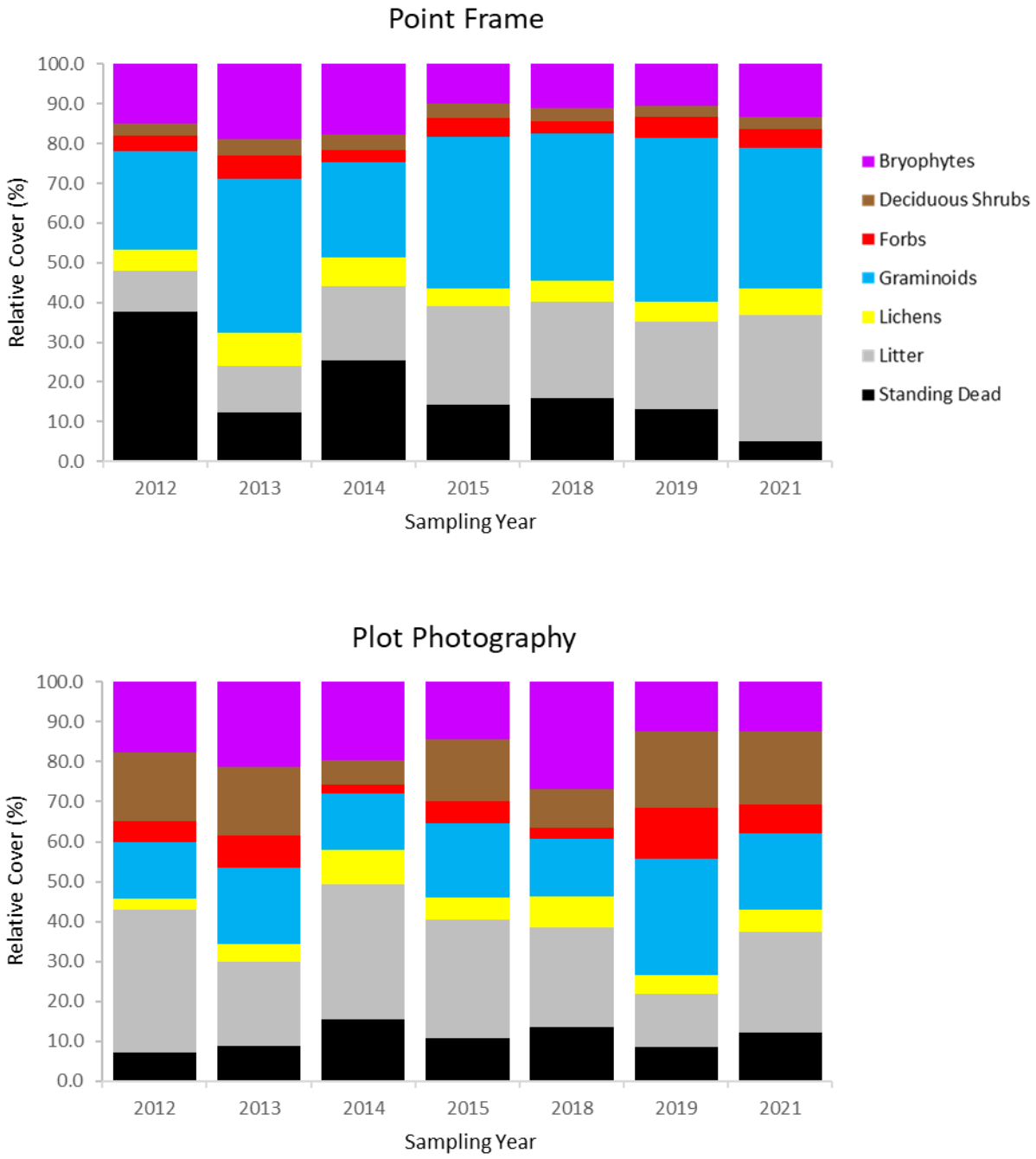

Supplemental Figure 3.S3. Relative cover estimates from the point frame (upper panel) and plot photography (lower panel) vegetation sampling methods. Bars are colored according to growth form: Bryophytes = Purple, Deciduous Shrubs = Brown, Forbs = Red, Graminoids = Blue, Lichens = Yellow, Litter = Gray, Standing Dead = Black.

Annotated R Code

Caret stands for **C**lassification **A**nd **Re**gression **T**raining, which allows the user to execute a variety of machine learning classifiers using standard syntax. Auxiliary tasks such as data preparation, data splitting, variable selection, and model evaluation can also be integrated using this package. Caret is described in great detail with practical examples by the original author, Max Kuhn, at https://topepo.github.io/caret/index.html. Technical issues can be submitted to him directly at https://github.com/topepo/caret/issues, as he continues to maintain this package.

All statistical analyses were performed using RStudio v. 1.4 (Boston, Massachusetts). Annotated samples of code are included for each statistical test. Additional code and data sets are included in the supplemental materials for this thesis, which are saved to the shared Arctic Ecology Program (AEP) computer drive.

```
#Install and load packages.

     install.packages(c("tidyverse", "dplyr", "caret", "tictoc",
     "e1071", "ranger", "gbm", "rpart", "kernlab"))

     Packages <- c("tidyverse", "dplyr", "caret", "tictoc", "e1071",
     "ranger", "gbm", "rpart", "kernlab")

     lapply(Packages, library, character.only = TRUE)


#Set privileges:

     setwd("D:/R/...")


#Anderson-Darling Normality Test:

     #Shapiro-Wilk normality test only supports a sample size of 3 -
     5,000 records, which exceeds my sample size of 15,000 records.

     install.packages('nortest')

     library(nortest)

     a <- lapply(select(trainee,-class), ad.test)
```

```
ad <- sapply(a, '[', c("statistic","p.value"))

t(ad)


#Feature selection:

    #Note: correlation coefficients are standardized when they are
    calculated, allowing for comparison between numerical predictors
    with different scales.

    #trainee is the labeled data set (n = 15,000 records). trainee
    contains a column for class (eight vegetation classes) and
    numerous columns for features.

    cor_trainee <- cor(dplyr::select(trainee,-class), method =
    "spearman") #Pearson is default.

    findCorrelation(cor_trainee, cutoff = 0.95, names = TRUE)
    #Reveals predictors that result in pairwise correlations greater
    than 95%, i.e., proposed index of column numbers for removal.

    filtered.95 <- subset(trainee, select = -c(v1, v2, v3 ... vx))
    #Find the two correlated variables: keep the most logical
    variable, remove the least logical variable.


#Split into training (70%) and test (30%):

    set.seed(1)

    f.95.100 <- createDataPartition(y=filtered.95$class, p=.7, list =
    FALSE) #Creates balanced split of the data (stratified random
    sampling).

    f95.100.trn <- filtered.95[f.95.100,]

    f95.100.tst <- filtered.95[-f.95.100,]

    #Summarize the data to confirm stratified counts:

    f95.100.trn %>%

      group_by(class) %>%

      summarise(n())

    f95.100.tst %>%

      group_by(class) %>%

      summarise(n())
```

```
#Split test into validation (15%) and test (15%):
     set.seed(2)
     f.95 <- createDataPartition(y=f95.100.tst$class, p=.5, list =
     FALSE)
     f95.100.val <- f95.100.tst[f.95,]
     f95.100.tst <- f95.100.tst[-f.95,]
     #Summarize the data to confirm counts:
     f95.100.val %>%
       group_by(class) %>%
       summarise(n())
     f95.100.tst %>%
       group_by(class) %>%
       summarise(n())


#Establish five repeats of 10-fold cross validation:
     tc <- trainControl(
       method = "repeatedcv",
       number = 10,
       repeats = 5,
       sampling = "down")


#Train the model
     #This is an iterative process, which requires different tuning
     grids or tuning values (tuneLength).
     #Set an identical seed across all models to ensure resampling
     sets are identical for each model.
     tic("rf.model")
     rf_grid <- expand.grid(mtry = c(2,4,6,8,10,12,14,16,18,20,22),
                            splitrule = c("gini", "extratrees"),
                            min.node.size = 1)
     set.seed(2021) #Pre-processing requirements: none
```

```
rf.model2 <- train(class ~ ., data = f95.100.trn,
                   method = "ranger",
                   trControl = tc,
                   tuneGrid = rf_grid,
                   importance = "impurity")
toc()
saveRDS(rf.model2, "./rf.model.rds") #Save model
rf.model <- readRDS("./rf.model.rds") #Open and re-name model

tic("gbm.model")
gbm_grid <- expand.grid(interaction.depth = c(1,2,3,5,9),
                        n.trees = c(50,100,150,200,250,300),
                        shrinkage = 0.1,
                        n.minobsinnode = 10)
set.seed(2021) #Pre-processing requirements: none
gbm.model <- train(class ~ ., data = f95.100.trn,
                   method = "gbm",
                   trControl = tc,
                   tuneGrid = gbm_grid,
                   verbose = FALSE)
toc()

tic("cart.model")
set.seed(2021) #Pre-processing requirements: none
cart.model <- train(class ~ ., data = f95.100.trn,
                    method = "rpart",
                    trControl = tc,
                    tuneLength = 10)
toc()
```

```
      tic("svm.model")
      set.seed(2021) #Pre-processing requirements: center, scale
      svm.model <- train(class ~ ., data = f95.100.trn,
                         method = "svmRadial",
                         preProcess = c("center", "scale"),
                         trControl = tc,
                         tuneLength = 10)
      toc()

      tic("knn.model")
      set.seed(2021) #Pre-processing requirements: center, scale, nzv
      knn.model <- train(class ~ ., data = f95.100.trn,
                         method = "knn",
                         preProcess = c("center", "scale", "nzv"),
                         trControl = tc,
                         tuneLength = 20)
      toc()

#Update model with selected parameters
      tic("final.rf")
      set.seed(2021)
      final.rf <- update(rf.model, param = list(mtry=36,
      splitrule="extratrees", min.node.size=1))
      toc()

#Options to visualize results:
      splom(res, metric = "Accuracy") #Scattermatrix
      xyplot(res, metric = "Accuracy") #Close up scattermatrix
      dotplot(res, metric = "Accuracy")

#Examine and test performance of the trained model only:
```

```
      res <- resamples(list(RF = rf.model,
                            GBM = gbm.model,
                            CART = cart.model,
                            SVM = svm.model,
                            KNN = knn.model))
      summary(res)
      modelDiffs <- diff(res) #Are there differences between the
      models?
      summary(modelDiffs) #Null hypothesis: There is no difference
      between the models. P-values are on the lower diagonal.


#Validate or test the model:
      set.seed(2021)
      rf.predict <- predict(rf.model, f95.100.tst)
      confusionMatrix(rf.predict, f95.100.tst$class)


#View the importance scores for the model:
      varImp(rf.model)$importance %>%
        mutate(names = row.names(.)) %>%
        arrange(-Overall)
      #Note: varImp will only work if the importance values have been
      calculated in the train function for random forest.


#Spearman-Rank Correlations:
      #Correlations are repeated for every vegetation class (bryophyte,
      deciduous shrub, forb, graminoid, lichen, litt, standing dead)
      between the two sampling methods (OBIA and PF) for each year
      (2012:2015, 2018, 2019, 2021).
      cor.test(a2021$bryo_OBIA, a2021$bryo_PF, method = "spearman")
      cor.test(a2021$dshr_OBIA, a2021$dshr_PF, method = "spearman")
      cor.test(a2021$forb_OBIA, a2021$forb_PF, method = "spearman")
      cor.test(a2021$gram_OBIA, a2021$gram_PF, method = "spearman")
```

```
cor.test(a2021$lich_OBIA, a2021$lich_PF, method = "spearman")
cor.test(a2021$litt_OBIA, a2021$litt_PF, method = "spearman")
cor.test(a2021$dead_OBIA, a2021$dead_PF, method = "spearman")
```

Bibliography

Aitken, S. N., Yeaman, S., Holliday, J. A., Wang, T., & Curtis-McLane, S. (2008). Adaptation, migration or extirpation: climate change outcomes for tree populations. *Evol. App.*, *1*(1), 95–111. https://doi.org/10.1111/j.1752-4571.2007.00013.x

Allen, M. R., Dube, O. P., Solecki, W., Aragón-Durand, F., Cramer, W., Humphreys, S., Kainuma, M., Kala, J., Mahowald, N., Mulugetta, Y., Perez, R., Wairiu, M., & Zickfeld, K. (2018). IPCC 2018: Framing and Context. In V. Masson-Delmotte, P. Zhai, H.-O. Pörtner, D. Roberts, J. Skea, P. R. Shukla, A. Pirani, W. Moufouma-Okia, C. Péan, R. Pidcock, S. Connors, J. B. R. Matthews, Y. Chen, X. Zhou, M. I. Gomis, E. Lonnoy, T. Maycock, M. Tignor, & T. Waterfield (Eds.), *Global Warming of 1.5°C. An IPCC Special Report on the impacts of global warming of 1.5°C above pre-industrial levels and related global greenhouse gas emission pathways, in the context of strengthening the global response to the threat of climate change*.

Altman, N. S. (1992). An introduction to kernel and nearest-neighbor nonparametric regression. *The American Statistician*, *46*(3), 175–185. https://doi.org/10.1080/00031305.1992.10475879

Anderson, H. B., Nilsen, L., Tommervik, H., Rune Karlsen, S., Nagai, S., & Cooper, E. J. (2016). Using ordinary digital cameras in place of near-infrared sensors to derive vegetation indices for phenology studies of high Arctic vegetation. *Remote Sens.*, *8*(847), 1–17.

Anderson, K., & Gaston, K. J. (2013). Lightweight unmanned aerial vehicles will revolutionize spatial ecology. *Front. Ecol. Environ.*, *11*(3), 138–146.

Aplin, P. (2006). On scales and dynamics in observing the environment. *Int. J. Remote Sens.*, *27*, 2123–2140.

Arft, A. M., Walker, M. D., Gurevitch, J., Alatalo, J. M., Bret-Harte, M. S., Dale, M., Diemer, M., Gugerli, F., Henry, G. H. R., Jones, M. H., Hollister, R. D., Jonsdottir, I. S., Laine, K., Levesque, E., Marion, G. M., Molau, U., Molgaard, P., Nordenhall, U., Raszhivin, V., … Wookey, P. A. (1999). Responses of tundra plants to experimental warming: Meta-analysis of the International Tundra Experiment. *Ecol. Monogr.*, *69*(4), 491–511. https://doi.org/10.2307/2657227

Arvor, D., Durieux, L., Andrés, S., & Laporte, M. A. (2013). Advances in Geographic Object-Based Image Analysis with ontologies: A review of main contributions and limitations from a remote sensing perspective. *ISPRS Journal of Photogrammetry and Remote Sensing*, *82*, 125–137. https://doi.org/10.1016/j.isprsjprs.2013.05.003

Baatz, M., & Schaape, A. (2000). A multiresolution segmentation: an optimization approach for high quality multi-scale image segmentation. In J. Strobl (Ed.), *Proceedings of Angewandte Geographische Informations-verarbeitung XII* (pp. 12–23).

Beamish, A. L., Nijland, W., Edwards, M., Coops, N. C., & Henry, G. H. R. (2016). Phenology and vegetation change measurements from true colour digital photography in high Arctic tundra. *Arctic Science*, *2*, 33–49. https://doi.org/10.1139/as-2014-0003

Beamish, A., Raynolds, M. K., Epstein, H. E., Frost, G. V., Macander, M. J., Bergstedt, H., Bartsch, A., Kruse, S., Miles, V., Tanis, C. M., Heim, B., Fuchs, M., Chabrillat, S., Shevtsova, I., Verdonen, M., & Wagner, J. (2020). Recent trends and remaining challenges for optical remote sensing of Arctic tundra vegetation: A review and outlook. *Remote Sens. Environ.*, *246*, 111872. https://doi.org/10.1016/j.rse.2020.111872

Belgiu, M., & Drăgut, L. (2016). Random forest in remote sensing: A review of applications and future directions. *ISPRS Journal of Photogrammetry and Remote Sensing*, *114*, 24–31.

https://doi.org/10.1016/j.isprsjprs.2016.01.011

Bennett, L. T., Judd, T. S., & Adams, M. A. (2000). Close-range vertical photography for measuring cover changes in perennial grasslands. *J. Range Manage.*, *53*(6), 634–641.

Benz, U. C., Hofmann, P., Willhauck, G., Lingenfelder, I., & Heynen, M. (2004). Multi-resolution, object-oriented fuzzy analysis of remote sensing data for GIS-ready information. *ISPRS J. Photogramm. Remote Sens.*, *58*, 239–258.

Bhatt, U. S., A, W. D., K, R. M., A, B. P., E, E. H., Comiso, J. C., E, P. J., J, T. C., Michael, S., Ermold, W., & Jinlun, Z. (2017). Changing seasonality of panarctic tundra vegetation in relationship to climatic variables. *Environ. Res. Lett.*, *12*(5), 055003.

Bhatt, U. S., Walker, D. A., Raynolds, M. K., Bieniek, P. A., Epstein, H. E., Comiso, J. C., Pinzon, J. E., Tucker, C. J., & Polyakov, I. V. (2013). Recent declines in warming and vegetation greening trends over pan-Arctic tundra. *Remote Sens.*, *5*(9), 4229–4254. https://doi.org/10.3390/rs5094229

Bjorkman, A.D., Garcia-Criado, M., Myers-Smith, I. H., Ravolainen, V., Jonsdottir, I. S., Bakke Westergaard, K., Lawler, J. P., Aronsson, M., Bennett, B., Gardfjell, H., Heidmarsson, S., Stewart, L., & Normand, S. (2019). Status and trends in Arctic vegetation: evidence from experimental warming and long-term monitoring. *Ambio*, *49*, 678–692.

Bjorkman, Anne D., Myers-Smith, I. H., Elmendorf, S. C., Normand, S., Ruger, N., Beck, P. S. A., Blach-Overgaard, A., Blok, D., Cornelissen, J. H. C., Forbes, B. C., Georges, D., Goetz, S. J., Guay, K. C., Henry, G. H. R., HilleRisLambers, J., Hollister, R. D., Karger, D. N., Kattge, J., Manning, P., … Weiher, E. (2018). Plant functional trait change across a warming tundra biome. *Nature*, *562*(7725), 57–62.

Blaschke, T. (2005). Towards a framework for change detection based on image objects. In

Göttinger Geographische Abhandlungen: Vol. Vol. 113 (pp. 1–9).

Blaschke, T. (2010). Object based image analysis for remote sensing. *ISPRS J. Photogramm.*, *65*, 2–16.

Blaschke, T., Hay, G. J., Kelly, M., Lang, S., Hofmann, P., Addink, E., Queiroz Feitosa, R., van der Meer, F., van der Werff, H., van Coillie, F., & Tiede, D. (2014). Geographic Object-Based Image Analysis - Towards a new paradigm. *ISPRS J. Photogramm.*, *87*, 180–191.

Blaschke, T., Lang, S., Lorup, E., Strobl, J., & Zeil, P. (2000). Object-oriented image processing in an integrate GIS/remote sensing environment and perspectives for environmental applications. In A. B. Cremers & K. Greve (Eds.), *Umweltinformatik '00 Umweltinformation für Planung, Politik und Öffentlichkeit* (pp. 555–570). Metropolis.

Blaschke, T., & Strobl, J. (2001). What's wrong with pixels? Some recent developments interfacing remote sensing and GIS. *GIS*, *14*(6), 12–17.

Bliakharskii, D. P., Florinsky, I. V., & Skrypitsyna, T. N. (2019). Modelling glacier topography in Antarctica using unmanned aerial survey: assessment of opportunities. *Remote Sens.*, *40*(7), 2517–2541.

Booth, D. T., Cox, S. E., Fifield, C., Phillips, M., & Willlamson, N. (2005). Image analysis compared with other methods for measuring ground cover. *Arid Land Research and Management*, *19*(2), 91–100. https://doi.org/10.1080/15324980590916486

Box, J. E., Colgan, W. T., Christensen, T. R., Schmidt, N. M., Lund, M., Parmentier, F.-J. W., Brown, R., Bhatt, U. S., Euskirchen, E. S., Romanovsky, V. E., Walsh, J. E., Overland, J. E., Wang, M., Corell, R. W., Meier, W. N., Wouters, B., Mernild, S., Mård, J., Pawlak, J., & Olsen, M. S. (2019). Key indicators of Arctic climate change: 1971–2017. *Environ. Res. Lett.*, *14*, 045010. https://doi.org/10.1088/1748-9326/aafc1b

Breiman, L. (1996). Bagging predictors. *Mach. Learn.*, *24*, 123–140.

Breiman, L. (2001). Random Forest. *Machine Learning*, *45*, 5–32.

Brown, J., Hinkel, K. M., & Nelson, F. E. (2000). The Circumpolar Active Layer Monitoring (CALM) program: Research designs and initial results. *Polar Geogr.*, *24*(3), 165–258.

Brown, J., Miller, P. C., Tieszen, L. L., & Bunnell, F. L. (Eds.). (1980). *An arctic ecosystem: the coastal tundra at Barrow, Alaska*. Dowden, Hutchinson, & Ross, Inc.

Buchhorn, M., Walker, D. A., Heim, B., Raynolds, M. K., Epstein, H. E., & Schwieder, M. (2013). Ground-based hyperspectral characterization of Alaska tundra vegetation along environmental gradients. *Remote Sens.*, *5*, 3971–4005.

Bunn, A. G., & Goetz, S. J. (2006). Trends in satellite-observed circumpolar photosynthetic activity from 1982 to 2003: The influence of seasonality, cover type, and vegetation density. *Earth Interactions*, *10*(1), 1–19. https://doi.org/10.1175/EI190.1

Chandrashekar, G., & Sahin, F. (2014). A survey on feature selection methods. *Computers & Electrical Engineering*, *40*(1), 16–28.

Chapin, F. S., BretHarte, M. S., Hobbie, S. E., & Zhong, H. L. (1996). Plant functional types as predictors of transient responses of arctic vegetation to global change. *Journal of Vegetation Science*, *7*(3), 347–358.

Chapin, F. S., Sturm, M., Serreze, M. C., McFadden, J. P., Key, J. R., Lloyd, A. H., McGuire, A. D., Rupp, T. S., Lynch, A. H., Schimel, J. P., Beringer, J., Chapman, W. L., Epstein, H. E., Euskirchen, E. S., Hinzman, L. D., Jia, G., Ping, C. L., Tape, K. D., Thompson, C. D. C., … Welker, J. . (2005). Role of land-surface changes in Arctic summer warming. *Science*, *310*(5748), 657–660. https://doi.org/10.1126/science.1117368

Chen, G., Hay, G. J., Carvalho, L. M. T., & Wulder, M. A. (2012). Object-based change

detection. *Int. J. Remote Sens.*, *33*, 4434–4457.

Chen, Gang, Weng, Q., Hay, G. J., & He, Y. (2018). Geographic object-based image analysis (GEOBIA): emerging trends and future opportunities. *GIScience and Remote Sensing*, *55*(2), 159–182. https://doi.org/10.1080/15481603.2018.1426092

Chen, Z., Chen, E. W., Leblanc, S. G., Henry, G. H. R., & Chen, W. (2010). Digital photograph analysis for measuring percent plant cover in the Arctic. *Arctic*, *63*(3), 315–326.

Clark, J. S., Nemergut, D., Seyednasrollah, B., Turner, P. J., & Zhang, S. (2017). Generalized joint attribute modeling for biodiversity analysis: median-zero, multivariate, multifarious data. *Ecol. Monogr.*, *87*, 34–56. https://doi.org/10.1002/ecm.1241

Clarke, T. A., & Fryer, J. G. (1998). The development of camera calibration methods and models. *Photogrammetric Record*, *16*(91), 51–66.

Cohen, J. (1960). A coefficient of agreement for nominal scales. *Educational and Psychological Measurement*, *20*(1), 37–40.

Congalton, R. G. (1991). A review of assessing the accuracy of classifications of remotely sensed data. *Remote Sensing of Environment*, *37*(1), 35–46. https://doi.org/10.1016/0034-4257(91)90048-B

Congalton, R. G., & Green, K. (2009). *Assessing the Accuracy of Remotely Sensed Data: Principles and Practices* (2nd Editio). Lewis Publishers.

Congalton, R. G., Oderwald, R. G., & Mead, R. A. (1983). Assessing Landsat classification accuracy using discrete multivariate analysis statistical techniques. *Photogrammetric Engineering and Remote Sensing*, *49*, 1671–1678.

Cortes, C., & Vapnik, V. (1995). Support-vector networks. *Machine Learning*, *20*, 273–297. https://doi.org/10.1007/BF00994018.

Davidson, S. J., Santos, M. J., Sloan, V. L., Watts, J. D., Phoenix, G. K., Oechel, W. C., & Zona, D. (2016). Mapping Arctic tundra vegetation communities using field spectroscopy and multispectral satellite data in north Alaska, USA. *Remote Sens.*, *8*(978), 1–24.

de Jong, R., de Bruin, S., de Wit, A., Schaepman, M. E., & Dent, D. L. (2011). Analysis of monotonic greening and browning trends from global NDVI time-series. *Remote Sens. Environ.*, *115*, 692–702.

de Valpine, P., & Harmon-Threatt, A. N. (2013). General models for resource use or other compositional count data using the Dirichlet-multinomial distribution. *Ecology*, *94*(12), 2678–2687. https://doi.org/10.1890/12-0416.1

Drăguţ, L., Csillik, O., Eisank, C., & Tiede, D. (2014). Automated parameterisation for multi-scale image segmentation on multiple layers. *ISPRS Journal of Photogrammetry and Remote Sensing*, *88*, 119–127. https://doi.org/10.1016/j.isprsjprs.2013.11.018

Dronova, I. (2015). Object-based image analysis in wetland research: a review. *Remote Sens.*, *7*, 6380–6413.

Dronova, I., Gong, P., Clinton, N. E., Wang, L., Fu, W., Qi, S., & Liu, Y. (2012). Landscape analysis of wetland plant functional types: The effects of image segmentation scale, vegetation classes and classification methods. *Remote Sens. Environ.*, *127*, 357–369.

Dronova, I., Gong, P., Wang, L., & Zhong, L. (2015). Mapping dynamic cover types in a large seasonally floodedwetland using extended principal component analysis and object-based classification. *Remote Sens. Environ.*, *158*, 193–206.

Du, J., Watts, J. D., Jiang, L., Lu, H., Cheng, X., Duguay, C., Farina, M., Qiu, Y., Kim, Y., Kimball, J. S., & Tarolli, P. (2019). Remote sensing of environmental changes in cold regions: methods, achievements and challenges. *Remote Sens.*, *11*(1952), 1–36.

Elmendorf, S. C., Henry, G. H. R., Hollister, R. D., Björk, R. G., Bjorkman, A. D., Callaghan, T. V., Siegwart-Collier, L., Cooper, E. J., Cornelissen, J. H. C., Day, T. A., Fosaa, A. M., Gould, W. A., Gretarsdottir, J., Harte, J., Hermanutz, L., Hik, D. S., Hofgaard, A., Jarrad, F., Svala Jonsdottir, I., … Wookey, P. A. (2012). Global assessment of experimental climate warming on tundra vegetation: heterogeneity over space and time. *Ecol. Lett.*, *15*, 164–175.

Elmendorf, S. C., Henry, G. H. R., Hollister, R. D., Björk, R. G., Boulanger-Lapointe, N., Cooper, E. J., Cornelissen, J. H. C., Day, T. A., Dorrepaal, E., Elumeeva, T. G., Gill, M., Gould, W. A., Harte, J., Hik, D. S., Hofgaard, A., Johnson, D. R., Johnstone, J. F., Jónsdóttir, I. S., Jorgenson, J. C., … Wipf, S. (2012). Plot-scale evidence of tundra vegetation change and links to recent summer warming. *Nat. Clim. Change*, *2*, 453–457. https://doi.org/10.1038/nclimate1465

Epstein, H. E., Raynolds, M. K., Walker, D. A., Bhatt, U. S., Tucker, C. J., & Pinzon, J. E. (2012). Dynamics of aboveground phytomass of the circumpolar Arctic tundra during the past three decades. *Environ. Res. Lett.*, *7*(1), 015506.

Epstein, Howard E., Myers-Smith, I. H., & Walker, D. A. (2013). Recent dynamics of Arctic and sub-Arctic vegetation. *Environ. Res. Lett.*, *8*, 1–6.

Everitt, B. S., Laundau, S., Leese, M., & Stahl, D. (2006). *Miscellaneous Cluster Methods in Cluster Analysis* (5th ed.). John Wiley & Sons, Ltd.

Ewertowski, M., Tomczyk, A., Evans, D., Roberts, D., & Ewertowski, W. (2019). Operational framework for rapid, very-high resolution mapping of glacial geomorphology using low-cost unmanned aerial vehicles and structure-from-motion approach. *Remote Sens.*, *11*(1).

Foody, G. M. (2002). Status of land cover classification accuracy assessment. *Remote Sens.*

Environ., *80*, 185–201.

Fraser, L. H., Henry, H. A. L., & Etc. (2012). Coordinated distributed experiments: an emerging tool for testing global hypotheses in ecology and environmental science. *Front. Ecol. Environ.* https://doi.org/10.1890/110279

Fraser, R. H., Olthof, I., Lantz, T. C., & Schmitt, C. (2016). UAV photogrammetry for mapping vegetation in the low-Arctic. *Arctic Science*, *2*, 79–102.

Freund, Y., & Schapire, R. E. (1997). A decision-theoretic generalization of on-line learning and an application to boosting. *J. Comput. Syst. Sci.*, *55*(119–139).

Friedman, J. H. (2001). Greedy function approximation: A gradient boosting machine. *Ann. Statist.*, *29*(5), 1189–1232. https://doi.org/10.1214/aos/1013203451

Friedman, J. H. (2002). Stochastic gradient boosting. *Computational Statistics & Data Analysis*, *38*(4), 367–378. https://doi.org/10.1016/S0167-9473(01)00065-2

Gitelson, A. A., Kaufman, Y. J., Stark, R., & Rundquist, D. (2002). Novel algorithms for remote estimation of vegetation fraction. *Remote Sens.*, *80*, 76–87.

Goetz, A. F., Vane, G., Solomon, J. E., & Rock, B. N. (1985). Imaging spectrometry for earth remote sensing. *Science*, *228*(4704), 1147–1153.

Gorrod, E. J., & Keith, D. A. (2009). Observer variation in field assessments of vegetation condition: implications for biodiversity conservation. *Ecol. Manag. Restor.*, *10*, 31–40. https://doi.org/10.1111/j.1442-8903.2009.00437.x

Guay, K. C., Beck, P. S. A., Berner, L. T., Goetz, S. J., Baccini, A., & Buermann, W. (2014). Vegetation productivity patterns at high northern latitudes: a multi-sensor satellite data assessment. *Glob Chang Biol*, *20*, 3147–3158.

Halabisky, M., Moskal, L. M., & Hall, S. A. (2011). Object-based classification of semi-arid

wetlands. *J. Appl. Remote Sens.*, *5*(1), 053511. https://doi.org/10.1117/1.3563569

Haralick, R. (1979). Statistical and structural approaches to texture. *Proceedings of the IEEE*, *67*(5), 786–804.

Haralick, R. M., Shanmugan, K., & Dinstein, I. (1973). Textural features for image classification. *IEEE Transactions on Systems, Man and Cybernetics*, *SMC-3*(6), 610–621.

Harris, J. A., Hollister, R. D., Botting, T. F., Tweedie, C. E., Betway, K. R., May, J. L., Barrett, R. T. S., Leibig, J. A., Christoffersen, H. L., Vargas, S. A., Orejel, M., & Fuson, T. L. (2021). Understanding the climate impacts on decadal vegetation change in northern Alaska. *Arctic Science*. https://doi.org/10.1139/as-2020-0050

Hay, G. J., & Castilla, G. (2008). Geographic object-based image analysis (GEOBIA): A new name for a new discipline. In Thomas Blaschke, S. Lang, & G. J. Hay (Eds.), *Lecture Notes in Geoinformation and Cartography* (1st ed., Vol. 0, Issue 9783540770572, pp. 75–89). Springer-Verlag. https://doi.org/10.1007/978-3-540-77058-9_4

Hay, G. J., & Castilla, G. (2006). Object-Based Image Analysis: Strengths, Weaknesses, Opportunities and Threats (SWOT). *The International Archives of the Photogrammetry, Remote Sensing and Spatial Information Sciences*, 1–3.

Hay, G. J., Marceau, D. J., Dube, P., & Bouchard, A. (2001). A multiscale framework for landscape analysis: object-specific analysis and upscaling. *Landsc. Ecol.*, *16*(6), 471–490.

Healey, N. C., Oberbauer, S. F., Ahrends, H. E., Dierick, D., Welker, J. M., Leffler, A. J., Hollister, R. D., Vargas Zesati, S. A., & Tweedie, C. E. (2014). A mobile instrumented sensor platform for long-term terrestrial ecosystem analysis: an example application in an Arctic tundra ecosystem. *J. Environ. Inform.*, *24*(1), 1–10.

Henry, G. H. R., & Molau, U. (1997). Tundra plants and climate change: the International

Tundra Experiment (ITEX). *Global Change Biology*, *3*, 1–9. https://doi.org/10.1111/j.1365-2486.1997.gcb132.x

Hollister, R. D. (2003). *Response of tundra vegetation to temperature: Implications for forecasting vegetation change*. Michigan State University.

Hollister, R. D., Webber, P. J., Nelson, F. E., & Tweedie, C. E. (2006). Soil thaw and temperature response to air warming varies by plant community: Results from an open-top chamber experiment in northern Alaska. *Arctic, Antarctic, and Alpine Research*, *38*(2), 206–215.

Hossain, M. D., & Chen, D. (2019). Segmentation for Object-Based Image Analysis (OBIA): A review of algorithms and challenges from remote sensing perspective. *ISPRS J. Photogramm.*, *150*, 115–134.

Huang, C., Davis, L. S., & Townshend, J. R. G. (2002). An assessment of support vector machines for land cover classification. *International Journal of Remote Sensing*, *23*(4), 725–749. https://doi.org/10.1080/01431160110040323

Hussain, M., Chen, D., Cheng, A., Wei, H., & Stanley, D. (2013). Change detection from remotely sensed images: From pixel-based to object-based approaches. *ISPRS Journal of Photogrammetry and Remote Sensing*, *80*, 91–106. https://doi.org/10.1016/j.isprsjprs.2013.03.006

Husson, E., Ecke, F., & Reese, H. (2016). Comparison of manual mapping and automated object-based image analysis of non-submerged aquatic vegetation from very-high-resolution UAS images. *Remote Sensing*, *8*(9), 1–18. https://doi.org/10.3390/rs8090724

Ide, R., & Oguma, H. (2010). Use of digital cameras for phenological observations. *Ecol. Inform.*, *5*, 339–347.

Jensen, J. R. (2005). *Introductory Digital Image Processing: A Remote Sensing Perspective*. Prentice Hall, Inc.

Jensen, J. R. (2013). *Remote Sensing of the Environment: An Earth Resource Perspective* (2nd Edn.). Harlow: Pearson Eduction Ltd.

Johansen, K., Coops, N. C., Gergel, S. E., & Stange, Y. (2007). Application of high spatial resolution satellite imagery for riparian and forest ecosystem classification. *Remote Sens. Environ.*, *110*(1), 29–44. https://doi.org/10.1016/j.rse.2007.02.014

Joly, K., Jandt, R. R., & Klein, D. R. (2009). Decrease of lichens in Arctic ecosystems: the role of wildfire, caribou, reindeer, competition and climate in north-western Alaska. *Polar Res.*, *28*(3), 433–442. https://doi.org/10.1111/j.1751-8369.2009.00113.x

Kelsey, K., Pedersen, S., Leffler, A. J., Sexton, J., Feng, M., & Welker, J. M. (2021). Winter snow and spring temperature have differential effects on vegetation phenology and productivity across Arctic plant communities. *Global Change Biology*, *27*(8), 1572–1586.

Kim, M., Warner, T. A., Madden, M., & Atkinson, D. S. (2011). Multi-scale GEOBIA with very high spatial resolution digital aerial imagery: Scale, texture and image objects. *Int. J. Remote Sens.*, *32*, 2825–2850.

King, D. H., Wasley, J., Ashcroft, M. B., Ryan-colton, E., Lucieer, A., Chisholm, L. A., Robinson, S. A., & King, D. H. (2020). Semi-automated analysis of digital photographs for monitoring east Antarctic vegetation. *Frontiers in Plant Science*, *11*(766), 1–16. https://doi.org/10.3389/fpls.2020.00766

Kowk, R. (2018). Arctic sea ice thickness, volume, and multiyear ice coverage: losses and coupled variability (1958–2018). *Environ. Res. Lett.*, *13*, 105005. https://doi.org/10.1088/1748-9326/aae3ec

Kruschke, J. K. (2014). *Doing Bayesian Data Analysis: A tutorial with R, JAGS, and Stan* (2nd Editio). Elsevier Inc.

Kucharczyk, M., Hay, G. J., Ghaffarian, S., & Hugenholtz, C. H. (2020). Geographic object-based image analysis: A primer and future directions. *Remote Sensing*, *12*(12), 1–33. https://doi.org/10.3390/rs12122012

Kuhn, M. (2008). Building predictive models in R using the caret package. *Journal of Statistical Software*, *28*(5), 1–26. https://doi.org/https://doi.org/10.18637/jss.v028.i05

Laliberte, A. S., & Rango, A. (2011). Image processing and classification procedures for analysis of sub-decimeter imagery acquired with an unmanned aircraft over arid rangelands. *GIScience and Remote Sensing*, *48*(1), 4–23. https://doi.org/10.2747/1548-1603.48.1.4

Laliberte, A. S., Rango, A., & Herrick, J. (2007). Unmanned aerial vehicles for rangeland mapping and monitoring: A comparison of two systems. *American Society for Photogrammetry and Remote Sensing - ASPRS Annual Conference 2007: Identifying Geospatial Solutions*, *1*, 379–388.

Laliberte, A. S., Rango, A., Herrick, J. E., Fredrickson, E. L., & Burkett, L. (2007). An object-based image analysis approach for determining fractional cover of senescent and green vegetation with digital plot photography. *Journal of Arid Environments*, *69*(1), 1–14. https://doi.org/10.1016/j.jaridenv.2006.08.016

Laliberte, Andrea S., & Rango, A. (2008). Incorporation of texture, intensity, hue, and saturation for rangeland monitoring with unmanned aircraft imagery. *GEOBIA Proceedings*, *37*, 4.

Lang, S. (2008). Object-based Image Analysis for remote sensing applications: modeling reality – dealing with complexity. In T. Blaschke, S. Lang, & G. J. Hay (Eds.), *Object-based Image Analysis* (pp. 1–25). Springer.

Lang, Stefan. (2008). Why object-based image analysis. In Thomas Blaschke, S. Lang, & G. J. Hay (Eds.), *Object-based image analysis: Lecture notes in geoinformation and cartography* (pp. 3–27). Springer.

Langford, Z., Kumar, J., Hoffman, F. M., Norby, R. J., Wullschleger, S. D., Sloan, V. L., & Iversen, C. M. (2016). Mapping arctic plant functional type distributions in the Barrow Environmental Observatory using WorldView-2 and LiDAR datasets. *Remote Sens.*, *8*(9), 733. https://doi.org/10.3390/rs8090733

Lawrence, R. L., Wood, S. D., & Sheley, R. L. (2006). Mapping invasive plants using hyperspectral imagery and Breiman Cutler classifications (randomForest). *Remote Sens. Environ.*, *100*, 356–362.

Leffler, A. J., Klein, E. S., Oberbauer, S. F., & Welker, J. M. (2016). Coupled long-term summer warming and deeper snow alters species composition and stimulates gross primary productivity in tussock tundra. *Oecologia*, *181*(1), 287–297.

Liu, N., & Treitz, P. (2016). Modelling high arctic percent vegetation cover using field digital images and high resolution satellite data. *Int. J. Appl. Earth Obs.*, *52*, 445–456.

Liu, T., Abd-Elrahman, A., Morton, J., & Wilhelm, V. L. (2018). Comparing fully convolutional networks, random forest, support vector machine, and patch-based deep convolutional neural networks for object-based wetland mapping using images from small unmanned aircraft system. *GIScience and Remote Sensing*, *55*(2), 243–264. https://doi.org/10.1080/15481603.2018.1426091

Luscier, J. D., Thompson, W. L., Wilson, J. M., Gorhara, B. E., & Dragut, L. D. (2006). Using digital photographs and object-based image analysis to estimate percent ground cover in vegetation plots. *Front. Ecol. Environ.*, *4*(8), 408–413.

Ma, L., Cheng, L., Li, M., Liu, Y., & Ma, X. (2015). Training set size, scale, and features in Geographic Object-Based Image Analysis of very high resolution unmanned aerial vehicle imagery. *ISPRS Journal of Photogrammetry and Remote Sensing*, *102*, 14–27. https://doi.org/10.1016/j.isprsjprs.2014.12.026

Ma, L., Manchun, L., Ma, X., Cheng, L., Du, P., & Liu, Y. (2017). A review of supervised object-based land-cover image classification. *ISPRS J. Photogramm.*, *130*, 277–293.

Malenovský, Z., Lucieer, A., King, D. H., Turnbull, J. D., & Robinson, S. A. (2017). Unmanned aircraft system advances health mapping of fragile polar vegetation. *Methods in Ecology and Evolution*, *8*(12), 1842–1857. https://doi.org/10.1111/2041-210X.12833

Mamet, S. D., Young, N., Chun, K. P., & Johnstone, J. F. (2016). What is the most efficient and effective method for long-term monitoring of alpine tundra vegetation? *Arctic Science*, *2*(3), 127–141. https://doi.org/10.1139/as-2015-0020

Marceau, D. J. (1999). The scale issue in the social and natural sciences. *Canadian Journal of Remote Sensing*, *25*(4), 347–356. https://doi.org/10.1080/07038992.1999.10874734

Marcial-Pablo, M. de J., Gonzalez-Sanchez, A., Jimenez-Jimenez, S. I., Ontiveros-Capurata, R. E., & Ojeda-Bustamante, W. (2019). Estimation of vegetation fraction using RGB and multispectral images from UAV. *International Journal of Remote Sensing*, *40*(2), 420–438. https://doi.org/10.1080/01431161.2018.1528017

Marris, E. (2013). Fly, and bring me data. *Nature*, *498*, 156–158.

Maxwell, A. E., Warner, T. A., & Fang, F. (2018). Implementation of machine-learning classification in remote sensing: An applied review. *International Journal of Remote Sensing*, *39*(9), 2784–2817. https://doi.org/10.1080/01431161.2018.1433343

May, J.L., Hollister, R. D., Betway, K. R., Harris, J. A., Tweedie, C. E., Welker, J. M., Gould,

W. A., & Oberbauer, S. F. (2020). NDVI changes show warming increases the length of the green season at Tundra communities in Northern Alaska: a fine-scale analysis. *Frontiers in Plant Science*, *11*, 1174. https://doi.org/10.3389/fpls.2020.01174

May, J.L., Parker, T., Unger, S., & Oberbauer, S. F. (2018). Short term changes in moisture content drive strong changes in Normalized Difference Vegetation Index and gross primary productivity in four Arctic moss communities. *Remote Sens. Environ.*, *212*, 114–120.

May, Jeremy L., & Hollister, R. D. (2012). Validation of a simplified point frame method to detect change in tundra vegetation. *Polar Biol.*, *35*, 1815–1823.

McFeeters, S. (1996). The use of the Normalized Difference Water Index (NDWI) in the delineation of open water features. *Int. J. Remote Sens.*, *17*, 1425–1432.

McPartland, M. Y., Falkowski, M. J., Reinhardt, J. R., Kane, E. S., Kolka, R., Turetsky, M. R., Douglas, T. A., Anderson, J., Edwards, J. D., Palik, B., & Montgomery, R. A. (2019). Characterizing boreal peatland plant composition and species diversity with hyperspectral remote sensing. *Remote Sens.*, *11*(4), 1685. https://doi.org/10.3390/rs11141685

Menon, S. (2014). *ArcGIS 10.3: The next generation of GIS is here*. ESRI, Inc. https://www.esri.com/arcgis-blog/products/apps/3d-gis/arcgis-10-3-the-next-generation-of-gis-is-here/

Michel, P., Mathieu, R., & Mark, A. F. (2010). Spatial analysis of oblique photo-point images for quantifying spatio-temporal changes in plant communities. *Applied Vegetation Science*, *13*(2), 173–182. https://doi.org/10.1111/j.1654-109X.2009.01059.x

Molau, U., & Mølgaard, P. (1996). *International Tundra Experiment (ITEX) Manual* (2nd ed.). Danish Polar Center.

Motohka, T., Nasahara, K. N., Oguma, H., & Tsuchida, S. (2010). Applicability of green-red

vegetation index for remote sensing of vegetation phenology. *Remote Sens.*, *2*, 2369–2387.

Mountrakis, G., Im, J., & Ogole, C. (2011). Support vector machines in remote sensing: A review. *ISPRS Journal of Photogrammetry and Remote Sensing*, *66*(3), 247–259. https://doi.org/10.1016/j.isprsjprs.2010.11.001

Myers-Smith, I. H., Forbes, B. C., Wilmking, M., Hallinger, M., Lantz, T. C., Blok, D., Tape, K. D., Macias-Fauria, M., Sass-Klaassen, U., Levesque, E., Boudreau, S., Ropars, P., Hermanutz, L., Trant, A., Siegwart-Collier, L., Weijers, S., Rozema, J., Rayback, S. A., Martin Schmidt, N., … Hik, D. S. (2011). Shrub expansion in tundra ecosystems: dynamics, impacts and research priorities. *Environ. Res. Lett.*, *6*, 1–15.

Myers-Smith, I. H., Grabowski, M. M., Thomas, H. J. D., Angers-Blondin, S., Daskalova, G. N., Bjorkman, A. D., Cunliffe, A. M., Assmann, J. J., Boyle, J. S., McLeod, E., McLeod, S., Joe, R., Lennie, P., Arey, D., Gordon, R. R., & Eckert, C. D. (2019). Eighteen years of ecological monitoring reveals multiple lines of evidence for tundra vegetation change. *Ecol. Monogr.*, *89*(2), 1–21.

Myers-Smith, I. H., Kerby, J. T., Phoenix, G. K., Bjerke, J. W., Epstein, H. E., Assmann, J. J., John, C., Andreu-Hayles, L., Angers-Blondin, S., Beck, P. S. A., Berner, L. T., Bhatt, U. S., Bjorkman, A. D., Blok, D., Bryn, A., Christiansen, C. T., Cornelissen, J. H. C., Cunliffe, A. M., Elmendorf, S. C., … Wipf, S. (2020). Complexity revealed in the greening of the Arctic. *Nat. Clim. Change*, *10*, 106–117.

Myint, S. W., Gober, P., Brazel, A., Grossman-Clarke, S., & Qihao, W. (2011). Per-pixel vs. object-based classification of urban land cover extraction using high spatial resolution imagery. *Remote Sens. Environ.*, *115*(5), 1145–1161. https://doi.org/10.1016/j.rse.2010.12.017

Nie, Y., & Li, A. (2011). Assessment of alpine wetland dynamics from 1976-2006 in the Vicinity of Mount Everest. *Wetlands*, *31*, 875–884.

Nowak, M. M., Dziób, K., & Bogawski, P. (2018). Unmanned aerial vehicles (UAVs) in environmental biology: a review. *Eur. J. Ecol.*, *4*(2), 56–74.

Oberbauer, S. F., Elmendorf, S. C., Troxler, T. G., Hollister, R. D., Rocha, A. V., Bret-Harte, M. S., Dawes, M. A., Fosaa, A. M., Henry, G. H. R., Høye, T. T., Jarrad, F. C., Jónsdóttir, I. S., Klanderud, K., Klein, J. A., Molau, U., Rixen, C., Schmidt, N. M., Shaver, G. R., Slider, R. T., … Welker, and J. M. (2013). Phenological response of tundra plants to background climate variation tested using the International Tundra Experiment. *Philos Trans R Soc Lond B Biol Sci*, *368*(1624). https://doi.org/10.1098/rstb.2012.0481

Oberbauer, Steven F., Tweedie, C. E., Welker, J. M., Fahnestock, J. T., Henry, G. H. R., Webber, P. J., Hollister, R. D., Walker, M. D., Kuchy, A., Elmore, E., & Starr, G. (2007). Tundra CO2 fluxes in response to experimental warming across latitudinal and moisture gradients. *Ecol. Monogr.*, *77*(2), 221–238.

Olden, J. D., Lawler, J. J., & Poff, N. L. (2008). Machine learning methods without tears: A primer for ecologists. *Quarterly Review of Biology*, *83*(2), 171–193. https://doi.org/10.1086/587826

Pal, M., & Mather, P. M. (2003). An Assessment of the Effectiveness of Decision Tree Methods for Land Cover Classification. *Remote Sens. Environ.*, *86*, 554–565. https://doi.org/10.1016/S0034-4257 (03)00132-9

Pal, M., & Mather, P. M. (2005). Support vector machines for classification in remote sensing. *International Journal of Remote Sensing*, *26*(5), 1007–1011. https://doi.org/doi:10.1080/01431160512331314083

Pearson, R. G., Phillips, S. J., Loranty, M. M., Beck, P. S. A., Damoulas, T., Knight, S. J., & Goetz, S. J. (2013). Shifts in Arctic vegetation and associated feedbacks under climate change. *Nat. Clim. Change*, *3*, 673–677.

Pettorelli, N. (2013). *The Normalized Difference Vegetation Index*. Oxford University Press.

Phiri, D., & Morgenroth, J. (2017). Developments in Landsat land cover classification methods: A review. *Remote Sens.*, *9*(9), 967–992. https://doi.org/10.3390/rs9090967

Phoenix, G. K., & Bjerke, J. W. (2016). Arctic browning: extreme events and trends reversing arctic greening. *Glob. Change Biol.*, *22*, 2960–2962.

Platt, R. V., & Rapoza, L. (2008). An evaluation of an object-oriented paradigm for land use/land cover classification. *Prof. Geog.*, *60*(1), 87–100.

Pontius, R. G., & Millones, M. (2011). Death to Kappa: birth of quantity disagreement and allocation disagreement for accuracy assessment. *Int. J. Remote Sens.*, *32*(15), 4407–4429. https://doi.org/10.1080/01431161.2011.552923

Post, E., Alley, R. B., Christensen, T. R., Macias-Fauria, M., Forbes, B. C., Gooseff, M. N., Iler, A., Kerby, J. T., Laidre, K. L., Mann, M. E., Olofsson, J., Stroeve, J. C., Ulmer, F., R.A., V., & Wang, M. (2019). The polar regions in a 2°C warmer world. *Sci. Adv.*, *5*(1–12).

Prevéy, J., Vellend, M., Rüger, N., Hollister, R. D., Bjorkman, A. D., Myers-Smith, I. H., Elmendorf, S. C., Clark, K., Cooper, E. J., Elberling, B., Fosaa, A. M., Henry, G. H. R., Høye, T. T., Jónsdóttir, I. S., Klanderud, K., Lévesque, E., Mauritz, M., Molau, U., Natali, S. M., … Rixen, C. (2017). Greater temperature sensitivity of plant phenology at colder sites: implications for convergence across northern latitudes. *Glob Chang Biol*, *23*(7), 2660–2671. https://doi.org/10.1111/gcb.13619

Quinlan, J. R. (1986). Induction of decision trees. *Machine Learning*, *1*, 81–106.

Radoux, J., & Bogaert, P. (2017). Good practices for object-based accuracy assessment. *Remote Sensing*, *9*(7). https://doi.org/10.3390/rs9070646

Ramezan, C. A., Warner, T. A., Maxwell, A. E., & Price, B. S. (2021). Effects of training set size on supervised machine-learning land-cover classification of large-area high-resolution remotely sensed data. *Remote Sensing*, *13*(3), 1–27. https://doi.org/10.3390/rs13030368

Rawat, W., & Wang, Z. (2017). Deep convolutional neural networks for image classification: A comprehensive review. *Neural Computation*, *29*(9), 2352–2449. https://doi.org/10.1162/neco_a_00990

Raynolds, M. K., Walker, D. A., Balser, A., Bay, C., Campbell, M., Cherosov, M. M., Daniëls, F. J. A., Eidesen, P. B., Ermokhina, K., Frost, G. V., Jedrzejek, B., Jorgenson, M. T., Kennedy, B. E., Kholod, S. S., Lavrinenko, I. A., Lavrinenko, O. V., Magnússon, B., Matveyeva, N. V., Metúsalemsson, S., … Troeva, E. (2019). A raster version of the Circumpolar Arctic Vegetation Map (CAVM). *Remote Sens. Environ.*, *232*, 1–12.

Richardson, A.D., Braswell, B. H., Hollinger, D. Y., Jenkins, J. P., & Ollinger, S. V. (2009). Near-surface remote sensing of spatial and temporal variation in canopy phenology. *Ecol. App.*, *19*, 1417–1428.

Richardson, A.D., Jenkins, J. P., Braswell, B. H., Hollinger, D. Y., Ollinger, S. V., & Smith, M. L. (2007). Use of digital webcam images to track spring green-up in a deciduous broadleaf forest. *Oecologia*, *152*, 323–334.

Richardson, Andrew D., Hufkens, K., Milliman, T., Aubrecht, D. M., Chen, M., Gray, J. M., Johnston, M. R., Keenan, T. F., Klosterman, S. T., Kosmala, M., Melaas, E. K., Friedl, M. A., & Frolking, S. (2018). Tracking vegetation phenology across diverse North American biomes using PhenoCam imagery. *Scientific Data*, *5*, 180028.

https://doi.org/10.1038/sdata.2018.28

Rixen, C., Høye, T. T., Macek, P., Aerts, R., Alatalo, J. M., Anderson, J. T., Arnold, P. A., Barrio, I. C., Bjerke, J. W., Björkman, M. P., Blok, D., Blume-Werry, G., Boike, J., Bokhorst, S., Carbognani, M., Christiansen, C. T., Convey, P., Cooper, E. J., Cornelissen, J. H. C., … Zong, S. (2022). Winters are changing: snow effects on Arctic and alpine tundra ecosystems. *Arctic Science*, 1–37. https://doi.org/10.1139/as-2020-0058

Rogers, G. F., Turner, R. M., & Malde, H. E. (1983). Using Matched Photographs to Monitor Resource Change. In J. F. Bell & T. Atterbury (Eds.), *Renewable resource inventories for monitoring changes and trends: proceedings of an international conference* (pp. 90–92).

Schapeman-Strub, G., Limpens, J., Menken, M., Bartholomeus, H. M., & Schaepman, M. E. (2009). Towards spatial assessment of carbon sequestration in peatlands: Spectroscopy based estimation of fractional cover of three plant functional types. *Biogeosciences*, *6*, 275–284.

Schapire, R. E. (1990). The strength of weak learnability. *Mach. Learn.*, *5*, 197–227.

Schuur, E. A., McGuire, A. D., Schädel, C., Grosse, G., Harden, J. W., Hayes, D. J., Hugelius, G., Koven, C. D., Kuhry, P., Lawrence, D. M., Natali, S. M., Olefeldt, D., Romanovsky, V. E., Schaefer, K., Turetsky, M. R., Treat, C. C., & Vonk, J. E. (2015). Climate change and the permafrost carbon feedback. *Nature*, *520*(7546), 171–179.

Shiklomanov, A. N., Bradley, B. A., Dahlin, K. M., Fox, A. M., Gough, C. M., Hoffman, F. M., Middleton, E. M., Serbin, S. P., Smallman, L., & Smith, W. K. (2019). Enhancing global change experiments through integration of remote-sensing techniques. *Front. Ecol. Environ.*, *17*(4), 215–224.

Shiklomanov, N. I., Streletskiy, D. A., Nelson, F. E., Hollister, R. D., Romanovsky, V. E.,

Tweedie, C. E., Bockheim, J. G., & Brown, J. (2010). Decadal variations of active-layer thickness in moisture-controlled landscapes, Barrow, Alaska. *J. Geophys. Res.*, *115*, G00I04. https://doi.org/10.1029/2009JG001248

Simonis, J. L., White, E. P., & Ernest, S. K. M. (2021). Evaluating probabilistic ecological forecasts. *Ecology*, *102*, e03431. https://doi.org/10.1002/ecy.3431

Smith, A. (2010). Image segmentation scale parameter optimization and land cover classification using the Random Forest algorithm. *Journal of Spatial Science*, *55*(1), 69–79. https://doi.org/10.1080/14498596.2010.487851

Story, M., & Congalton, R. G. (1986). Accuracy assessment: A user's perspective. *Photogramm. Eng. Rem. S.*, *52*(3), 397–399.

Stow, D. A., Hope, A., McGuire, D., Verbyla, D., Gamon, J., Huemmrich, F., Houston, S., Racine, C., Sturm, M., Tape, K., Hinzman, L., Yoshikawa, K., Tweedie, C., Noyle, B., Silapaswan, C., Douglas, D., Griffith, B., Jia, G. J., Epstein, H., … Myneni, R. (2004). Remote sensing of vegetation and land-cover change in Arctic tundra ecosystems. *Remote Sens.*, *89*, 281–308. https://doi.org/10.1016/j.rse.2003.10.018

Strahler, A., Woodcock, C., & Smith, J. (1986). On the nature of models in remote sensing. *Remote Sens. Environ.*, *20*, 121–139.

Sturm, M., Douglas, T., Racine, C., & Liston, G. E. (2005). Changing snow and shrub conditions affect albedo with global implications. *J. Geophys. Res.*, *110*(1), 1–13. https://doi.org/10.1029/2005JG000013

Tempfli, K., Kerle, N., Huurneman, G. C., & Janssen, L. L. F. (Eds.). (2009). *Principles of Remote Sensing*. International Institute for Geo-Information Science and Earth Observation.

Tieszan, L. L. (1978). Photosynthesis in the principal Barrow, Alaska species: a summary of

field and laboratory responses. In L. L. Tieszen (Ed.), *Vegetation and Production Ecology of an Alaskan Arctic Tundra*. Springer.

Torres-Sánchez, J., López-Granados, F., & Peña, J. M. (2015). An automatic object-based method for optimal thresholding in UAV images: Application for vegetation detection in herbaceous crops. *Computers and Electronics in Agriculture*, *114*, 43–52. https://doi.org/10.1016/j.compag.2015.03.019

Trimble Germany GmbH. (2019). *Trimble Documentation eCognition Developer 9.5 Reference Book* (9.5.1). Trimble Germany GmbH.

Tucker, C. J. (1979). Red and photographic infrared linear combinations for monitoring vegetation. *Remote Sens. Environ.*, *8*, 127–150.

Turner, D. J., Malenovský, Z., Lucieer, A., Turnbull, J. D., & Robinson, S. A. (2019). Optimizing spectral and spatial resolutions of unmanned aerial system imaging sensors for monitoring Antarctic vegetation. *IEEE Journal of Selected Topics in Applied Earth Observations and Remote Sensing*, *12*(10), 3813–3825. https://doi.org/JSTARS.2019.2938544

van der Welle, M. E. W., Vermeulen, P. J., Shaver, G. R., & Berendse, F. (2003). Factors determining plant species richness in Alaskan Arctic tundra. *Journal of Vegetation Science*, *14*(5), 711–720.

Vittoz, P., & Guisan, A. (2007). How reliable is the monitoring of permanent vegetation plots? A test with multiple observers. *J. Veg. Sci.*, *18*, 413–422.

Wahren, C. H., Walker, M. D., & Bret-Harte, M. S. (2005). Vegetation responses in Alaskan arctic tundra after 8 years of a summer warming and winter snow manipulation experiment. *Glob Chang Biol*, *11*(4), 537–552.

Walker, M. D., Wahren, C. H., Hollister, R. D., Henry, G. H. R., Ahlquist, L. E., Alatalo, J. M., Bret-Harte, M. S., Calef, M. P., Callaghan, T. V., Carroll, A. B., Epstein, H. E., Jónsdóttir, I. S., Klein, J. A., Magnússon, B., Molau, U., Oberbauer, S. F., Rewa, S. P., Robinson, C. H., Shaver, G. R., … Wookey, P. A. (2006). Plant community responses to experimental warming across the tundra biome. *PNAS*, *103*(5), 1342–1346.

Wallace, L., Saldias, D. S., Reinke, K., Hillman, S., Hally, B., & Jones, S. (2019). Using orthoimages generated from oblique terrestrial photography to estimate and monitor vegetation cover. *Ecological Indicators*, *101*, 91–101. https://doi.org/10.1016/j.ecolind.2018.12.044

Webber, P. J., & Walker, M. D. (1991). Resolution: International Tundra Experiment (ITEX). *Arctic and Alpine Research*, *23*, 125.

Willmott, C. J., & Matsuura, K. (2005). Advantages of the mean absolute error (MAE) over the root mean square error (RMSE) in assessing average model performance. *Climate Research*, *30*(1), 79–82. https://doi.org/10.3354/cr030079

Witharana, C., Bhuiyan, A. E., Liljedahl, A. K., Kanevskiy, M., Jorgenson, T., Jones, B. M., Daanen, R., Epstein, H. E., Griffin, C. G., Kent, K., & Jones, M. K. W. (2021). *An Object-Based Approach for Mapping Tundra Ice-Wedge Polygon Troughs An Object-Based Approach for Mapping Tundra Ice-Wedge Polygon Troughs from Very High Spatial Resolution Optical Satellite Imagery*. *February*. https://doi.org/10.3390/rs13040558

Witharana, C., & Civco, D. L. (2014). Optimizing multi-resolution segmentation scale using empirical methods: Exploring the sensitivity of the supervised discrepancy measure Euclidean distance 2 (ED2). *ISPRS Journal of Photogrammetry and Remote Sensing*, *87*, 108–121. https://doi.org/10.1016/j.isprsjprs.2013.11.006

Wrona, F. J., Johansson, M., Culp, J. M., Jenkins, A., Mård, J., Myers-Smith, I. H., Prowse, T. D., Vincent, W. F., & Wookey, P. A. (2016). Transitions in Arctic ecosystems: Ecological implications of a changing hydrological regime. *J. Geophys. Res.*, *121*(3), 650–674. https://doi.org/10.1002/2015JG003133

Xue, J., & Su, B. (2017). Significant remote sensing vegetation indices: a review of developments and applications. *J. Sens.*, *2017*, 1–17.

Ye, S., Pontius, R. G., & Rakshit, R. (2018). A review of accuracy assessment for object-based image analysis: From per-pixel to per-polygon approaches. *ISPRS Journal of Photogrammetry and Remote Sensing*, *141*, 137–147. https://doi.org/10.1016/j.isprsjprs.2018.04.002

Zhou, Y., Dong, J., Xiao, X., Xiao, T., Yang, Z., Zhao, G., Zou, Z., & Qin, Y. (2017). Open Surface Water Mapping Algorithms: A Comparison of Water-Related Spectral Indices and Sensors. *Water*, *9*(4). https://doi.org/10.3390/w9040256

Zhu, Z., Piao, S., Myneni, R. B., Huang, M., Zeng, Z., Canadell, J. G., Ciais, P., Sitch, S., Friedlingstein, P., Arneth, A., Cao, C., Cheng, L., Kato, E., Koven, C., Li, Y., Lian, X., Liu, Y., Liu, R., Mao, J., … Zeng, N. (2016). Greening of the Earth and its drivers. *Nat. Clim. Change*, *6*, 791–795.